HHS Public Access

Author manuscript

Chem Soc Rev. Author manuscript; available in PMC 2017 January 10.

Published in final edited form as:

Chem Soc Rev. 2015 August 07; 44(15): 5552–5595. doi:10.1039/c4cs00382a.

Suspension arrays based on nanoparticle-encoded microspheres for high-throughput multiplexed detection

Yuankui Leng[a], **Kang Sun**[a], **Xiaoyuan Chen**[b], and **Wanwan Li**[a]

[a]The State Key Lab of Metal Matrix Composites, School of Materials Science and Engineering, Shanghai Jiao Tong University, Shanghai 200240, China

[b]Laboratory of Molecular Imaging and Nanomedicine, National Institute of Biomedical Imaging and Bioengineering, National Institutes of Health, Bethesda, Maryland 20892, USA

Abstract

Spectrometrically or optically encoded microsphere based suspension array technology (SAT) is applicable to the high-throughput, simultaneous detection of multiple analytes within a small, single sample volume. Thanks to the rapid development of nanotechnology, tremendous progress has been made in the multiplexed detecting capability, sensitivity, and photostability of suspension arrays. In this review, we first focus on the current stock of nanoparticle-based barcodes as well as the manufacturing technologies required for their production. We then move on to discuss all existing barcode-based bioanalysis patterns, including the various labels used in suspension arrays, label-free platforms, signal amplification methods, and fluorescence resonance energy transfer (FRET)-based platforms. We then introduce automatic platforms for suspension arrays that use superparamagnetic nanoparticle-based microspheres. Finally, we summarize the current challenges and their proposed solutions, which are centered on improving encoding capacities, alternative probe possibilities, nonspecificity suppression, directional immobilization, and "point of care" platforms. Throughout this review, we aim to provide a comprehensive guide for the design of suspension arrays, with the goal of improving their performance in areas such as multiplexing capacity, throughput, sensitivity, and cost effectiveness. We hope that our summary on the state-of-the-art development of these arrays, our commentary on future challenges, and some proposed avenues for further advances will help drive the development of suspension array technology and its related fields.

1. Introduction

The rapid development of disease diagnosis and therapeutic treatment has led to increasing demand for a multiplex and high throughput analysis of large numbers of biomolecules within a single sample.[1–3] Large-scale screening of biomolecules has attracted much attention for its use in various applications, including the functional analysis of unknown genes to identify those that are disease-related,[4] clinical diagnostics,[5] and screening for drug discovery.[6,7] As a result, many multiplexing technologies have recently been developed, including predominantly planar microarray[8–11] and suspension array technologies

Correspondence to: Kang Sun; Xiaoyuan Chen; Wanwan Li.

(SATs).[12–19] Multiplexing technologies can conveniently integrate multiple variables to overcome the clinical sensitivity and/or specificity limitations found with a single marker. When compared to multiple, single-analyte assays, multiplexing can dramatically increase the efficiency of these analyses by reducing costs through lower reagent consumption, faster analysis, and decreased labor.[20] As shown in Fig. 1, the growth in multiplex research is most clearly shown in the increasing number of published papers related to the topic.

1.1. Significance of suspension array technology

Compared to methods of traditional, quantitative analysis, the key to realizing multiplexed analysis is in efficiently addressing various analytes for their separate quantifications.[21] To fulfill the demand for large-scale biomolecule screening, planar microarrays such as the two-dimensional probe grids (*e.g.* oligonucleotides, proteins, and drug candidates) have molecules deposited onto flat solid supports and can address and separately quantify thousands of analytes *via* a positional encoding method.[22] Although planar microarray technology plays an important role in ultra-high-density analysis,[23] it has limitations on the quality of its results, binding rates, decoding speed, and its overall flexibility.[21] To address this problem, suspension arrays that use encoded microparticles as solid-supports in combination with tracking codes for analytes offer significant advantages. These advantages include:[21,23–25]

1. Faster binding kinetics and convenient separation steps.[26] The small size and 3D exposure of the microcarriers allow for near solution-phase kinetics, which is in contrast to planar microarrays, which are limited by solid-phase kinetics.[27,28]
2. Flexibility in target selection and immobilization of probe molecules. Analytes can be freely customized according to the user's specific needs. Furthermore, each probe can be separately immobilized *via* proven chemical methods and under conditions that are optimal for each probe. Planar microarrays use a uniform immobilization procedure, which may not be suitable for all probes.
3. Higher quality of results, including better reproducibility and higher sensitivity.[21] In planar microarray technology, the number of array spots being produced at the same time is limited, thus leading to variations in feature properties between arrays and even within the same array. This ultimately leads to relatively poor productivity and detection sensitivity. The high-volume production of encoded microcarriers allows for a standardized assay that planar microarrays cannot provide. This is in combination with the statistical calibration of batch results from many microcarriers, thus providing overall higher quality results.
4. Suspension array is a unique platform which can address the need for applications requiring simultaneous high-density and high-throughput.[25] Modern flow cytometers can read fluorescent barcodes at extremely high speeds (50 million events per day).[25] In contrast, planar microarrays can

provide ultra-high-density analysis, but with low sample throughput due to its relatively low decoding speed.[23]

5. Easy fabrication and cost-effectiveness.[29] When compared to planar microarrays, the fabrication of suspension arrays shows a lower demand on both equipment and raw materials, leading to enhanced cost-effectiveness.

1.2. Why do suspension arrays based on nanoparticle-encoded microspheres hold great promise for high-throughput, multiplexed detection?

The core technology of the suspension array is the use of encoded microcarriers to identify different biomolecular binding events (Fig. 2).[30] A sufficient number of accurate barcodes are critical to fulfill the high density analysis, and various encoding schemes have been used to this end, including spectrometric encoding,[12,15,18,30,31] graphical encoding,[19,32–35] chemical encoding,[36–40] electronic encoding,[41,42] physical encoding,[43,44] and magnetic encoding.[45,46] Furthermore, the combination of different encoding techniques can produce an even larger amount of barcodes.[30,33,47] Among these schemes, spectrometric encoding is the most widely used, due to its flexible encoding, convenience, and high-speed decoding. In comparison, graphical encoding utilizes structural recognition and requires complex instrumentation for both synthesis and readout. This makes it especially limited, due to its relatively low decoding speed.[21,33] Chemical encoding[36] also suffers from a complicated and time-consuming decoding process, with its high cost being another concern. Additionally, barcodes from electronic encoding are limited by size,[41,42] thus seriously affecting their multiplexing capacity.

Physical characteristics such as size and refractive index can limit encoding capacity. Since size and refractive index can be conveniently decoded using modern flow cytometers, they are usually used as additional encoding dimensions for spectrometric encoding.[30,48] However, for planar, multi-bit, magnetic barcodes,[46] magnetic elements show controlled spatial distribution, making the manufacture and decoding processes more complicated than those for spectrometric barcodes. Therefore, spectrometric barcodes and those combined with other compatible encoding elements, such as size, refractive index and lifetime, are more popular for applications in high-throughput, multiplexed detection. For example, the first commercial suspension array platform, a Luminex®xMAP™ system,[25,49] incorporates 5.6 μm polystyrene microspheres internally dyed with two or three spectrally distinct fluorochromes, and has been used in a variety of applications.[50–53]

The main advantage of using a planar microarray is that it allows for thousands of individual tests to be performed in parallel, lending it well-suited to powerful applications in genomics, proteomics, and drug discovery. Since suspension array technology can provide higher quality results, the question is whether it has the potential to confer the same array density. In the Luminex system[49] and BD cytometric bead array system,[54] microspheres are encoded with various organic dyes with different wavelengths and intensities to create a library of barcodes for the parallel detection of multiple targets. However, organic dye-based barcodes suffer from several drawbacks.[55] For one, the available barcode number (typically <500) is limited by the number of spectrally, well-resolved organic dyes that do not interfere with

commonly used biological markers.[21,56] Moreover, multiple excitation lasers are required if dyes with different excitation wavelengths are used, which is costly for decoding instruments.[30,57] Additionally, interference between encoding fluorescence and labeled fluorescence is inevitable, thus complicated and tedious color compensations are needed. Finally, organic dyes that are incorporated into microspheres also suffer from low photobleaching thresholds.

Thanks to the recent advances in nanotechnology, new functional nanoparticles with unique spectrometric properties make it possible to overcome the limitations of organic dyes. Quantum dots (QDs)[56] with narrow, size-tunable, and stable emissions possess much higher encoding capacities than organic dyes. Moreover, the possibility for exciting all QDs at the same wavelength is important to allow for the further simplification of decoding instruments. Upconversion nanoparticles (UCNPs)[58] are excited by near-infrared (NIR) light and would be able to minimize background noise. The tunable lifetime of UCNPs can also be used as a supplemental encoding dimension. Noble metal particle-based surface enhanced Raman scattering (SERS) signals[59] can be used as encoded labels for ultra-sensitive multiplexed detection. Periodic nanostructures[60] could also be used, providing for extremely stable barcodes. Moreover, all of the aforementioned nanoparticles provide much higher resistance to photobleaching than conventional, organic dyes. Therefore, the use of functional nanoparticles in suspension array technology would allow for significant advancement, making them an excellent tool for high-throughput analysis. Specifically, suspension arrays can provide high array density, which is not only comparable to planar microarray capabilities, but to better reproducibility, higher sensitivity, and increased throughput.

In this review article, we will first introduce the different nanoparticles used for barcode preparation, focusing mainly on their encoding patterns and capacities as well as how to take full advantage of their physicochemical properties. We will then compare different barcode synthetic techniques, discuss their advantages and disadvantages. Conducting a bioanalysis (*e.g.* disease diagnosis) based on either the presence or concentration of certain biomolecules requires assays that can detect molecules of interest or other targets with a high degree of sensitivity. Given this importance, five routes to obtain a high signal-to-noise ratio in high sensitivity assays will be reviewed, including new materials that can generate high signal or low background, signal amplification strategies, suppression of nonspecific events, oriented immobilization, and better probing ligands for target recognition. Moreover, suspension arrays are currently equipped with large and complex instruments that typically require highly skilled personnel to operate and are oftentimes remote from the site of patient care. With this in mind, we will briefly introduce the development of robust, portable, and low-cost suspension arrays for “point-of-care” diagnosis. It is anticipated that nanoparticle-encoded microsphere-based suspension array technology will elicit broad interest and provide guidance for research in related disciplines such as material chemistry, disease diagnosis, drug discovery, and medical instrument engineering.

2. Spectrometrically or optically encoded microspheres with nanoparticles

The microsphere barcode is the key to the suspension array. As such, there are six properties which must be met:

1. The more barcode number the better, as more barcodes confer a higher capacity for multiplex analysis;
2. The encoded signal should be of considerable stability. Good stability means increased resistance to environmental conditions[61] such as pH, temperature, and buffer concentrations, resulting in robust, long-term stability;
3. Easily implemented decoding methods. The decoding methods should be simple and flexible enough to be compatible with multiple decoding instruments;
4. Decreased mutual interference between signals from barcodes, labels, and biomolecules. When the suspension arrays work, there are at least three optical signals: those from the barcodes, the labels and the biomolecules that are attached onto the microspheres;
5. Ability to manufacture the individually encoded microspheres in large, replicable quantities;
6. Proper size and density of encoded microspheres. Falling under the common denominator of miniaturization[62] coupled with high density analysis, the working volume of the microspheres will be decreased while maintaining a high enough density for adequate analysis. Thus, the size of the barcode will need to be small enough. On the one hand, large and/or dense microspheres require vigorous mixing to maintain them in suspension, while the vigorous mixing might damage the probe, target molecules, and even the microspheres themselves. On the other, the microspheres should also be (i) large enough to host some form of code and (ii) slightly denser than water for effective separation from the solution. Adequate microspheres should be made from materials with a proper density (*e.g.* polystyrene, poly(styrene-*co*-maleic anhydride), silica, *etc.*) and have a diameter in the range of 0.3–10 μm.[21]

Although the commercial suspension array platforms currently available from Luminex and BD[54] use organic dyes as their encoding fluorochromes, these may not be the most suitable choice as mentioned above. Fortunately, many functional nanoparticles with unique spectrometric properties can function as alternatives, greatly improving the multiplexing capacity, sensitivity, and photostability of suspension arrays (see Table 1).

2.1. Quantum dot-encoded microspheres

Quantum dots (QDs) have excellent and unique optical properties[12,57,63,64] including narrow and symmetrical emission spectra, broad excitation wavelength (*i.e.* QDs with different emission spectra can be excited by a single wavelength excitation source), tunable emission

wavelengths, and high brightness. These characteristics make QDs ideal candidates for the creation of a diverse array of barcodes for suspension assays. Since this concept was proposed by the Nie[12] group in 2001, the spectroscopic encoding of microspheres based on QD color and intensity has been regarded as one of the most promising approaches, owing both to its flexible encoding and convenient decoding by modern flow cytometers and/or spectrometers.

The primary advantage of QDs over other barcode sources (*e.g.* traditional organic dyes) is their significantly increased encoding capacity. By trapping QDs with different emission spectra at different concentrations (*i.e.* intensities), different barcodes can be obtained, with the number of barcodes calculated according to the following formula: $C = N^m - 1$ (where C = the barcode number, N = the number of intensity levels and m = the number of colors) (Fig. 3). Their narrow, tunable emission spectra (full width at half maximum (FWHM) of 20–30 nm) can provide 10–12 different colors in the visible region with acceptable spectral overlap. This concept was conclusively demonstrated, with at least 10 intensity levels being used effectively in microsphere barcodes.[12]

Theoretically, more than one million barcodes could be generated, which is significantly more than that capable of being produced using organic dyes alone. To this end, Chan *et al.*[65] generated 105 spectrally distinct barcodes *via* partial use of five different QDs at three different intensities. Since modern flow cytometers can decode particles on the basis of size, many more barcodes could be generated by encoding a combination of QD color, intensity, and microsphere size. As shown in Fig. 3(b), a 3D barcode library based on FL1-FL4-FS signals of a flow cytometer (Beckman Coulter FC500) was generated by incorporating 520 nm QDs and 680 nm QDs into differentially-sized polymer microspheres.[30] NIR (near-infrared) QDs (650–800 nm) with wide PL spectra (FWHM > 50 nm) can also be utilized, and a "single wavelength" encoding method[66] was developed to take advantage of QDs in the NIR region. With this method, the spectra of NIR QDs span over FL4 and FL5 fluorescent channels of the flow cytometer. The encoding principle is shown in Fig. 3(c), whereby distinct NIR QDs with different PL wavelengths provide separate FL4/FL5 PL intensity ratios, resulting in different encoding signals. This increases the encoding capacity of QDs within the NIR region.

In practice, the encoding capacity is also limited by overlap between different intensities,[21] which is one of the main challenges in QD encoding. Currently, the probable solution is to control the locations of different colored QDs in the microspheres (discussed further in Section 7). It is also worth noting that it is necessary to use a label for multiplexed assays, with the region of the spectrum reserved for the label then not available for encoding purposes.

The method for reading QD barcodes (or read-out algorithms) also determines the number of available QD barcodes used in bioassays. Simple and effective signal processing methods can not only decrease false signal detection, but can also improve QD encoding capacity. For example, Chan *et al.*[61] developed a deconvolution algorithm to identify QD barcodes, whereby QD barcodes with similar fluorescence spectra can be clearly distinguished. When compared to fluorescence channel-based decoding methods (*e.g.* flow cytometry), this PL

spectra-based decoding method has an obvious benefit in the decreased need for filters and single light detectors.

Finally, the type of short-wavelength excitation that is usually used in bioanalysis with organic dyes and QDs leads to significant background signals.[57] Conventionally, the fluorescence lifetimes of organic dyes are too short (<10 ns) to allow for efficient temporal discrimination of the short-lived fluorescence interference induced by the excitation. In the case of QDs, the relatively long lifetime (10–100 ns) enables robust temporal discrimination of the background signal by time-gated measurements, thereby enhancing overall sensitivity.[67] However, the use of time-gated measurements in a suspension array may reduce its decoding speed, increasing the burden on decoding instruments like flow cytometers.

2.2. Upconversion nanoparticle-encoded microspheres

Background interference from biomolecules usually occurs in organic dye- or QD-based suspension arrays due to the use of short-wavelength excitation. The background signals derive primarily from Rayleigh scattering and autofluorescence of bio-molecules under excitation of short wavelength light.[58] However, there is little interaction between NIR light and biomolecules, leading to almost no NIR light-induced background luminescence or photodamage. Several strategies have been developed to take advantage of NIR light, including the use of long-wavelength absorbing organic fluorochromes[69,70] and anti-Stokes emissions[71–73] (*e.g.* two photon excitation). However, long-wavelength absorbing organic fluorochromes often show low quantum yields[57] and require the use of expensive and powerful pulsed lasers since high energy excitations are usually required in most anti-Stokes processes. To directly address this limitation, upconversion nanoparticles (UCNPs) are lanthanide-doped nanocrystals that allow for low energy anti-Stokes emission.[74] UCNPs can emit multi-colored light with narrow emission bands and a large anti-Stokes shift with continuous use of a NIR diode laser.[75,76] UCNPs also show low toxicity, high photostability,[77] and their multi-color fluorescence emission can be fine-tuned by varying either the lanthanide dopants[75,78] or the optical surface layers.[79,80] Furthermore, when compared to QDs or organic dyes, lanthanide ion emissions only involve atomic transitions and are considerably more stable. Additionally, a FRET effect does not happen among UCNPs, which is different from both QDs and organic dyes. Therefore, UCNPs are suitable candidates for use as fluorochromes in microsphere barcodes and have been widely used in multicolor encoding[16,19,79,81] based on their tunable, multicolor emission spectra.

As shown in Fig. 4(a), Zhang *et al.*[16] presented an encoding scheme for UCNPs of "n intensity levels with m colors generating ($n^m - 1$) unique codes", which is similar to that of QDs. When using one of the emissions within a nanocrystal as an internal standard, the relative fluorescence intensities of other emissions give m colors, which can be obtained by varying the composition of the UCNPs. Additionally, if different organic dyes were used as labels (Fig. 4(b)), the optical crosstalk between barcodes and label dyes under different excitation conditions could be avoided. Therefore, the labels could be selected in a wide emission range and the labels could even act as another coding dimension, further increasing the overall number of codes.

However, a platform combining the use of UCNP barcodes with organic labels has two drawbacks. First, there is a likelihood of background interference due to short-wavelength excitation of the organic dye labels. Second, at least two light sources would be needed. Moreover, the signals from the barcodes and labels of the microspheres should be excited and detected separately to avoid optical crosstalk, thus compounding the burden on decoding instruments. Gorris *et al.*[79] tuned emission spectra of $NaYF_4$:Yb,Er and $NaYF_4$:Yb,Tm by coating different concentrations of organic dyes on the surface of the upconversion nanoparticles (Fig. 5(a) and (b)). One of the two emission bands was selectively re-absorbed at different degrees by the organic dyes and resulted in different values of I_{code}/I_{ref} (Fig. 5(c) and (d)). These were then used as ratiometric coding elements (Fig. 5(e) and (f)). Here, $I_{code}(I_{ref})$ denotes the intensity of the tuned (untuned) emission (Fig. 5(c)). It should also be noted that lanthanide doped downconversion nanoparticles[82] have also been used for encoding through the use of their multicolor emission properties.

When compared to QDs, UCNPs possess a lower encoding capacity. This is due to the fact that the peak positions of the multicolor emission UCNPs are determined by the doped lanthanide ions, leading to an underutilization of spectral space. Another obstacle is finding labels suitable for use in UCNPs encoded-microspheres for a suspension array. Organic dyes and QDs are less than suitable, since they need extra excitation in the form of a short wavelength laser. A better choice might be UCNPs. However, most UCNPs are not used as matched labels due to their multicolor emission spectra. Currently, efforts to develop UCNPs with single-band emissions are ongoing,[83–88] with UCNPs at a red emission peak of 650 nm and an NIR emission peak of 800 nm having been produced.

2.3. Luminescence life-time-encoded microspheres

Currently, fluorescence color encoding in combination with a modern, multi-color flow cytometer[89] as the decoding equipment is one of the most popular methods for multiplexing. Despite this popularity, it has several limitations. First, the crowded spectral domain allows for fewer than 20 channels in the decoding instrument, resulting in practical limits on the number of codes. Second, there are several equipment constraints, including: three to five lasers (QD-encoded microspheres only need a single laser[30]), tens of filters, and up to 20 light detectors. Moreover, the unavoidable spectral overlap leads to complicated and tedious color compensations. Therefore, the use of additional, distinguishable coding dimensions (*e.g.* spatial fluorescence encoding,[19,33] SERS encoding,[59,90] metal ion-based mass encoding,[38,39] and lifetime encoding[17,91]) have all been exploited for multiplexing. The luminescence lifetime is an intrinsically, self-referential parameter that is insensitive to variations in excitation light intensity and dye concentration.[58] Moreover, lifetime multiplexing relies on dyes with sufficiently different lifetimes, yet that can be excited at the same wavelength and detected within the same spectral window.[92]

In recent years, life-time encoding methods based on organic dyes,[92] QDs,[93,94] and metal ligand complexes[95] have been developed. Chen *et al.*[94] developed NIR-emitting, 2D codes based on emission (λ) and lifetime (τ) of lattice-strained CdTe/CdS QDs (with short lifetime, q-dots) and lattice strained CdTe/CdS:Cu QDs (with long lifetime, d-dots). However, most fluorescence chromophores (including organic dyes and QDs) are not the

most optimal choices due to their short lifetimes.[57] Some rare-earth metal-based materials can exhibit longer lifetimes—from microseconds to even milliseconds—and have been widely used in time-resolved luminescence immunoassays.[96,97] The lifetimes of downconversion lanthanide complexes can be tuned using the scheme of lanthanide-based resonance energy transfer (LRET).[98,99] Recently, Lu *et al.*[100] utilized a LRET scheme to tune the lifetimes of downconversion lanthanide complex-containing microspheres. Meanwhile, lifetimes of lanthanide doped UCNPs (called '**τ**-dots') were able to be tuned by controlling the doping amount of lanthanide ions, crystal phases[17] and sizes,[101] or the surface ligand passivation.[17] Given this wide range of tuning ability, dozens of lifetime barcodes could be generated (Fig. 6(a)). When combined with time-gated, orthogonal scanning automated microscopy (OSAM, on-the-fly scanning cytometry) as a decoding instrument (Fig. 6(b)),[102,103] the realization of a lifetime barcode-based suspension array would be possible (Fig. 6(c)).[100] '**τ**-dots' encoded barcodes have several advantages over fluorescent color and intensity based barcodes. Firstly, similar to the multicolor encoding scheme of UCNPs, '**τ**-dots' show high stability and no background interference due to the NIR excitation and time-resolved measurement.[97] Secondly, since luminescence lifetime is independent of absolute PL intensity, '**τ**-dots' are more tolerant of ambient background, as well as instrument disturbances including electronic noise, varying collection efficiencies and chromatic aberration associated with optical defocusing. While compared with fluorescence color barcodes, the decoding speed of lifetime barcodes is much slower.

2.4. Surface-enhanced Raman scattering (SERS) spectrum-encoded microspheres

SERS[104,105] is a widely used optical signal in biological imaging[109,110] and biological sensing[59,111,112] that is traditionally based on plasmonic materials such as noble and coinage metals (*e.g.* silver,[106] gold,[107] and copper[108]) that have nanoscale features (*e.g.* roughened surfaces and nanoparticles). Some nanomaterials including graphene,[113] TiO_2[114] and QDs[115] have also been reported to show SERS. When SERS is used as a coding element, it offers several unique advantages, such as:

1. Ultrasensitive detection, which is of greater sensitivity than fluorescence-based methods,[116–118] offering detection capabilities down to the level of a single molecule;
2. No photobleaching in Raman scattering;[119]
3. Excitation light wavelength falls within a flexible range, covering the UV to NIR regions;[104]
4. High capacity of multiplexing.[120] Owing to the narrow spectral features of SERS, large numbers of different Raman signatures can be obtained using different reporter molecules.

In recent years, various SERS-encoding nanomaterials[9,121,122] and readout techniques[90,123,124] have been reported. Most SERS-encoding nanomaterials are based on composite organic–inorganic nanoparticles (COINs),[120] also called "SERS dots". In suspension array technology, SERS signatures can be used to encode carriers as well as labels, due to their high encoding capacity and high sensitivity (Fig. 7). Jun *et al.*[125] generated spectroscopically-distinguishable SERS barcodes by using three different Raman

labels in silver nanoparticle-embedded sulfonated polystyrene beads (Ag NPs). SERS signals were then used to distinguish various targets, with a Cy5 fluorescent label used for quantitative analysis (Fig. 7(a)). To prevent fluorescence quenching, Cy5 was separated from the Ag NPs by coating a silica shell on the nanoparticles. Moreover, additional barcodes were generated by coating several types of SERS dots together with different intensities onto the microspheres.[122] It is worth noting that signals from the fluorescent labels can overlap with the SERS signal. In the future, overlap will have to be avoided in this platform *via* careful selection of Raman dyes and fluorescent labels.

SERS dots can also act as simultaneous barcodes and labels (Fig. 7(b)).[18,126–128] Mirkin and colleagues[128] encoded different oligonucleotide sequences by conjugating each oligonucleotide with a unique combination of fluorescent dyes onto gold nanoparticles. The Raman probes were then used as labels in microbead assays and the Raman signals of the bound labels were enhanced by gold-nanoparticle-catalyzed silver deposition. Thirteen oligonucleotide sequences were encoded by using Cy3 and Cy3.5 fluorescent labels at five different intensity levels, resulting in the generation of approximately 8000 barcodes by using six dyes with non-overlapping SERS spectra. However, the Raman spectra will contain an increasingly large amount of unwanted features as more dyes are used, thus it is unlikely to produce a large number of barcodes that will have robust and precise readouts. In 2007, Oxonica developed Nanoplex technology, which is based on the Nanoplex™ biotag[127] and designed for use in multiplex bioassays (Fig. 7(c)). The Nanoplex™ biotag is composed of Raman active molecule-tagged gold nanoparticles encapsulated within a silica shell. In a typical multiplex assay, the biotags, analytes, and magnetic beads are immobilized with capture probes to form two-particle sandwich complexes. These are then concentrated and detected at a specific location reaction vessel under application of a magnetic field. This platform permits a fast, homogeneous reaction, no-washing, multiplexed analysis of biomolecules with high sensitivity (pg mL^{-1} for protein). Furthermore, infrared light excitation is used in this platform, resulting in reduced background fluorescence. However, the achievable multiplexing capacity depends on precise decoding of the signals from mixed Raman labels. Therefore, the Raman dyes suitable for this platform are limited to those with a simple molecular structure that provide less complicated SERS signals. Typically, the Nanoplex™ biotag platform can multiplex about ten tests using a low-cost, handheld decoding reader.

According to theoretical calculations[129,130] and work on the distribution of site enhancements,[131] use of the Nanogap area[118] (or the so called “hot spot”[116]) of a noble metal colloidal aggregation can dramatically increase the SERS signal and potentially enhance its detection sensitivity. Therefore, SERS probes with built-in nanogap hot spots have attracted much attention, and various multimeric ensembles of metal nanostructures with tailored interparticle nanogaps have been produced using self-assembly approaches.[132,133] The anisotropic SERS signal from multimeric ensembles suffers from poor reproducibility of the SERS-active sites, and the nonuniform SERS signal resulting from the wide distribution of the enhancement factor (EF) values brings down detection sensitivity.[134] Recently, both the Nam[134] and Duan groups[135] reported core–shell SERS nanoprobes with interior nanogaps, which showed highly uniform and efficient SERS activity (Fig. 8). This kind of nanoprobe would be an ideal label for suspension arrays, since

it can provide uniform and high EF values (narrowly distributed between 10^8 and 5×10^9), which result in its high sensitivity.

2.5. Structure color-encoded microspheres

Structure color comes from the reflection of periodic nanostructures of dielectric materials (called "photonic crystals"[136]) and is another novel coding element. Structure colors are electromagnetic waves that fall in a specific frequency range and are prohibited by photonic crystals (PCs).[137] Their colors are determined by the structural period and the system refractive index of the dielectric system according to Bragg's law, $m\lambda = 2nd\sin\theta$, where m is the diffraction order, λ is the light wavelength in a vacuum, n is the refractive index of the material, d is the diffracting plane spacing, and θ is the Bragg glancing angle. Thus, structure color is tunable and resistant to photo bleaching. Stable barcodes can then be obtained from the tunable reflectance peaks of photonic crystals.[138,139] For instance, Cunin *et al.*[138] prepared PC-encoded, porous silicon microparticles by galvanostatic anodic etching of crystalline silicon wafers. Silicon particles with porosity variation were prepared, with the periodicity of the porosity variation controlled by the etching parameters. In this way, particles with different reflectance peaks could be produced. Importantly, particles with multiple reflectance bands could also be precisely produced.[140] The wavelengths of peak reflectance were used as encoding elements, resulting in the fabrication of more than one million encoded porous silicon PC microparticles. Of note is that the decoding process required that the anisotropic 2D microparticles were properly dispersed and correctly orientated,[140] which is difficult to achieve. However, this problem can be solved by using isotropic 3D PC microspheres.[60]

Gu *et al.*[15,60,141–143] have done comprehensive work on photonic crystal microsphere-based suspension arrays. As shown in Fig. 9, an opal colloidal photonic crystal structure composed of either submicron silica nanobeads or submicron polystyrene nanobeads, and an inverse opal colloidal photonic crystal structure were used to generate barcodes. However, the number of photonic crystal barcodes is limited because it is a one-dimensional encoding method. Given this limitation, other encoding elements such as QDs[144] were added to enrich the barcode library. Recently, multiple-core photonic crystal barcodes[145] with multiple structure colors have also been produced. When photonic crystal microsphere barcodes were applied in a suspension array, high sensitivity (0.92 ng mL^{-1} for IgG) was obtained due to the high surface-to-volume ratio (SVR) resulting from the ordered and porous nanostructure.[60] However, the photonic crystal barcodes were found to be larger than 100 μm, which would pose a challenge for high-density multiplexing.

3. Fabrication technologies for nanoparticle-tagged barcodes

Most suspension arrays using nanoparticle-tagged barcodes require uniform and biocompatible microspheres that are incorporated with different nanoparticles. It is therefore of great importance to develop techniques that allow for (i) highly efficient and reproducible barcode preparation, and that (ii) have excellent properties. Currently, most of the reported fabrication processes can be divided into the following five categories:[56]

i. Trapping nanoparticles into porous microspheres through the use of swelling methods;

ii. Coating nanoparticles onto spherical template surfaces using layer-by-layer self-assembly methods;

iii. Embedding nanoparticles into microspheres during their formation process *via* emulsification and/or polymerization methods;

iv. Micro-engineering emulsification and/or spray technique-assisted methods;

v. Using sol–gel processes to encapsulate nanoparticles into the silica shell of spherical templates or silica microspheres.

It is important to evaluate these manufacturing techniques and assess whether or not they are well-suited to barcode production. First, barcodes should be efficiently and reproducibly generated with corresponding high yields. Second, the methods employed should have low requirements on the need for synthesis equipment in addition to as simple a protocol (including purification steps) as possible. Third, barcode properties including size, monodispersity, stability, interior nanoparticle distribution, and the compatibility with probe molecules coupling should all be evaluated.

As for QD barcodes, poor monodispersity—as indicated by a large coefficient of the variation (CV) value—leads to variations in QD incorporation. This has adverse effects on deconvoluting the intensity part of the barcodes, thus limiting their encoding capacity.[12] Furthermore, the non-uniformity of barcode sizes will also lead to large CV values of detection, resulting in limited sensitivity. Maldistribution of QDs in microspheres increases the FRET effect among different QDs, resulting in limited encoding capacity. Note that the FRET effect among different QDs can be prevented by controlling the locations of different colored QDs within microbeads.[146] The stability of barcodes may also impact the accuracy of barcode identification.[61] Additionally, the raw material for barcodes should be carefully chosen for subsequent functional modification and probe immobilization. A comparison of some typical manufacturing techniques is shown in summary, Table 2.

3.1. Swelling method

In commercial suspension array systems, barcode preparation processes usually involve swelling the polymer beads in an organic dye-containing solvent, thereby allowing the dye molecules to infiltrate the beads.[21,147] After removing the solvent, the beads shrink and effectively trap the dye molecules. Nie *et al.* were the first encoded polystyrene microspheres with hydrophobic QDs *via* a swelling method.[12] By using a modified procedure, Nabiev *et al.*[148] doped water-soluble CdSe/ZnS QDs into polystyrene latex beads with the carboxylic groups on the surfaces to allow for further bioconjugation. Afterwards, Nie *et al.*[68] transformed commercial polystyrene microspheres into mesoporous microspheres (a pore diameter of 2–50 nm), and doped them with QDs. This doping was shown to be much more efficient than when used on nonporous beads, resulting in barcodes with fluorescence intensities that were 1000-fold brighter and five-fold more uniform than those of nonporous beads.

The key principle behind the success of the swelling method is the driving force of penetration.[149] In the swelling method employed by Nie *et al.*[12,13,68,150] and Nabiev *et al.*,[148] QDs were pushed into microspheres using either a hydrophobic[12] or hydrophilic interaction,[148] with poor solvents used to increase the driving force. Another driving force is the difference of QD concentration between the interior and exterior of the microspheres. Thus concentrating the QDs outside the microsphere during the doping process can more effectively drive penetration. Song *et al.*[151] combined these two types of driving forces *via* a gradual solvent evaporation method. However, the fluorescence intensities of the QDs were often decreased during the swelling process due to the use of a poor solvent.[149] To address this issue, a "swelling-evaporation" method[149] was recently developed, in which the swelling process was combined with gradual solvent evaporation, avoiding the use of a poor solvent (Fig. 10). The relationship found between pore size and fluorescence indicates that when used with microspheres that have no or small pores, QDs will remain on the surface. In contrast, microspheres with pores that are too large will fail to trap QDs efficiently.

As mentioned above, mesoporous microspheres facilitate efficient incorporation of QDs, but of concern is the fluorescence stability of barcodes produced by this method.[61] In order to obtain stable QD-encoded barcodes, QDs should be positioned well inside the polymer matrix to prevent leakage from the microspheres.[152,153] To this end, Gao *et al.*[152] encapsulated QD-doped mesoporous microspheres (QDMMs) with silica shells to prevent potential leakage and/or chemical-induced degradation of the embedded QDs. To create anchor points for silane condensation, a polyvinyl alcohol layer should be coated onto QDMM firstly *via* a microemulsion procedure. Song *et al.*[153] proposed a "self-healing" encapsulation strategy to seal the surfaces of QD-embedded porous poly(styrene-*co*-EGDMA-*co*-MAA) microspheres. The QD barcodes obtained *via* this "self-healing" encapsulation strategy were promising and showed high stability. However, both methods are complex and time consuming and will need further refinement.

Since the use of swelling methods has resulted in excellent monodispersity of barcodes, they have been widely employed to produce other nanoparticle-encoded microspheres, including multicolor UCNP encoded barcodes[16] and '**τ**-dots' encoded barcodes.[17] Compared with QDs, UCNPs (or '**τ**-dots') are more tolerant of degradative chemical environments.

3.2. Layer-by-layer (LBL) self-assembly method

Traditionally, the LBL deposition method[154] is based on alternating adsorption of oppositely charged species. This then allows for various nanostructures to be held together by electrostatic forces and hydrogen bonding interactions. Incorporating QDs onto microspheres through layer-by-layer technology was first used by Rogach *et al.*[155] Furthermore, multicolor QDs have been shown to be rapidly and precisely deposited onto different spherical templates (Fig. 11).[144,156–158] Usually, the LBL method for QD-encoding uses hydrophilic and charged QDs, which are transferred from hydrophobic QDs either through ligand exchange techniques[155] or encapsulation with amphiphilic copolymers.[158] However, oftentimes the quantum yields (QYs) of QDs significantly decrease during the solvent transfer process. Hydrophobic QDs have also been deposited onto microspheres,[157] but the resulting QD fluorescence intensities are compromised due to the poor solvent

capacity of water. Moreover, an extra layer is always needed to protect the QDs. Instead of utilizing electrostatic forces, Rauf and coworkers[159,160] deposited multilayer QDs onto microspheres containing magnetic nanoparticles by a biotin–streptavidin system (Fig. 12). This method provided a reagent-less, self-assembly process for barcode production that was stable even at high temperatures (as indicated by no fluorescence signal variation after treatment at 95 °C for 15 min). Moreover, streptavidin also provided a blocking coating to minimize non-specific biofouling.

The LBL process is also suitable for deposition of other nanoparticles, such as magnetic iron oxide[161] and colloidal metal nanoparticles.[162] However, the LBL process will become more complex and time-consuming as more and more layers are needed.

3.3. Embedding nanoparticles during the formation of microspheres

Embedding nanoparticles into microspheres during the formation of the microspheres themselves is another popular method and can be divided into two types according to a synthesis process of either polymerization or emulsification/solvent evaporation.

The most direct application of the polymerization method is to introduce hydrophobic nanoparticles into drops containing monomers, an initiator, and a crosslinking agent, and then trigger the polymerization.[163] However, using this method results in QD barcodes that have a maldistribution of QDs within the microspheres. This is due to the incompatibility between QDs and the polymer, thus requiring surface modifications of the QDs to allow for a more equal distribution.[164,165] Bawendi *et al.*[166] modified QDs with various phosphorus oligomer ligands, then encapsulated QDs in polystyrene beads. Although the results indicated that a uniform, spatial distribution of QDs within the polystyrene beads could be obtained, the microspheres showed poor monodispersity. As for hydrophilic nanoparticles, hydrophobic modifications would need to occur prior to encapsulation. For instance, Gao *et al.*[167–169] transferred hydrophilic nanoparticles to hydrophobic ones by using various surfactants and ligands. These nanoparticle-tagged microspheres were then synthesized by emulsion polymerization.

Although polymerization methods provide high yield with a low demand on synthesis equipment, modifications to nanoparticles are needed to improve the compatibility between nanoparticles and polymers. In turn, these modifications may reduce the fluorescence intensity of nanoparticles such as QDs. Gao *et al.*[168] found that several oxidative initiators such as benzoyl peroxide, potassium persulfate, and hydrogen peroxide caused fluorescence quenching of QDs during the polymerization process. The reactive QDs could adversely affect the nucleation and growth of the copolymerization process, leading to broad particle size distribution.[166] Additionally, lengthy and tedious purification steps are needed, providing further limitations.

When compared to the polymerization method, the emulsification/solvent evaporation process can encapsulate nanoparticles into polymeric microspheres without the need for chemical modifications to the nanoparticles. Moreover, the mild emulsification conditions are beneficial and provide protection to the nanoparticles. During the emulsification method, the polymers and nanoparticles are dissolved directly into the dispersed phase solvent.

Stirring action (*e.g.* homogenization) or ultrasonic dispersion then enables the formation of emulsion droplets in a continuous phase containing surfactants. Finally, the droplets solidify into microspheres *via* solvent evaporation and the nanoparticles are embedded into the resulting polymer matrix.[170–172] However, the broad distribution of the bead size also renders this method problematic for barcoding applications.

Self-assembly processes have been introduced into emulsification methods.[146,173,174] For instance, Ku *et al.*[146] developed multi-color emitting, hybrid block copolymer (BCP)-QD microspheres by locating differentially-colored QDs in different BCP micelles. The FRET effect among different QDs was completely suppressed due to the thick protective micellar corona. Gao *et al.*[173] reported a synthetic route for QD nanobarcodes based on the epitaxial assembly of nanoparticle amphiphilic polymer complexes in homogeneous solution. When polar solvent dimethylformamide (DMF) was added into QD and poly(maleic anhydride-octadecene) (PMAO) containing tetrahydrofuran (THF) solution, the QD-PMAO complexes epitaxially grew into highly fluorescent nanobeads with narrow size dispersity *via* multivalent hydrophobic interactions. Furthermore, the polymer chains in the nanobeads were cross-linked with small-molecule diamines, resulting in enhanced stability.

SERS microspheres and UCNP-embedded microspheres can also be synthesized using both the polymerization[175,176] and emulsification methods.[174,177] Fenniri *et al.*[175] synthesized SERS-active microspheres *via* suspension polymerization, whereby AgNPs that had been functionalized with polymerizable groups (*i.e.* the Raman labels) were used as cross-linking agents. Wang *et al.*[174] fabricated UCNP-encoded superparticles (SPs) *via* a convenient microemulsion, self-assembly technique. A colloidal cyclohexane solution containing one or more kinds of NaYF4:Yb^{3+}/Ln^{3+} nanocrystals was added to anionic surfactant SDS-(sodium dodecyl sulfate) containing aqueous solution, then the system was emulsified by vigorous stirring. After evaporation of cyclohexane, UCNPs had assembled to form highly-ordered, 3D SPs.

3.4. Microengineering emulsification and spray techniques

Nanoparticle embedded microspheres that have been prepared by either the polymerization[166] to traditional emulsification methods[174] are not uniform enough in size for use in a suspension array. To solve this problem, microengineering emulsification techniques,[178] including microfluidic technology[65,82,145,179–183] and membrane emulsification techniques,[30,66] have been introduced that can produce monodispersed droplets. The mechanisms underlying microfluidic and membrane emulsification are similar, both of which involve two steps: (i) the formation of emulsion droplets and (ii) the solidification of droplets (*via* solvent evaporation[30,65] or polymerization[181,183]). However, these two methods differ in the formation process of emulsion droplets. With microfluidic emulsification, the disperse phase containing polymers or monomers is broken into emulsion droplets by a continuous phase in the microfluidic channel (Fig. 13). Contrastingly, membrane emulsification employs a disperse phase that passes through a number of uniform pores of rigid membranes (*e.g.* Shirasu porous glass (SPG) membranes) under appropriate pressure. This then enters into the continuous phase to yield uniform emulsion droplets (Fig. 14).

Microfluidic techniques offer excellent control of emulsion droplets, thereby providing a powerful platform for continuous and reproducible production of polymer microspheres with precise control over their monodispersity, structure, and composition.[179] Thus, uniform nanoparticle-tagged microspheres with a controlled structure and composition can be produced by taking advantage of the controllable structures and independently tunable compositions of microfluidic emulsions (Fig. 13). Chan *et al.*[65] developed a set of concentration-controlled flow-focusing (CCFF) devices (Fig. 13(a)) based on microfluidic technology, resulting in the production of 4–20 μm uniform QD-encoded microspheres. The size of the encoded microspheres could be controlled by varying the polymer concentration and/or flow rates. Both increasing the focusing flow (the flow of the continuous phase, water) and decreasing the focused flow (the flow of the disperse phase, QDs/polymer-containing CH_3Cl_3 which is broken into droplets by the continuous focusing flow) led to smaller particles. By using the microfluidic device shown in Fig. 13(b), uniform microspheres (46.4 ± 1.0 μm) encoded with lanthanide nanophosphors were also produced.[82] Hydrophilic lanthanide nanoparticles and pre-polymer-containing water flow (disperse phase) were broken into uniform droplets by a continuously flowing oil stream at the T-junction of the device. The droplets were then polymerized into beads *via* UV light illumination.

Microfluidic devices have also been engineered to operate a double emulsification process, resulting in the production of multi-core microsphere barcodes.[181,184,185] Gu *et al.*[181] produced 50 μm QD-encoded microspheres with PEG shells by polymerizing O/W/O type emulsion using a capillary microfluidic device shown in Fig. 13(c). By using double-emulsion droplets with two inner droplets (QD- and magnetic nanoparticle-dispersed droplets) as templates, they fabricated 100 μm anisotropic magnetic barcode microspheres with either two separate cores or with a Janus core. Chen *et al.*[184] generated multicolor QD-encoded core–shell microspheres by using double emulsions using multiple cores as templates. By embedding different QDs into different cores, the FRET effect among different QDs could be effectively avoided. Furthermore, using the protection of hydrogel shells, the QD leakage was prevented, leading to a significant enhancement of barcode stability. Kim *et al.*[185] developed an encoding scheme by using core droplets with three distinct colors (red, green, and blue, (RGB)) and optically identifiable codes were generated by controlling the number of RGB core droplets encapsulated within the shell droplet. As shown in Fig. 13(d), by using a photocurable resin flow with silica nanoparticles (indicated as the middle flow), silica particle arrays were formed on the surfaces of both the core and shell of the barcodes. Moreover, microfluidic-assisted methods have also been widely used to prepare photonic crystal barcodes.[60,143] By using a capillary microfluidic device with multiple injecting channels (see Fig. 13(e)) and silica nanoparticles-dispersed ETPTA (ethoxylated trimethylolpropane triacrylate) solutions as the inner phase, Gu *et al.*[145] generated multiple-core opal colloidal photonic crystal barcodes.

Although microfluidic techniques provide the versatility necessary for precise control over the monodispersity, structure, and composition of barcodes, their productivity is limited and most resulting barcodes—especially those with complex structures—are too large for use in high-density, multiplexing applications. When compared to microfluidic techniques, the membrane emulsification technique results in higher productivity,[30] since many droplets can

be produced simultaneously. The most commonly used membranes for membrane emulsification are SPG[186,187] and microsieve membranes.[188] Membrane emulsification techniques have been widely used to produce uniform particles, with the mean particle size ranging from sub-micrometer to several hundred micrometers in diameter, with a typical CV of 10–20%.[178] Recently, SPG membrane emulsification was successfully used to prepare QD-encoded microspheres.[30,66] This method has the potential to provide approximately 1000-fold increased productivity over that of the CCFF technique, resulting in encoded microspheres that show good monodispersity (CV ≤10%). By using SPG membranes with different pore sizes, a barcode library combining color encoding and size encoding could be produced (Fig. 14 and Fig. 3(b)).

A spray technique[190] that is based on the atomization of uniform droplets has also been successfully introduced for the high yield production of uniform barcodes.[165,191,192] Previous work has shown that it is capable of producing uniform microspheres with sizes ranging from nano to micron.[190] Couzis *et al.*[165] produced 50 μm QD barcodes using a spraying-suspension polymerization method (see Fig. 15(a)). The QDs and pre-polymer containing solutions were ultrasonically atomized into droplets with resulting barcodes polymerized from the droplets showing good monodispersity. Yang *et al.*[191] generated highly monodisperse (CV <1%) photonic crystal microspheres *via* an electrospray device as shown in Fig. 15(b). Further, Sun *et al.*[192] produced QD barcodes with a mean size of approximately 1 μm by using an electrospray/solvent evaporation method.

3.5. Encapsulating nanoparticles by a sol–gel process

Silica materials obtained *via* the solution–gelation ("sol–gel") inorganic polymerization process[193] are of particular interest since they are resistant to degradation and can be easily modified with a wide range of functional groups.[194] The sol–gel method[194,195] is a widely used approach for encapsulating organic dyes or nanoparticles into silica microspheres or the silica shell of template microspheres (Fig. 16), with resulting microspheres showing good monodispersity. Insin *et al.*[194] encapsulated water-soluble QDs and iron oxide nanoparticles into silica shells to generate dual-functional silica microspheres. Zhang *et al.*[81] encapsulated hydrophilic UCNPs *via* a traditional sol–gel process and generated upconversion nano-barcodes (≤90 nm). Ma *et al.*[196] developed multicolor-encoded silica microspheres using a stepwise encapsulation of quantum dot/silica multilayers and a reverse microemulsion method. In this manner, hydrophobic QDs were used without the need for phase transfer, lending further protection to the QDs. Moreover, energy transfer processes between different QDs leads to a deviation of the designed signal ratios that can be suppressed by the pure silica layers. Wang *et al.*[197] produced multi-component barcode nanospheres that contain a magnetic nanoparticle (MNPs) core, with different emission QDs separated into spatially distinct silica layers (shells) and QD-free silica layers (insulation layers) using a stepwise sol–gel process.

Sol–gel methods are also versatile for producing dual-functional[198] or multi-functional particles, for tuning the optical properties of nanoparticles,[199] or for producing protective layers for SERS dots.[125,200] Moreover, the silica surface is amenable to later modification and bioconjugation.

4. Optical label and signal amplification

In order to apply the barcodes in a suspension array, an additional labeling step is usually required to monitor biomolecular binding events. Various types of optical labels have been used in suspension arrays, including organic dyes, QDs, and SERS dots (see Table 3).[30,65,126,151] However, some label-free patterns have also been developed.[202–204] Moreover, various patterns for signal amplification have been developed to increase overall sensitivity.[205–209]

Usually, labels are used to generate a quantitative signal for binding events, with label elements capable of acting as bar-codes for the recognition of different binding events (*e.g.* SERS label). When combined with special structures such as dendrimer-like DNA[210] and/or nanostring,[211] organic dyes can produce a number of encoded labels by varying the color and amount of the organic dyes. This scheme can be expanded to other types of labels, including QDs and SERS dots, as well as other structures such as polymer beads.

4.1. Label-based suspension arrays

Using a suitable label leads to high sensitivity. In order to obtain a high signal-to-noise ratio, labels can be chosen according to the following principles:

1. Minimization of the background signal (*e.g.* a less background signal produced when NIR-exciting rather than UV-exciting dyes are used; using labels with relatively long lifetimes, using time-resolved measurements to temporally discriminate the background signal from the label signal[97]).
2. Avoiding interference between barcodes and labels (*e.g.* minimizing spectral overlap and FRET effects between labels and barcodes).
3. Maximization of label brightness: (*e.g.* QDs have higher molar absorption coefficients and quantum yields than organic dyes, making them brighter labels).

Traditional labels such as organic dyes[65,157,212,213] (*e.g.* FITC, Alexa488, Alexa647, Cy5) and fluorescent proteins[30] (*e.g.* R-phycoerythrin) are still the most widely-used labels in suspension array technology. When compared to FITC, R-phycoerythrin[214] and Alexa488[215] are brighter dyes due to their high extinction coefficients and quantum yields. R-phycoerythrin has a large Stokes shift, which can make it easier to separate its signal from background.[214] Cy5 is one of the most popular organic dye labels and gives a high signal-to-noise ratio due to its low background signals with long wavelength excitation.[216]

Inorganic nanoparticles[217,218] (*e.g.* QDs, UCNPs) and nanostructures[219] (*e.g.* SERS dots, nanoparticle-containing organic dyes) are more stable and carry higher density optical signals. As such, they have also been widely used as labels in planar microarrays[111,220,221] and suspension arrays.[126,151] When compared to traditional organic dyes, QDs exhibit brighter fluorescence due to their much higher extinction coefficients, which are beneficial for highly sensitive biosensing.[57,221] The increased brightness of QDs also minimizes the working concentration of QD conjugations (labels), thus reducing the type of non-specific binding that can occur using highly concentrated QD conjugations.[22] Moreover, the large

Stokes shifts of QDs provide a way to easily separate the QD fluorescence from background autofluorescence, even if excited by UV light.[222]

SERS dots have also been used as barcode labels in suspension arrays (*e.g.* Nanoplex™ biotag), which enable an ultrasensitive, fast, no-washing, homogenous reaction and multiplexed analysis of biomolecules. Moreover, higher sensitivity can be achieved by taking advantage of the nanogap areas of noble metal colloidal aggregations[132] or core–shell SERS nanoparticles.[134] As discussed in Section 2, UCNPs can provide high sensitivity, but they have not yet been used as labels for suspension arrays due to their multi-color emission properties. Fortunately, UCNPs with a single-band emission have been developed.[83–88]

Currently, there are several unaddressed concerns regarding the use of nanoparticles in biosensing.[57,221,223] First, nanoparticles should be modified with an amount of ligand that not only introduces suitable functional groups for conjugation with biomolecules, but also maintains long-term colloidal stability and the stability of the nanoparticles' optical properties.[224] For a more detailed discussion regarding the surface modification of inorganic nanoparticles, please refer a recent review by Sperling and Parak.[225]

Second, nanoparticle conjugation techniques have not yet been perfected.[226] Pathak *et al.*[227] studied two models for antibody labeling with QDs: (1) direct coupling of functionalized QDs with monoclonal antibodies *via* standard bio-conjugation techniques, and (2) indirect coupling *via* the biotin–streptavidin binding of streptavidin-coated QDs with biotinylated antibodies. Their results demonstrated that there were very few antibodies available for target binding in the direct coupling approach. This was due to the orientation of the recognition sites (Fab region) of most antibodies, which were located close to the QD surface, ultimately resulting in inadequate target binding (Fig. 17). Comparatively, biotin–streptavidin conjugations increased the space between the QD and antibody, thus offering more structural opportunities for light chain fragments (Fab region) to bind to their targets. When used in immunoassays (including suspension arrays), the biotinylated antibodies were shown to bind with the target protein first, after which they were captured by the QDs-streptavidin (labels) through the specific biotin–streptavidin conjugation. This sequence of events thus eliminated all of the worst possible orientations.

Finally, to overcome the shortcomings of the traditional random orientation binding methods, directional-oriented conjugation techniques[226] have been developed. Directional orientation immobilization of mAbs occurs when the Fab region (the recognition site) is oriented away from the support surface to preserve the full functionality of the antibody. Kumar *et al.*[228] developed a directional-oriented conjugation protocol by attaching a heterofunctional linker to the nontargeting portion (Fc region) of a glycosylated antibody, thereby leaving the antigen-binding portion (Fab region) unhindered (Fig. 17(c)).

4.2. Label-free suspension arrays

Label-based detection strategies have several limitations, such as the limited number of matched-pair antibodies,[230] alterations of surface characteristics of the reporter molecules, and time and effort required for the labeling procedure, to name a few. Label-free techniques that monitor inherent property changes of reaction carriers induced by target binding events

could be used to avoid these problems. To this end, a number of label-free planar arrays[231] have been developed, including microarrays based on surface plasmon resonance (SPR),[232] carbon nanotubes (CNTs),[233] and nanowires.[234] In recent years, a few label-free suspension array methods[15,203,204] and some bead-based label-free patterns which can also be expanded for multiplexing[235–238] have been developed (see Table 4).

Gu *et al.*[15,202] developed an inverse photonic crystal-based label-free platform, in which the target quantity can be detected by monitoring the reflection-peak shift of photonic crystal microbeads (Fig. 18). Although this platform is promising, the sensitivity is low (1 nM for DNA), and needs further improvement.

Jun *et al.*[203] reported a label-free method based on a molecular beacon (MB) approach. They introduced an RNA aptamer-based molecular beacon that can undergo spontaneous conformational changes upon hybridization between proteins and aptamers. Such spontaneous conformational changes lead to blocking of the FRET effect between fluorophores and quenchers, thus "turning on" the fluorescent light of the MB. However, only a few RNA aptamers have been reported for protein targeting, thus limiting the number of applicable target proteins that can be detected by this method.

Label-free patterns using conjugated polymers (CPs) as signal transducers have also been developed.[204,235,236] As novel optoelectronic materials, CPs have been widely used in biosensing, bioimaging, therapy,[239–243] and barcoding[244] due to their high fluorescence quantum yields and large extinction coefficients. Jun *et al.*[204] coated a polydiacetylene (PDA, a water-soluble fluorescent conjugated polymer[241]) layer onto optically-encoded microspheres, with the PDA layer exhibiting a blue to red color change induced by external stress. However, color change of the PDA can be induced not only by antibody-antigen binding but also by other stressors, including pH and temperature, thus limiting their practical application for high-throughput, multiplexing of targets. Moreover, the blue to red color change of PDA occupies a broad spectral range, thereby compressing the total encoding space.

Further work reported by Liu *et al.* showed the feasibility of label-free, bead-based biomolecular detection based on conjugated polymer staining.[235,236] As shown in Fig. 19(a),[235] lysozymal selective aptamer-coated silica nanoparticles were used as carriers and binding events resulted in an alternation of the surface charge from negative to partially positive. A highly fluorescent, anionic poly (fluorene-*alt*-vinylene) ($PFVSO_3$) was then stained onto protein–aptamer-NP complexes *via* electrostatic interactions, which transferred the binding events into fluorescent signals. However, this convenient, label-free bead based assay gave a low limit of detection (~0.36 μg mL^{-1} for lysozymes). This CP staining-based label-free scheme can be expanded for multiplexing by using proper barcodes like QD barcodes instead of silica nanoparticles. To obtain high multiplexing capacity, a large portion of the visible light region should be reserved for QD barcodes. Thus water-soluble anionic CPs with a narrow band or near-infrared band emission spectrum would be preferred.

Moreover, CPs also show efficient energy-transfer properties and excitations can be efficiently transferred to lower electron/energy acceptor sites over long distances, leading to

fluorescence superquenching of CPs or signal amplification of acceptors.[245] Liu *et al.*[236] developed a label-free, single-nucleotide polymorphism (SNP) detection platform by utilizing the FRET effect of CPs. As shown in Fig. 19(b), after the sequence-specific hybridization between the DNA probes on the silica nanoparticles to the targets of interest, DNA molecules were successively treated with ethidium bromide (EB) and a cationic tetrahedralfluorene. The target recognition events were then transferred into enhanced sensitized EB emission *via* FRET. Due to the selective response of tetrahedralfluorene to intercalated EB, the complementary DNA targets were differentiated from those with a single base mismatch. Moreover, this FRET-based SNP DNA detection platform is capable of conducting multiplexed detection if proper barcodes, rather than silica nanoparticles, are used. However, fluorescent or SERS barcodes are not suitable for this multiplexed detection scheme due to their severely restricted excitation and emission bands. Similarly, Boudreau *et al.*[237] developed a label-free, DNA sensing strategy combining the molecular recognition capabilities of a cationic conjugated polymer (CCP) transducer with highly fluorescent, core–shell nanoparticles (NPs with an Ag core and a fluorescent silica shell) (Fig. 19(c)). The binding events were monitored *via* enhanced FRET effects between the CCP transducer (donor) and fluorophores (acceptor), which had been doped in the silica shell of the Ag nanoparticles. The presence of the metal core has been shown to efficiently enhance dye emission,[246,247] thereby reducing the lifetime[248] of the excited states and resulting in enhanced sensitivity and photostability. Moreover, the plasmonic enhancement can be beneficial for the FRET efficiency, range, and transfer rate.[249,250]

Recently, an enzyme-assisted target recycling scheme[251,252] has been used in ultra-sensitive, label-free biomolecules detection. Importantly, for this method, the cyclical utilization of the target acts as a signal amplification mechanism,[253] which can dramatically increase detection sensitivity and is comparable to that of polymerase chain reaction (PCR) amplification. Lu *et al.*[238] developed exonuclease III-aided target recycling amplified bead-based DNA detection (Fig. 20). When compared to conventional, direct hybridization, bead-based assays, sensitivity was greatly enhanced by a factor greater than 56.8. This route has clear transferability to suspension arrays that have high multiplexing capacity and ultra-sensitivity by encoding the magnetic beads used. Moreover, an enzyme-assisted, target recycling scheme can also be extended to rapid, label-free, and multiplexed detection of various nucleic acids and proteins by using different kinds of fluorescent nucleotide analogues and specific aptamers as probes.[252]

4.3. Signal amplification

Various methods have been used to obtain higher detection sensitivity, including signal amplification and target amplification (pre-concentrating targets) (see Table 5).

Analytes of interest in serum or plasma can be pre-concentrated by specific solid phase extraction, but this is not suitable for high-throughput multiplexing. Methods for pre-concentrating all serum proteins have also been developed, such as the freeze–thaw technique.[254] Although analytes can be pre-concentrated by the freeze–thaw method, the concentrations of interferents will also become higher, thus increasing background signals. PCR amplification—a classical method used for ultrasensitive detection of nucleic acids—

has also been used for the pre-amplification step in suspension arrays.[255] Chan *et al.*[256] used an isothermal amplification technology, termed recombinase polymerase amplification (RPA),[257] in QD barcode-based multiplexed detection. When compared to PCR technology, RPA offers a portable, low-cost method for nucleic acid analysis, which is ideally suited for point-of-care use. As mentioned above, the enzyme-assisted target recycling scheme almost always increases target concentration (Fig. 20).[238]

Signal amplification in suspension arrays can also be achieved through amplification of labels (creating more labels) and signal enhancement. Lowe *et al.*[205] developed a signal amplification approach by introducing biotinylated dendrimers in order to provide increased binding sites for streptavidin–phycoerythrin (SA–PE) molecular labels (Fig. 21(a)). Similar amplification approaches have been used in immunoassays that are based on various structures, including branched DNA,[258] fluorescent vesicles,[259] polymer chains[260] and dye-doped nanoparticles.[261] This approach has also been used in suspension arrays, with further expansion possible.[258,260]

Another scheme to increase label amount is based on step-by-step label amplification.[262] Xiang *et al.*[206] achieved a layer-by-layer assembly of CdS QDs through the use of a biotin–avidin interaction, resulting in a 17-fold signal enhancement (Fig. 21(b)). Ren *et al.*[263] reported the use of a linear hybridization chain reaction (HCR)-based layer-by-layer signal amplification to detect DNA. The detection limit was about three orders of magnitude lower than that performed without HCR amplification (Fig. 21(c)). There have also been additional reports on other cascade label amplification strategies for immunoassays, such as rolling circle amplification (RCA),[264,265] loop-mediated isothermal amplification (LAMP),[266] and nonlinear HCR,[267] which are all extendable for use in suspension arrays (see Table 6 for a brief summary of these isothermal nucleic acid amplification technologies).

Enzymatic amplification methods can also be used to increase the generated signal as well as improve detection sensitivity. Commercially available catalyzed reporter deposition (CARD)[268] has been widely used for *in situ* hybridization and microarray analysis.[269,270] Tyramide signal amplification (TSA) is a CARD technique that converts tyramide derivatives to highly reactive intermediates using peroxidase, leading to enrichment of the tyramide substrate on the surface of the enzyme (Fig. 22). When fluorescent tyramide derivatives are used as labels, localized enhancement of fluorescent signals will occur.[271] George *et al.*[209] assessed the potential to improve sensitivity of CARD for the Luminex100 platform. Their results showed that (i) TSA was better than dye-labeled antibodies for signal amplification and (ii) that it improved the detection limit up to 100-fold over Cy3-labeled antibodies. Recently, Liu *et al.*[272] developed a label amplification strategy based on the integration of TSA and polymerization-assisted signal amplification.[273] As shown in Fig. 22, in the TSA system, HRP can catalyze the deposition of QD–tyramide conjugates on the enzymatic site, resulting in localized, high-density labeling. Meanwhile the increased loading of HRP *via* ATRP further increases the accumulation of the QD signal, thus providing a near 10-fold improvement in sensitivity. Importantly, this strategy is extensible to suspension arrays, as indicated by previous TSA[209] and polymerization-assisted signal amplification[205] work.

Moreover, conjugated polymer-based FRET[236] and nanoplasmonic-assisted fluorescence enhancement[237] has also been developed for signal enhancement. Liu *et al.*[207] used a cationic conjugated polymer (CCP) poly(fluorenyldivinylene-alt1,4-phenylene) (PFVP) as either a signal amplifier (FRET pattern) or a signal reporter (label-free pattern) in a bead-based array for DNA detection (Fig. 23) with SNP selectivity. The presence of CCP provided a 110-fold increase in amplification, the FRET pattern yielded a detection limit of 10^{-17} M, and the label-free pattern yielded a detection limit of 5×10^{-13} M. In a separate study,[274] they added CCP as an energy donor to the protein immunoassay sandwich structure, thus resulting in a six-fold higher increase in detection sensitivity.

Nanoplasmonic-assisted fluorescence enhancement based on metal nanostructures[275] is another promising pattern for use in signal amplification in suspension arrays. Goldys *et al.*[208] demonstrated that silver nanostructures deposited on a silica bead surface can be used to enhance the signal of fluorophores for bead-based immunoassay. Specifically, the silver deposited silica beads enhanced the emission intensity of an Alexa 430 fluorophore by factors of 8.5 and 10.1 for 400 nm and 5 μm beads, respectively. Furthermore, Chan *et al.*[276] synthesized metal nanoshell-coated QD barcodes using a seed-mediated strategy (Fig. 24), which exhibited enhanced stability and two orders of magnitude improvement in analytical sensitivity when compared to QD barcodes that lacked the metal coating. They also developed nanobarcodes composed of gold nanoparticle cores and quantum dot-encoded shells *via* layer-by-layer polyelectrolyte deposition,[277] which showed enhanced fluorescence and suppressed blinking. Suppression of blinking from plasmon interaction[278] is of great importance for single-molecule level detection, as blinking of labels may lead to false-negative signals.

5. Taking advantage of fluorescence resonance energy transfer (FRET)

The fluorescence resonance energy transfer (FRET) effect[279] is a non-radiative energy transfer process which requires good overlap between donor emission and acceptor absorption bands. It is strongly dependent on the distance between donor and acceptor molecules. The FRET effect usually acts as a negative factor for suspension arrays, as FRET among QDs in QD barcodes limits their encoding capacity.[21] Similarly, FRET amongst fluorescence intensities of barcodes and labels always leads to complicated and tedious color compensations. However, the FRET effect can also be a positive factor in bioimaging and biodetection, including use in suspension arrays.

5.1. FRET-based encoding

One of the shortcomings in using organic dyes to produce barcodes is their narrow absorption band. This requires the use of multiple excitation lasers when several organic dyes are used. Recently, Wagh *et al.*[280] proposed a sequential and multiple FRET cascade mechanism to overcome this issue (Fig. 25). They produced polymer nanoparticles encapsulated with combinations of four lipophilic carbocyanine-based fluorophores: 3,3′-dioctadecyloxacarbocyanine (DiO), 1,1′-dioctadecyl-3,3,3′,3′-tetramethylindocarbocyaine (Dil), 1,1′-dioctadecyl-3,3,3′,3′-tetramethylindodicarbocyanine (DiD), and 1,1′-dioctadecyl-3,3,3′,3′-tetramethylindotricarbocyanine (DiR). This approach resulted in the

production of more than 30 barcodes. The sequential and multiple FRET cascade mechanism was based on overlaps between absorptions of DiO, Dil, DiD, and emissions of Dil, DiD, DiR, thus multicolor emission spectra of these nanoparticles could be excited with a single excitation at 485 nm.

FRET can also be utilized to tune the emission of upconversion nanoparticles[79] and lifetime of downconversion lanthanide complexes,[100] which have both been used to fabricate barcodes. The peak positions of multicolor emission UCNPs are determined by the doping lanthanide ions, thus the spectrum are underused which limits the encoding capacity of UCNPs. UCNP-dye complexes based on FRET can overcome this disadvantage.[76] By incorporating QDs or FITC into a silica shell, $NaYF_4$:Yb,Tm@FITC-silica and $NaYF_4$:Yb,Tm@QD-silica nanoparticles have been produced, which adds another emission to $NaYF_4$:Yb,Tm nanoparticles. By using UCNP@dye-silica nanoparticles, more 980 nm exciting barcodes can be obtained than what can be produced by using UCNPs alone.

5.2. FRET-based ultrasensitive detection

The FRET effect has been widely used in biosensing because it leads to enhancement of detection sensitivity. First, FRET is very sensitive to the distance between the donor and acceptor (or quencher), which can be used to realize single molecule detection.[281,282] Second, the FRET effect always results in a larger Stokes shift when a fluorescent donor is used, which can then be used to separate the label signal from background autofluorescence. Finally, FRET is very attractive for bioanalysis since it is simple to build ratiometric systems.[283–285] Notably, the ratiometric systems which use the ratio of the two fluorescence intensities to quantitatively analyze the targets can eliminate most detection disturbances by self-calibration of the two emission bands.[286,287] External factors, such as excitation source fluctuations and, in homogenous systems, sensor concentration, have no effect on ratiometric systems. Several FRET-based suspension assays have already been reported[203,288–291] and as discussed in Section 4, label-free suspension arrays[203] and signal amplification strategies[207] based on FRET have also been developed.

Sukhanova *et al.*[288] developed a FRET-based detection platform for autoantibodies between labels (AlexaFluor633) and QDs located in the pre-surface layer of the QD barcodes (Fig. 26). Since there is sufficient spectral overlap between QD emission and the absorption of the dye, excitation energy can efficiently transfer from QDs to the neighboring dye labels on secondary antibodies, thus confirming the binding effect. When a QD-selective excitation lamp is focused on a single bead, the QDs from the pre-surface layer of the microbeads can be highly effective FRET donors and can excite those specifically-bound AlexaFluor633-labeled secondary antibodies. In this way, both the QDs and label dye emissions can be detected, but free labels near the microbeads will not be excited. However, if a laser fit for Alexa633 is used, any nearby free labels are also excited. Therefore, the FRET detection scheme that operates under a QD-selective excitation lamp could be more specific and sensitive than the latter, which uses a laser fit for labels.

6. Magnetic nanoparticle-based suspension arrays

Magnetic microbeads composed of superparamagnetic nanoparticles have gained much attention in the bioanalytic field, including the use of suspension arrays.[292] Immunomagnetic separation-based suspension arrays have some advantages over nonmagnetic suspension arrays, such as facilitating assay automation and improving both detection sensitivity and specificity.

In recent years, magnetic separation-based, optically encoded suspension arrays have been developed. They have been based on one of the two approaches: (1) using magnetic nanoparticles or magnetic microbeads in mutiplexing detection as carriers for the separation and encoding of labels, respectively (*e.g.* the Nanoplex™ biotag technology[127]); (2) combining magnetic properties and optical barcodes in carriers to create magnetic optical barcodes (*e.g.* MicroPlex® Microspheres from Luminex corporation[292]). Of the two, the latter is the more commonly used.

In the first approach, encoded labels provide simultaneous signals for different binding events and quantitative target analysis. This results in a limited number of barcodes, since intensity levels cannot be fully used for encoding. The second approach is based on magnetic-optical bifunctional particles (*e.g.* luminescent magnetic particles[293]). The most common strategy for developing magnetic-optical bifunctional particles is by the incorporation of superparamagnetic nanoparticles together with encoding elements (such as QDs and organic dyes) into polymer microspheres.[13,66,294] The Luminex corporation[25] developed a MagPlex® Microspheres platform by incorporating iron oxide nanoparticles and organic dyes into polystyrene microbeads. As previously discussed, Nie *et al.*[13] embedded magnetic nanoparticles and QDs into mesoporous silica beads by using the swelling method. However, it was found that iron oxide nanocrystals decreased QD fluorescence intensities by absorbing excitation light and QD fluorescence emissions.[13] NIR-emitting QDs and Fe_3O_4 nanoparticles were capsulated into PSMA microspheres[66] resulting in a similar decrease in fluorescence intensity, but to a lesser extent than visible light-emitting QDs due to the minimal NIR absorption of magnetic nanoparticles. Jun *et al.*[125] coated SERS dots onto magnetic microspheres to produce magnetic SERS barcodes. Nanoparticles that simultaneously provide superparamagnetism and SERS substrates have also been developed (*e.g.*, Au–Fe nanoalloys,[295] Fe_3O_4@Ag nanoparticles[296]).

Nonspecific adsorption effect (or so-called cross-reactivity)[297] is a major challenge for multiplexing biodetection, especially for antibody-based protein detection. Cross-reactivity among immobilized captured ligands, detection antibodies, and nonspecific analytes limits the number of proteins capable of being subjected to multiplexing. Moreover, nonspecific binding may produce a high background signal, resulting in decreased assay sensitivity. Theoretically, cross-reactivity between proteins is more likely to happen in suspension assays due to the high, specific surface area of the microbeads, subsequently limiting its multiplexing ability.[20] However, immunomagnetic separation can partially decrease nonspecific absorption,[298] which is a step towards improving detection sensitivity.

Manual operation is a negative factor for detection robustness, reproducibility, and reliability,[297] thus there is a trend to develop automatic immune detection systems.[299,300] In recent years, microfluidic-based sample-in/answer-out systems[301,302] have attracted much attention, including bead-based microfluidic immunoassays or arrays.[303,304] The key for operating a bead-based suspension array on an automated system is how to more easily manipulate and transport the microspheres.[305] Immunomagnetic microspheres make it more convenient for assay automation,[306] and many magnetic bead-based automated immunoassay platforms have been reported.[299,307–310] Sasso *et al.*[299] developed a microfluidic platform and demonstrated that it could fully automate a three-stage, multiplexed magnetic bead-based immunoassay, with the Luminex xMAP system chosen as a typical case.

Mechanistically, the microfluidic immunoassay system utilizes a magnetic separation scheme, whereby magnetic microbeads are pulled from one reagent stream to the next under application of an external magnetic field (Fig. 27(a)). After magnetic separation, the bead carrier solution flows into a waste outlet, while the beads flow into a spiral-like incubation chamber. The device uses three layers in combination with a single magnet to automatically operate the three-stage assay (Fig. 27(b)): one layer for the antigen capture incubation, one for secondary antibody incubation and the other for labeling streptavidin-PE. Moreover, the sensitivity of the suspension array operated on-chip is comparable with the off-chip assay (Fig. 27(c)). Chan *et al.*[311] designed an automated microfluidic biochip for operating multiple steps in a magnetic QD barcode assay (Fig. 28(a)) and the barcodes were detected by a diagnostic system as illustrated in Fig. 28(b).[312] As shown in Fig. 28(a), the barcodes were magnetically controlled in the microfluidic chip and the key to this control is the identification of optimal magnet(s) position(s). Furthermore, the integrated automated detection system (Fig. 28(b)) has been shown to be more sensitive than currently available, FDA-approved methods in a proof of concept infectious disease detection assay.[312] This automated system is close to the initially discussed “sample-in/answer-out” system and—with future development—shows promise as an eventual handheld point-of-care diagnostic system.

7. Challenges and possible solutions

In recent years, researchers have invested enormous energy to improve the performance of microsphere-based suspension array technology, including multiplexing capacity (or array density), sensitivity, robustness, portability,[313] and assay throughput. However, there are still several foreseeable challenges. Here, we focus on the following important issues: improving encoding capacity, developing better probes, nonspecific biofouling suppression, directional immobilization, and “point-of-care” diagnosis.

7.1. Improving encoding capacity

The most popular encoding scheme involves wavelengths and intensities. Two approaches have been evaluated to increase their collective encoding capacity and are in accordance with the formula: $C = N^m - 1$. The first approach is to use the narrow emission bands of dyes such as QDs[12] and Raman dyes,[127] leading to the fabrication of thousands of barcodes.

Raman scattering bands have smaller FWHM values than those of QDs, theoretically resulting in a higher number of total codes. However, the presence of multiple Raman bands and relatively weak signals has seriously limited the possible number of codes.[24] Another approach is to increase the number of intensity levels used for encoding, which subsequently depends on the decoding precision of the instruments used as well as the dye loading accuracy.[24]

To boost the loading accuracy of nanoparticles, the monodispersity of nanoparticle-tagged microspheres and the distribution of nanoparticles inside microspheres will need to be improved. This relies heavily on the further development of manufacturing techniques. Microengineering emulsification techniques such as CCFF techniques[65] and the membrane emulsification solvent evaporation (MESE) method[30] can provide one-step synthesis of uniform (both in size and distribution of nanoparticles) barcodes. However, the CV value of the barcode signal is usually up to 10%, so further improvement in the size monodispersity is needed. Swelling methods can also be used to synthesize barcodes with excellent size monodispersity, but the stabilities of the resulting barcodes remain relatively poor.[61] Since the overlap between different intensities of nanoparticles (especially QDs) is the main practical limitation, controlling the locations of different-colored nanoparticles inside microspheres[146,184,196] seems to be a probable solution. Barcodes with spatially isolated nanoparticles[184] can be fabricated through microfluidic techniques, but the large size of the barcode would prove problematic. Self-assembled BCPs[146] can yield various nanostructures when the volume fraction and molecular weight of the blocks are controlled, while needing an improvement in the size monodispersity of the barcode. Stepwise encapsulation of nanoparticles into multilayers is a lengthy process with cumbersome steps.[196] Similarly, in order to obtain highly uniform SERS barcodes, the loading accuracy of Raman dyes and the distribution of dyes will need to be improved. Importantly, noble metal substrates should provide highly uniform loading sites for Raman dyes.[134]

Combining spectrometric encoding with other encoding schemes can dramatically increase the achievable amount of barcodes. Some promising encoding schemes have been proposed, including combining with physical encoding,[30,48,314] lifetime encoding[17,94] and graphical encoding.[33,315,316] As proposed by Lu *et al.*,[17] more than 10 000 distinguishable codes can be generated using a combination of color, intensity, and lifetime. However, the operations for lifetime tuning can result in changes to colors or intensities of lanthanide complexes and UCNPs. Furthermore, decoding barcodes with mixed lifetime components is still relatively inaccurate.[17] Therefore, it remains a challenge to encode UCNPs using a combination of color, intensity, and lifetime.

A combination of graphical encoding and spectrometric encoding can produce significantly more barcodes, but it requires knowledge of the location of the encoding elements on the supports as well as their spectra.[19,315,316] This would result in a dramatically reduced barcode reading speed. Since physical characteristics (including size and refractive index) can be conveniently decoded by modern flow cytometers, they can be used as an additional encoding element with good compatability.[30,314] To this end, Trau *et al.*[314] prepared microspheres encoded with up to six fluorescent dyes located in separate shells alternating with nonfluorescent shells around a silica core. The resulting microspheres displayed a

diverse range of optical signatures combined with fluorescence wavelength as well as intensity with size and refractive index.

7.2. Alternative probes for selective recognition

Solutions are needed to address the limitations presented by the use of antibodies, such as cross-reactivity (nonspecificity)[297] and the limited number of matched antibody pairs available.[230] Recently, these have included label-free systems, plastic antibody based on molecule imprinted technology (MIT),[317] semisynthetic DNA–protein conjugates,[318] and alternative capture ligands. A few label-free suspension arrays have been proposed, but currently have problems with both sensitivity[15,202] and multiplexing capacity.[203] Artificial receptors prepared *via* MIT by using target molecules as templates have garnered extensive attention because of their desired selectivity, high physical robustness, and thermal stability, as well as their low cost and ease of preparation.[317] Although this technique has been shown to be particularly effective for small molecules, expanding the technology for selective recognition of biotemplates such as proteins, DNA, viruses, and bacteria will be challenging.[319]

Conjugation with artificial nucleic acids allows proteins to be modified with a synthetically accessible, robust tag.[318,320,321] This DNA-directed immobilization (DDI) method allows for DNA-conjugated proteins to be immobilized onto either microcarriers or nano-labels with conformational freedom and lack of denaturation. Moreover, utilizing DNA allows for easier signal amplification by means of HCR (hybridization chain reaction), RCA (rolling circle amplification),[322] or LAMP (loop-mediated isothermal amplification). Alternative ligands such as engineered protein scaffolds and nucleic acid scaffolds have also been evaluated.[323,324] For example, aptamers, which are highly specific nucleic acid molecules, possess target recognition features similar to antibodies and can also distinguish different protein isoforms and conformations.[325]

As for nucleic acid detection, nucleic acid analogues such as peptide nucleic acids (PNA)[326] and locked nucleic acids (LNA)[327] can overcome the specific limitations presented by natural nucleic acids. As such, they have attracted much attention for the development of high-performance affinity biosensors. For instance, LNA-modified oligonucleotides with enhanced hybridization affinity for complementary DNA and RNA have been successfully applied in the suspension array of the FlexmiR™ system for microRNA detection.[328] Incorporating LNA into the array to capture probes greatly increased their affinity for miRNA targets, thus increasing the overall selectivity of the array. PNAs, which are DNA analogues containing neutral amide backbone linkages, possess stronger affinity for their complementary DNA or RNA molecules due to the lack of electrostatic repulsion between the uncharged PNA backbone and that of the natural nucleic acid. Moreover, a single mismatch between the PNA and its target leads to a 10–20 °C decrease in melting temperature,[329] thus PNA probes can provide high SNP selectivity. To this end, Darrell *et al.*[330] have shown that PNA probe-conjugated microbeads have much higher sensitivity than DNA probe-conjugated microbeads in a bead-based assay.

7.3. Nonspecific biofouling suppression and oriented immobilization

Although suppressing the nonspecific biofouling and oriented immobilization of biomolecules for both label parts and carrier parts are important for improving specific biorecognition,[331] they have been underdeveloped for suspension arrays. With the exception of better ligand development, particular efforts have focused on preventing nonspecific binding at the surface modifications of either microcarriers or nano-labels. Bovine serum albumin (BSA) has been widely used as a blocking agent in suspension arrays.[30] Nonspecific biofouling can be robustly suppressed after BSA treatment, but it is often insufficient. Moreover, BSA may have been contaminated by undesired particulates such as bacteria and/or viruses. Therefore, various synthetic, water-soluble polymers ("polymer brushes") have been investigated as blocking agents, especially the popular poly(ethylene glycol) (PEG).[332,333] Dense PEG-chain-tethered surfaces with proper structures can not only prevent nonspecific adsorption,[334,335] but also improve immune response and the orientation of capture probes (*e.g.* DNA and antibody).[336,337] However, PEG may degrade after long-term storage and functionalized PEG derivatives are also expensive.

Recently, viral-based hybrid materials have been used to build highly selective and sensitive biosensors.[338] It has been demonstrated that nonspecific binding can be extensively suppressed through the formation of virus-like, biocompatible, and hydrophilic self-assembled monolayers (SAMs)[339,340] on the surfaces of microspheres. Jeon *et al.*[339] produced Au-layered magnetic microspheres with biomimetic architectures (viral filamentous morphology SAMs) on their surfaces to decrease nonspecific binding. Extremely low non-specific adsorption and increased sensitivity were obtained when compared to bare polymer beads. Moreover, captured antibodies also showed well-oriented binding to the nanoparticle containing the virus-like monolayer.[341] Well-oriented immobilization of captured probes on substrates is expected to have high reactivity, theoretical binding capacity,[342] and low nonspecific absorption. The widely used nondirectional immobilization methods result in random orientations of captured antibodies, thus the fraction of active antibodies drops well below 4%.[343] Given this, developing mild chemical procedures for the directional immobilization of captured probes (especially protein probes) has attracted much attention. To this end, substantial progress has been made in planar microarray technology[344–348] which is extensible for bead-based assays.

7.4. Optifluidics and "point of care"

There is a strong demand for developing "point-of-care" (POC) diagnostic platforms, which are cheap and can be operated by untrained personnel. Such POC platforms have been strongly promoted by microfluidic techniques.[349] In the past few decades, the microfluidic technique has strongly driven the exploitation of miniaturized analytical devices ("lab-on-a-chip" (LOC) or the "micro total analysis system" (μTAS)[350]), catalyzing an efficiency revolution in bioanalytics.[351] Combining microfluidic technologies with bioanalysis, including monoplex assays (*e.g.* qPCR[352,353]) and multiplexing assays (*e.g.* microarray[354] and suspension array[311,312,355]), is expected to yield much higher throughput and faster automated biosystems. To exploit accurate, fast, miniaturized, and cheap innovative suspension array systems for POC diagnosis, past studies have focused on three aspects: (1) operation of bead-based assays in automated microfluidic systems; (2) development of

miniaturized decoding devices; (3) integration of assay operation modules and decoding modules. The key areas for the development of automated suspension arrays are the propulsion of microfluidics and the manipulation of microspheres (particle trapping and sorting).[355] Compared to expensive, conventional decoding instruments (*e.g.* flow cytometers and high resolution imaging systems), integrating detection instruments "on-chip" for micro bioanalysis has the potential to dramatically improve cost-efficiency.

Although developing miniaturized decoding devices for optical barcodes is still in its infancy, there have been some promising examples recently reported. For instance, Ozcan *et al.*[356–358] developed mobile phone with imaging, sensing, diagnostics, and measurement functions by embedding high-end components within the device. Gu *et al.*[359] reported a strategy of automated image decoding with a photonic crystal bead (PCB) array in the microfluidic chip for multiplex assays. Tassaneewan *et al.*[360] designed a smartphone accessory ("dongle") for cost-effective POC diagnostic of infectious diseases. With this method, results can be obtained quickly (within 15 min) and conveniently using a single finger prick. The dongle then performs a triplex test based on silver deposition on gold nanoparticle seeds bound to the secondary antibodies. The final diagnostic results are comparable to those generated by the gold standard of laboratory-based ELISA testing. Chan *et al.*[256] designed a simple and low-cost chip-based wireless multiplex diagnostic device by combining quantum dot barcode technology with smartphones and RPA. Both the isothermal amplification of samples as well as the immunoassay on QD barcodes could be run on-chip. The results of the multiplex, on-chip assays could then be obtained by the smartphone reader. This device was shown to be capable of detecting multiple targets with high speed (in less than 1 hour) and high sensitivity (1000 viral genetic copies per milliliter). Meanwhile, the micro-flow cytometer or the lab-on-a-chip FACS system (μFACS) has also attracted much attention.[361–363] However, integrating these decoding modules together with microfluidic chips into optofluidic systems is challenging due to the need to consider both cost and flexibility. Still, we believe that the miniaturization of biomedical instruments and microfluidics-based, automated biochips may bring us closer to high-throughput multiplexing "sample-in/answer-out" POC diagnostic platforms. For more detailed information about the development of optofluidics, please refer to these recently published reviews.[364–366]

8. Concluding remarks

In this review article, we have provided a comprehensive view of the current development of suspension arrays based on spectrometric nanoparticle-encoded microspheres. Thanks to the rapid development of nanotechnology, tremendous progress has been made in recent years. Given scientific and financial factors, further development of nanoparticle-encoded microsphere-based suspension array technology is anticipated to achieve both higher performance (*i.e.*, higher multiplexing capacity, higher sensitivity) as well as simple and cost-effective devices for point-of-care diagnoses. Undoubtedly, nanoparticles with unique spectrometric properties have a bright future for suspension array technology, since they can improve multiplexed detecting capabilities, photostability, and sensitivity. Magnetic nanoparticles also play an important role in developing automatic immunoassay systems. To obtain high signal-to-noise ratios for higher sensitivity, various labels and signal

amplification methods—as well as nonspecific suppression methods—have been developed. In many cases, the use of microfluidic techniques has promoted and will continually improve suspension array technology, including more versatile preparation of barcodes, miniaturization of bioanalysis, and exploitation of miniaturized and automatic systems for point-of-care diagnosis. Comprehensive and detailed guidelines are provided in this review for designing suspension arrays with excellent performance and provide a strong impetus which is expected to help drive the development of suspension arrays and their related areas (*e.g.* nanotechnology, material chemistry, barcode production techniques, optofluidics, and biomedical instruments). It is also anticipated that nanoparticle barcode-based suspension array technology will elicit broad interest in biomedical applications including disease diagnosis, drug discovery, genomics, and proteomics.

Acknowledgments

This work was supported in part by the National Basic Research Program of China (973 program, 2010CB933901, 2013CB733802, 2014CB744503), the National Natural Science Foundation of China (Project No. 50902093, 81371596 and 81371645), Medicine & Engineering Cross Research Foundation of Shanghai Jiao Tong University (Project No. YG2012MS61, YG2014MS33), and the Intramural Research Program of National Institute of Biomedical Imaging and Bioengineering, National Institutes of Health.

References

1. Chin L, Andersen JN, Futreal PA. Nat Med. 2011; 17:297–303. [PubMed: 21383744]
2. McDermott U, Downing JR, Stratton MR. N Engl J Med. 2011; 364:340–350. [PubMed: 21268726]
3. Lander ES. Nature. 2011; 470:187–197. [PubMed: 21307931]
4. Han X, Wu X, Chung WY, Li T, Nekrutenko A, Altman NS, Chen G, Ma H. Proc Natl Acad Sci U S A. 2009; 106:12741–12746. [PubMed: 19617558]
5. Pritchard CC, Cheng HH, Tewari M. Nat Rev Genet. 2012; 13:358–369. [PubMed: 22510765]
6. MacArron R, Banks MN, Bojanic D, Burns DJ, Cirovic DA, Garyantes T, Green DVS, Hertzberg RP, Janzen WP, Paslay JW, Schopfer U, Sittampalam GS. Nat Rev Drug Discovery. 2011; 10:188–195. [PubMed: 21358738]
7. Kepp O, Galluzzi L, Lipinski M, Yuan J, Kroemer G. Nat Rev Drug Discovery. 2011; 10:221–237. [PubMed: 21358741]
8. Kim D, Daniel WL, Mirkin CA. Anal Chem. 2009; 81:9183–9187. [PubMed: 19874062]
9. Wang Z, Zong S, Li W, Wang C, Xu S, Chen H, Cui Y. J Am Chem Soc. 2012; 134:2993–3000. [PubMed: 22239121]
10. Cao YC, Jin R, Mirkin CA. Science. 2002; 297:1536–1540. [PubMed: 12202825]
11. Sendroiu IE, Gifford LK, Lupták A, Corn RM. J Am Chem Soc. 2011; 133:4271–4273. [PubMed: 21391582]
12. Han M, Gao X, Su JZ, Nie S. Nat Biotechnol. 2001; 19:631–635. [PubMed: 11433273]
13. Sathe TR, Agrawal A, Nie S. Anal Chem. 2006; 78:5627–5632. [PubMed: 16906704]
14. Mathur A, Kelso DM. Cytometry, Part A. 2010; 77:356–365.
15. Zhao Y, Zhao X, Tang B, Xu W, Li J, Hu J, Gu Z. Adv Funct Mater. 2010; 20:976–982.
16. Zhang F, Shi Q, Zhang Y, Shi Y, Ding K, Zhao D, Stucky GD. Adv Mater. 2011; 23:3775–3779. [PubMed: 21766355]
17. Lu Y, Zhao J, Zhang R, Liu Y, Liu D, Goldys EM, Yang X, Xi P, Sunna A, Lu J. Nat Photonics. 2014; 8:32–36.
18. Neng J, Harpster MH, Wilson WC, Johnson PA. Biosens Bioelectron. 2013; 41:316–321. [PubMed: 23021841]
19. Lee J, Bisso PW, Srinivas RL, Kim JJ, Swiston AJ, Doyle PS. Nat Mater. 2014; 13:524–529. [PubMed: 24728464]

20. Ling M, Ricks C, Lea P. Expert Rev Mol Diagn. 2007; 7:87. [PubMed: 17187487]
21. Wilson R, Cossins AR, Spiller DG. Angew Chem, Int Ed. 2006; 45:6104–6117.
22. Karlin-Neumann, G.; Sedova, M.; Falkowski, M.; Wang, Z.; Lin, S.; Jain, M. Quantum Dots. Springer; 2007. p. 239-251.
23. Nolan JP, Sklar LA. Trends Biotechnol. 2002; 20:9–12. [PubMed: 11742671]
24. Finkel NH, Lou X, Wang C, He L. Anal Chem. 2004; 76:352A–359A.
25. http://www.luminexcorp.com/.
26. Meza MB. Drug Discovery Today. 2000; 5(suppl 1):38–41.
27. Kusnezow W, Syagailo YV, Goychuk I, Hoheisel JD, Wild DG. Expert Rev Mol Diagn. 2006; 6:111–124. [PubMed: 16359272]
28. Situma C, Hashimoto M, Soper SA. Biomol Eng. 2006; 23:213–231. [PubMed: 16905357]
29. Birtwell S, Morgan H. Integr Biol. 2009; 1:345–362.
30. Wang G, Leng Y, Dou H, Wang L, Li W, Wang X, Sun K, Shen L, Yuan X, Li J. ACS Nano. 2012; 7:471–481. [PubMed: 23205725]
31. Eastman PS, Ruan W, Doctolero M, Nuttall R, de Feo G, Park JS, Chu JSF, Cooke P, Gray JW, Li S, Chen FF. Nano Lett. 2006; 6:1059–1064. [PubMed: 16683851]
32. Birtwell S, Broder G, Roach P, Morgan H. Biomed Microdevices. 2012; 14:651–657. [PubMed: 22391879]
33. Pregibon DC, Toner M, Doyle PS. Science. 2007; 315:1393–1396. [PubMed: 17347435]
34. Lin CH, Yeakley JM, McDaniel TK, Shen R. Methods in Molecular Biology. 2009; 496:129–142. [PubMed: 18839109]
35. Braeckmans K, De Smedt SC, Roelant C, Leblans M, Pauwels R, Demeester J. Nat Mater. 2003; 2:169–174. [PubMed: 12612674]
36. Hill HD, Mirkin CA. Nat Protoc. 2006; 1:324–336. [PubMed: 17406253]
37. Akhras MS, Pettersson E, Diamond L, Unemo M, Okamoto J, Davis RW, Pourmand N. PLoS One. 2013; 8:e76696. [PubMed: 24116138]
38. Liang Y, Abdelrahman AI, Baranov V, Winnik MA. Polymer. 2011; 52:5040–5052.
39. Abdelrahman AI, Dai S, Thickett SC, Ornatsky O, Bandura D, Baranov V, Winnik MA. J Am Chem Soc. 2009; 131:15276–15283. [PubMed: 19807075]
40. Song A, Zhang J, Lebrilla CB, Lam KS. J Am Chem Soc. 2003; 125:6180–6188. [PubMed: 12785850]
41. Moran EJ, Sarshar S, Cargill JF, Shahbaz MM, Lio A, Mjalli AMM, Armstrong RW. J Am Chem Soc. 1995; 117:10787–10788.
42. Nicolaou KC, Xiao X-Y, Parandoosh Z, Senyei A, Nova MP. Angew Chem, Int Ed Engl. 1995; 34:2289–2291.
43. Vaino AR, Janda KD. Proc Natl Acad Sci U S A. 2000; 97:7692–7696. [PubMed: 10884401]
44. Benecky MJ, Post DR, Schmitt SM, Kochar MS. Clin Chem. 1997; 43:1764–1770. [PubMed: 9299973]
45. Hayward T, Hong B, Vyas K, Palfreyman J, Cooper J, Jiang Z, Jeong J, Llandro J, Mitrelias T, Bland J. J Phys D: Appl Phys. 2010; 43:175001.
46. Jeong JR, Llandro J, Hong B, Hayward TJ, Mitrelias T, Kopper KP, Trypiniotis T, Steinmuller SJ, Simpson GK, Bland JAC. Lab Chip. 2008; 8:1883–1887. [PubMed: 18941689]
47. Banholzer MJ, Qin L, Millstone JE, Osberg KD, Mirkin CA. Nat Protoc. 2009; 4:838–848. [PubMed: 19444241]
48. Trau M, Battersby BJ. Adv Mater. 2001; 13:975–979.
49. Fulton RJ, McDade RL, Smith PL, Kienker LJ, Kettman JR. Clin Chem. 1997; 43:1749–1756. [PubMed: 9299971]
50. Siawaya JFD, Roberts T, Babb C, Black G, Golakai HJ, Stanley K, Bapela NB, Hoal E, Parida S, van Helden P. PLoS One. 2008; 3:e2535. [PubMed: 18596971]
51. Taniuchi M, Verweij JJ, Noor Z, Sobuz SU, van Lieshout L, Petri WA, Haque R, Houpt ER. Am J Trop Med Hyg. 2011; 84:332–337. [PubMed: 21292910]

52. Tait BD, Hudson F, Cantwell L, Brewin G, Holdsworth R, Bennett G, Jose M. Nephrology. 2009; 14:247–254. [PubMed: 19207861]
53. Dunbar SA. Clin Chim Acta. 2006; 363:71–82. [PubMed: 16102740]
54. Varro R, Chen R, Sepulveda H, Apgar J. Monoclonal Antibodies. 2007:125–152.
55. Akinfieva O, Nabiev I, Sukhanova A. Crit Rev Oncol Hematol. 2013; 86:1–14. [PubMed: 23058250]
56. Sukhanova A, Nabiev I. Crit Rev Oncol Hematol. 2008; 68:39–59. [PubMed: 18621543]
57. Resch-Genger U, Grabolle M, Cavaliere-Jaricot S, Nitschke R, Nann T. Nat Methods. 2008; 5:763–775. [PubMed: 18756197]
58. Gorris HH, Wolfbeis OS. Angew Chem, Int Ed. 2013; 52:3584–3600.
59. Jun BH, Kim G, Noh MS, Kang H, Kim YK, Cho MH, Jeong DH, Lee YS. Nanomedicine. 2011; 6:1463–1480. [PubMed: 22026382]
60. Zhao Y, Zhao X, Sun C, Li J, Zhu R, Gu Z. Anal Chem. 2008; 80:1598–1605. [PubMed: 18247635]
61. Lee JA, Mardyani S, Hung A, Rhee A, Klostranec J, Mu Y, Li D, Chan WCW. Adv Mater. 2007; 19:3113–3118.
62. Burbaum JJ. J Biomol Screening. 2000; 5:5–8.
63. Klarreich E. Nature. 2001; 413:450–452. [PubMed: 11586322]
64. Michalet X, Pinaud FF, Bentolila LA, Tsay JM, Doose S, Li JJ, Sundaresan G, Wu AM, Gambhir SS, Weiss S. Science. 2005; 307:538–544. [PubMed: 15681376]
65. Fournier-Bidoz S, Jennings TL, Klostranec JM, Fung W, Rhee A, Li D, Chan WC. Angew Chem, Int Ed. 2008; 120:5659–5663.
66. Wang X, Wang G, Li W, Zhao B, Xing B, Leng Y, Dou H, Sun K, Shen L, Yuan X. Small. 2013; 9:3327–3335. [PubMed: 23463727]
67. Dahan M, Laurence T, Pinaud F, Chemla DS, Alivisatos AP, Sauer M, Weiss S. Opt Lett. 2001; 26:825–827. [PubMed: 18040463]
68. Gao X, Nie S. Anal Chem. 2004; 76:2406–2410. [PubMed: 15080756]
69. Luo S, Zhang E, Su Y, Cheng T, Shi C. Biomaterials. 2011; 32:7127–7138. [PubMed: 21724249]
70. Gorris HH, Saleh SM, Groegel DB, Ernst S, Reiner K, Mustroph H, Wolfbeis OS. Bioconjugate Chem. 2011; 22:1433–1437.
71. Cheng A, Gonçalves JT, Golshani P, Arisaka K, Portera-Cailliau C. Nat Methods. 2011; 8:139–142. [PubMed: 21217749]
72. Larson DR, Zipfel WR, Williams RM, Clark SW, Bruchez MP, Wise FW, Webb WW. Science. 2003; 300:1434–1436. [PubMed: 12775841]
73. Pawlicki M, Collins HA, Denning RG, Anderson HL. Angew Chem, Int Ed. 2009; 48:3244–3266.
74. Wang F, Banerjee D, Liu Y, Chen X, Liu X. Analyst. 2010; 135:1839–1854. [PubMed: 20485777]
75. Wang F, Liu X. J Am Chem Soc. 2008; 130:5642–5643. [PubMed: 18393419]
76. Li Z, Zhang Y, Jiang S. Adv Mater. 2008; 20:4765–4769.
77. Zhou JC, Yang ZL, Dong W, Tang RJ, Sun LD, Yan CH. Biomaterials. 2011; 32:9059–9067. [PubMed: 21880365]
78. Wang F, Deng R, Wang J, Wang Q, Han Y, Zhu H, Chen X, Liu X. Nat Mater. 2011; 10:968–973. [PubMed: 22019945]
79. Gorris HH, Ali R, Saleh SM, Wolfbeis OS. Adv Mater. 2011; 23:1652–1655. [PubMed: 21472793]
80. Li Z, Wang L, Wang Z, Liu X, Xiong Y. J Phys Chem C. 2011; 115:3291–3296.
81. Zhang F, Haushalter RC, Haushalter RW, Shi Y, Zhang Y, Ding K, Zhao D, Stucky GD. Small. 2011; 7:1972–1976. [PubMed: 21726042]
82. Gerver RE, Gómez-Sjöberg R, Baxter BC, Thorn KS, Fordyce PM, Diaz-Botia CA, Helms BA, DeRisi JL. Lab Chip. 2012; 12:4716–4723. [PubMed: 23042484]
83. Wang J, Wang F, Wang C, Liu Z, Liu X. Angew Chem, Int Ed. 2011; 50:10369–10372.
84. Tian G, Gu Z, Zhou L, Yin W, Liu X, Yan L, Jin S, Ren W, Xing G, Li S. Adv Mater. 2012; 24:1226–1231. [PubMed: 22282270]

85. Zhang Y, Lin JD, Vijayaragavan V, Bhakoo KK, Tan TTY. Chem Commun. 2012; 48:10322–10324.
86. Chen D, Lei L, Zhang R, Yang A, Xu J, Wang Y. Chem Commun. 2012; 48:10630–10632.
87. Chan EM, Han G, Goldberg JD, Gargas DJ, Ostrowski AD, Schuck PJ, Cohen BE, Milliron DJ. Nano Lett. 2012; 12:3839–3845. [PubMed: 22713101]
88. Yi G, Peng Y, Gao Z. Chem Mater. 2011; 23:2729–2734.
89. Perfetto SP, Chattopadhyay PK, Roederer M. Nat Rev Immunol. 2004; 4:648–655. [PubMed: 15286731]
90. Watson DA, Brown LO, Gaskill DF, Naivar M, Graves SW, Doorn SK, Nolan JP. Cytometry, Part A. 2008; 73:119–128.
91. Cui HH, Valdez JG, Steinkamp JA, Crissman HA. Cytometry, Part A. 2003; 52:46–55.
92. Hoffmann K, Behnke T, Drescher D, Kneipp J, Resch-Genger U. ACS Nano. 2013; 7:6674–6684. [PubMed: 23837453]
93. Grabolle M, Kapusta P, Nann T, Shu X, Ziegler J, Resch-Genger U. Anal Chem. 2009; 81:7807–7813. [PubMed: 19705851]
94. Chen C, Zhang P, Gao G, Gao D, Yang Y, Liu H, Wang Y, Gong P, Cai L. Adv Mater. 2014; 26:6313–6317. [PubMed: 25066411]
95. Mayr T, Moser C, Klimant I. Anal Chim Acta. 2007; 597:137–144. [PubMed: 17658323]
96. Hagan A, Zuchner T. Anal Bioanal Chem. 2011; 400:2847–2864. [PubMed: 21556751]
97. Tu D, Liu L, Ju Q, Liu Y, Zhu H, Li R, Chen X. Angew Chem, Int Ed. 2011; 50:6306–6310.
98. Geißler D, Stufler S, Löhmannsröben H-G, Hildebrandt N. J Am Chem Soc. 2012; 135:1102–1109. [PubMed: 23231786]
99. Rajapakse HE, Gahlaut N, Mohandessi S, Yu D, Turner JR, Miller LW. Proc Natl Acad Sci U S A. 2010; 107:13582–13587. [PubMed: 20643966]
100. Lu Y, Lu J, Zhao J, Cusido J, Raymo FM, Yuan J, Yang S, Leif RC, Huo Y, Piper JA, Robinson JP, Goldys EM, Jin D. Nat Commun. 2014; 5:3741. [PubMed: 24796249]
101. Zhao J, Lu Z, Yin Y, McRae C, Piper JA, Dawes JM, Jin D, Goldys EM. Nanoscale. 2013; 5:944–952. [PubMed: 23223581]
102. Lu J, Martin J, Lu Y, Zhao J, Yuan J, Ostrowski M, Paulsen I, Piper JA, Jin D. Anal Chem. 2012; 84:9674–9678. [PubMed: 23098251]
103. Lu Y, Xi P, Piper JA, Huo Y, Jin D. Sci Rep. 2012; 2:837. [PubMed: 23150787]
104. Sharma B, Frontiera RR, Henry A-I, Ringe E, Van Duyne RP. Mater Today. 2012; 15:16–25.
105. Qian XM, Nie SM. Chem Soc Rev. 2008; 37:912–920. [PubMed: 18443676]
106. Mulvihill MJ, Ling XY, Henzie J, Yang P. J Am Chem Soc. 2009; 132:268–274.
107. Boisselier E, Astruc D. Chem Soc Rev. 2009; 38:1759–1782. [PubMed: 19587967]
108. Dendisová-Vyškovská M, Prokopec V, Člupek M, Matějka P. J Raman Spectrosc. 2012; 43:181–186.
109. Qian X, Peng X-H, Ansari DO, Yin-Goen Q, Chen GZ, Shin DM, Yang L, Young AN, Wang MD, Nie S. Nat Biotechnol. 2008; 26:83–90. [PubMed: 18157119]
110. Zavaleta CL, Smith BR, Walton I, Doering W, Davis G, Shojaei B, Natan MJ, Gambhir SS. Proc Natl Acad Sci U S A. 2009; 106:13511–13516. [PubMed: 19666578]
111. Rodriguez-Lorenzo L, Fabris L, Alvarez-Puebla RA. Anal Chim Acta. 2012; 745:10–23. [PubMed: 22938601]
112. Alvarez-Puebla RA, Liz-Marzán LM. Small. 2010; 6:604–610. [PubMed: 20108237]
113. Ling X, Xie L, Fang Y, Xu H, Zhang H, Kong J, Dresselhaus MS, Zhang J, Liu Z. Nano Lett. 2009; 10:553–561.
114. Musumeci A, Gosztola D, Schiller T, Dimitrijevic NM, Mujica V, Martin D, Rajh T. J Am Chem Soc. 2009; 131:6040–6041. [PubMed: 19364105]
115. Luther JM, Jain PK, Ewers T, Alivisatos AP. Nat Mater. 2011; 10:361–366. [PubMed: 21478881]
116. Camden JP, Dieringer JA, Wang Y, Masiello DJ, Marks LD, Schatz GC, Van Duyne RP. J Am Chem Soc. 2008; 130:12616–12617. [PubMed: 18761451]
117. Ewená Smith W. Analyst. 2004; 129:567–568. [PubMed: 15213819]

118. Lim DK, Jeon KS, Kim HM, Nam JM, Suh YD. Nat Mater. 2010; 9:60–67. [PubMed: 20010829]
119. Nie S, Emory SR. Science. 1997; 275:1102–1106. [PubMed: 9027306]
120. Su X, Zhang J, Sun L, Koo TW, Chan S, Sundararajan N, Yamakawa M, Berlin AA. Nano Lett. 2005; 5:49–54. [PubMed: 15792411]
121. Lutz BR, Dentinger CE, Nguyen LN, Sun L, Zhang J, Allen AN, Chan S, Knudsen BS. ACS Nano. 2008; 2:2306–2314. [PubMed: 19206397]
122. Kim JH, Kang H, Kim S, Jun BH, Kang T, Chae J, Jeong S, Kim J, Jeong DH, Lee YS. Chem Commun. 2011; 47:2306–2308.
123. Saute B, Premasiri R, Ziegler L, Narayanan R. Analyst. 2012; 137:5082–5087. [PubMed: 22977883]
124. Lee S, Joo S, Park S, Kim S, Kim HC, Chung TD. Electrophoresis. 2010; 31:1623–1629. [PubMed: 20419705]
125. Jun BH, Noh MS, Kim G, Kang H, Kim JH, Chung WJ, Kim MS, Kim YK, Cho MH, Jeong DH. Anal Biochem. 2009; 391:24–30. [PubMed: 19433055]
126. Sha MY, Xu H, Penn SG, Cromer R. Nanomedicine. 2007; 2:725–734. [PubMed: 17976033]
127. Doering WE, Piotti ME, Natan MJ, Freeman RG. Adv Mater. 2007; 19:3100–3108.
128. Jin R, Cao YC, Thaxton CS, Mirkin CA. Small. 2006; 2:375–380. [PubMed: 17193054]
129. Xu H, Aizpurua J, Käll M, Apell P. Phys Rev E: Stat Phys, Plasmas, Fluids, Relat Interdiscip Top. 2000; 62:4318–4324.
130. Jiang J, Bosnick K, Maillard M, Brus L. J Phys Chem B. 2003; 107:9964–9972.
131. Fang Y, Seong NH, Dlott DD. Science. 2008; 321:388–392. [PubMed: 18583578]
132. Wustholz KL, Henry A-I, McMahon JM, Freeman RG, Valley N, Piotti ME, Natan MJ, Schatz GC, Duyne RPV. J Am Chem Soc. 2010; 132:10903–10910. [PubMed: 20681724]
133. Alvarez-Puebla RA, Agarwal A, Manna P, Khanal BP, Aldeanueva-Potel P, Carbó-Argibay E, Pazos-Pérez N, Vigderman L, Zubarev ER, Kotov NA, Liz-Marzán LM. Proc Natl Acad Sci U S A. 2011; 108:8157–8161. [PubMed: 21536908]
134. Lim DK, Jeon KS, Hwang JH, Kim H, Kwon S, Suh YD, Nam JM. Nat Nanotechnol. 2011; 6:452–460. [PubMed: 21623360]
135. Song J, Duan B, Wang C, Zhou J, Pu L, Fang Z, Wang P, Lim TT, Duan H. J Am Chem Soc. 2014; 136:6838–6841. [PubMed: 24773367]
136. Zhao Y, Zhao X, Gu Z. Adv Funct Mater. 2010; 20:2970–2988.
137. Taubes G. Science. 1997; 278:1709–1710.
138. Cunin F, Schmedake TA, Link JR, Li YY, Koh J, Bhatia SN, Sailor MJ. Nat Mater. 2002; 1:39–41. [PubMed: 12618846]
139. Velev OD, Lenhoff AM, Kaler EW. Science. 2000; 287:2240–2243. [PubMed: 10731141]
140. Meade SO, Chen MY, Sailor MJ, Miskelly GM. Anal Chem. 2009; 81:2618–2625. [PubMed: 19271746]
141. Zhao YJ, Zhao XW, Hu J, Li J, Xu WY, Gu ZZ. Angew Chem, Int Ed. 2009; 48:7350–7352.
142. Tang B, Zhao X, Zhao Y, Zhang W, Wang Q, Kong L, Gu Z. Langmuir. 2011; 27:11722–11728. [PubMed: 21823629]
143. Zhao Y, Zhao X, Hu J, Xu M, Zhao W, Sun L, Zhu C, Xu H, Gu Z. Adv Mater. 2009; 21:569–572. [PubMed: 21161983]
144. Li J, Zhao X-W, Zhao Y-J, Hu J, Xu M, Gu Z-Z. J Mater Chem. 2009; 19:6492–6497.
145. Zhao Y, Xie Z, Gu H, Jin L, Zhao X, Wang B, Gu Z. NPG Asia Mater. 2012; 4:e25.
146. Ku KH, Kim MP, Paek K, Shin JM, Chung S, Jang SG, Chae WS, Yi GR, Kim BJ. Small. 2013; 9:2667–2672. [PubMed: 23401329]
147. Houser B. Arch Physiol Biochem. 2012; 118:192–196. [PubMed: 22852821]
148. Stsiapura V, Sukhanova A, Artemyev M, Pluot M, Cohen JHM, Baranov AV, Oleinikov V, Nabiev I. Anal Biochem. 2004; 334:257–265. [PubMed: 15494132]
149. Wang G, Zhang P, Dou H, Li W, Sun K, He X, Han J, Xiao H, Li Y. Langmuir. 2012; 28:6141–6150. [PubMed: 22428794]
150. Gao X, Nie S. J Phys Chem B. 2003; 107:11575–11578.

151. Song T, Zhang Q, Lu C, Gong X, Yang Q, Li Y, Liu J, Chang J. J Mater Chem. 2011; 21:2169–2177.
152. Hu S-H, Gao X. Adv Funct Mater. 2010; 20:3721–3726. [PubMed: 22389642]
153. Song T, Liu J, Li W, Li Y, Yang Q, Gong X, Xuan L, Chang J. ACS Appl Mater Interfaces. 2014; 6:2745–2752. [PubMed: 24495171]
154. Decher G. Science. 1997; 277:1232–1237.
155. Wang D, Rogach AL, Caruso F. Nano Lett. 2002; 2:857–861.
156. Wilson R, Spiller DG, Prior IA, Bhatt R, Hutchinson A. J Mater Chem. 2007; 17:4400–4406.
157. Wilson R, Spiller DG, Prior IA, Veltkamp KJ, Hutchinson A. ACS Nano. 2007; 1:487–493. [PubMed: 19206670]
158. Allen CN, Lequeux N, Chassenieux C, Tessier G, Dubertret B. Adv Mater. 2007; 19:4420–4425.
159. Rauf S, Glidle A, Cooper JM. Adv Mater. 2009; 21:4020–4024.
160. Rauf S, Glidle A, Cooper JM. Chem Commun. 2010; 46:2814–2816.
161. Yoon M, Kim Y, Cho J. ACS Nano. 2011; 5:5417–5426. [PubMed: 21688776]
162. Li H, Gao S, Zheng Z, Cao R. Catal Sci Technol. 2011; 1:1194–1201.
163. Yang X, Zhang Y. Langmuir. 2004; 20:6071–6073. [PubMed: 16459632]
164. Joumaa N, Lansalot M, Théretz A, Elaissari A, Sukhanova A, Artemyev M, Nabiev I, Cohen JH. Langmuir. 2006; 22:1810–1816. [PubMed: 16460111]
165. Vaidya SV, Gilchrist ML, Maldarelli C, Couzis A. Anal Chem. 2007; 79:8520–8530. [PubMed: 17927278]
166. Sheng W, Kim S, Lee J, Kim S-W, Jensen K, Bawendi MG. Langmuir. 2006; 22:3782–3790. [PubMed: 16584256]
167. Zhang H, Cui Z, Wang Y, Zhang K, Ji X, Lü C, Yang B, Gao M. Adv Mater. 2003; 15:777–780.
168. Yang Y, Wen Z, Dong Y, Gao M. Small. 2006; 2:898–901. [PubMed: 17193142]
169. Yang Y, Tu C, Gao M. J Mater Chem. 2007; 17:2930–2935.
170. Yin W, Liu H, Yates M, Du H, Jiang F, Guo L, Krauss T. Chem Mater. 2007; 19:2930–2936.
171. Pan J, Feng SS. Biomaterials. 2009; 30:1176–1183. [PubMed: 19062089]
172. Kim JS, Cho KJ, Tran TH, Nurunnabi M, Moon TH, Hong SM, Lee YK. J Colloid Interface Sci. 2011; 353:363–371. [PubMed: 20961554]
173. Yang J, Dave SR, Gao X. J Am Chem Soc. 2008; 130:5286–5292. [PubMed: 18361491]
174. Zhang Q, Wang X, Zhu Y. J Mater Chem. 2011; 21:12132–12138.
175. Farah AA, Alvarez-Puebla RA, Fenniri H. J Colloid Interface Sci. 2008; 319:572–576. [PubMed: 18187145]
176. Xiao Q, Ji Y, Xiao Z, Zhang Y, Lin H, Wang Q. Chem Commun. 2013; 49:1527–1529.
177. Kim MP, Kang DJ, Jung D-W, Kannan AG, Kim KH, Ku KH, Jang SG, Chae W-S, Yi G-R, Kim BJ. ACS Nano. 2012; 6:2750–2757. [PubMed: 22352689]
178. Vladisavljević GT, Kobayashi I, Nakajima M. Microfluid Nanofluid. 2012; 13:151–178.
179. Wang W, Zhang MJ, Chu LY. Acc Chem Res. 2014; 47:373–384. [PubMed: 24199893]
180. Kim SH, Cho YS, Jeon SJ, Eun TH, Yi GR, Yang SM. Adv Mater. 2008; 20:3268–3273.
181. Zhao Y, Shum HC, Chen H, Adams LL, Gu Z, Weitz DA. J Am Chem Soc. 2011; 133:8790–8793. [PubMed: 21574640]
182. Hwang H, Kim S-H, Yang S-M. Lab Chip. 2011; 11:87–92. [PubMed: 20959939]
183. Köhler JM, März A, Popp J, Knauer A, Kraus I, Faerber J, Serra C. Anal Chem. 2012; 85:313–318. [PubMed: 23206230]
184. Chen Y, Dong P, Xu J, Luo G. Langmuir. 2014; 30:8538–8542. [PubMed: 24956221]
185. Kim SH, Shim JW, Yang SM. Angew Chem, Int Ed. 2011; 123:1203–1206.
186. Nakashima T, Shimizu M, Kukizaki M. Key Eng Mater. 1992; 61:513–516.
187. Joscelyne SM, Trägårdh G. J Membr Sci. 2000; 169:107–117.
188. Wagdare NA, Marcelis ATM, Ho OB, Boom RM, van Rijn CJM. J Membr Sci. 2010; 347:1–7.
189. Chu LY, Park SH, Yamaguchi T, Nakao S. Langmuir. 2002; 18:1856–1864.

190. Nandiyanto ABD, Okuyama K. Adv Powder Technol. 2011; 22:1–19.
191. Moon JH, Yi GR, Yang SM, Pine DJ, Park SB. Adv Mater. 2004; 16:605–609.
192. Sun L, Yu X, Sun M, Wang H, Xu S, Dixon JD, Wang YA, Li Y, Yang Q, Xu X. J Colloid Interface Sci. 2011; 358:73–80. [PubMed: 21421221]
193. Ciriminna R, Fidalgo A, Pandarus V, Béland F, Ilharco LM, Pagliaro M. Chem Rev. 2013; 113:6592–6620. [PubMed: 23782155]
194. Insin N, Tracy JB, Lee H, Zimmer JP, Westervelt RM, Bawendi MG. ACS Nano. 2008; 2:197–202. [PubMed: 19206619]
195. Chan Y, Zimmer JP, Stroh M, Steckel JS, Jain RK, Bawendi MG. Adv Mater. 2004; 16:2092–2097.
196. Ma Q, Serrano IC, Palomares E. Chem Commun. 2011; 47:7071–7073.
197. Wang Q, Liu Y, Lin C, Yan H. Nanotechnology. 2007; 18:405604.
198. Ma Q, Nakane Y, Mori Y, Hasegawa M, Yoshioka Y, Watanabe TM, Gonda K, Ohuchi N, Jin T. Biomaterials. 2012; 33:8486–8494. [PubMed: 22906608]
199. Wu SL, Ye L, Ning YH, Niu WB, Zhang SF. Adv Mater Res. 2013; 679:69–74.
200. Sanles-Sobrido M, Exner W, Rodríguez-Lorenzo L, Rodríguez-González B, Correa-Duarte MA, Álvarez-Puebla RA, Liz-Marzán LM. J Am Chem Soc. 2009; 131:2699–2705. [PubMed: 19182903]
201. O'Brien P, Cummins SS, Darcy D, Dearden A, Masala O, Pickett NL, Ryley S, Sutherland AJ. Chem Commun. 2003:2532–2533.
202. Ye B, Ding H, Cheng Y, Gu H, Zhao Y, Xie Z, Gu Z. Adv Mater. 2014; 26:3270–3274. [PubMed: 24550084]
203. Jun BH, Kim JE, Rho C, Byun JW, Kim YH, Kang H, Kim JH, Kang T, Cho MH, Lee YS. J Nanosci Nanotechnol. 2011; 11:6249–6252. [PubMed: 22121695]
204. Jun BH, Baek J, Kang H, Park YJ, Jeong DH, Lee YS. J Colloid Interface Sci. 2011; 355:29–34. [PubMed: 21194704]
205. Lowe M, Spiro A, Zhang YZ, Getts R. Cytometry, Part A. 2004; 60:135–144.
206. Xiang Y, Zhang H, Jiang B, Chai Y, Yuan R. Anal Chem. 2011; 83:4302–4306. [PubMed: 21517090]
207. Wang C, Zhan R, Pu KY, Liu B. Adv Funct Mater. 2010; 20:2597–2604.
208. Deng W, Drozdowicz-Tomsia K, Jin D, Goldys EM. Anal Chem. 2009; 81:7248–7255. [PubMed: 19715357]
209. Anderson GP, Taitt CR. Biosens Bioelectron. 2008; 24:324–328. [PubMed: 18485692]
210. Li Y, Cu YTH, Luo D. Nat Biotechnol. 2005; 23:885–889. [PubMed: 15951805]
211. Geiss GK, Bumgarner RE, Birditt B, Dahl T, Dowidar N, Dunaway DL, Fell HP, Ferree S, George RD, Grogan T. Nat Biotechnol. 2008; 26:317–325. [PubMed: 18278033]
212. Vignali DA. J Immunol Methods. 2000; 243:243–255. [PubMed: 10986418]
213. Ma Q, Wang X, Li Y, Shi Y, Su X. Talanta. 2007; 72:1446–1452. [PubMed: 19071782]
214. Glazer A. J Appl Phycol. 1994; 6:105–112.
215. Berlier JE, Rothe A, Buller G, Bradford J, Gray DR, Filanoski BJ, Telford WG, Yue S, Liu J, Cheung CY, Chang W, Hirsch JD, Beechem Rosaria JM, Haugland P, Haugland RP. J Histochem Cytochem. 2003; 51:1699–1712. [PubMed: 14623938]
216. Mayr T, Moser C, Klimant I. J Fluoresc. 2009; 19:303–310. [PubMed: 18807154]
217. Alivisatos P. Nat Biotechnol. 2004; 22:47–52. [PubMed: 14704706]
218. Rosi NL, Mirkin CA. Chem Rev. 2005; 105:1547–1562. [PubMed: 15826019]
219. Yan J, Estévez MC, Smith JE, Wang K, He X, Wang L, Tan W. Nano Today. 2007; 2:44–50.
220. Päkkilä H, Ylihärsilä M, Lahtinen S, Hattara L, Salminen N, Arppe R, Lastusaari M, Saviranta P, Soukka T. Anal Chem. 2012; 84:8628–8634. [PubMed: 22985020]
221. Rousserie G, Sukhanova A, Even-Desrumeaux K, Fleury F, Chames P, Baty D, Oleinikov V, Pluot M, Cohen JH, Nabiev I. Crit Rev Oncol Hematol. 2010; 74:1–15. [PubMed: 19467882]
222. Sukhanova A, Devy J, Venteo L, Kaplan H, Artemyev M, Oleinikov V, Klinov D, Pluot M, Cohen JH, Nabiev I. Anal Biochem. 2004; 324:60–67. [PubMed: 14654046]

223. Rana S, Yeh YC, Rotello VM. Curr Opin Chem Biol. 2010; 14:828–834. [PubMed: 21035376]
224. Klostranec JM, Chan WCW. Adv Mater. 2006; 18:1953–1964.
225. Sperling RA, Parak WJ. Philos Trans R Soc, A. 2010; 368:1333–1383.
226. Li J, Ng CK. Antibody-Mediated Drug Delivery Systems: Concepts, Technology, and Applications. 2012; ch. 10:191–207.
227. Pathak S, Davidson MC, Silva GA. Nano Lett. 2007; 7:1839–1845. [PubMed: 17536868]
228. Kumar S, Aaron J, Sokolov K. Nat Protoc. 2008; 3:314–320. [PubMed: 18274533]
229. Boyer JC, Van Veggel FCJM. Nanoscale. 2010; 2:1417–1419. [PubMed: 20820726]
230. Jun BH, Kang H, Lee Y-S, Jeong DH. Molecules. 2012; 17:2474–2490. [PubMed: 22382526]
231. Lee HJ, Wark AW, Corn RM. Analyst. 2008; 133:975–983. [PubMed: 18645635]
232. Im H, Shao H, Park YI, Peterson VM, Castro CM, Weissleder R, Lee H. Nat Biotechnol. 2014; 32:490–495. [PubMed: 24752081]
233. Ahn JH, Kim JH, Reuel NF, Barone PW, Boghossian AA, Zhang J, Yoon H, Chang AC, Hilmer AJ, Strano MS. Nano Lett. 2011; 11:2743–2752. [PubMed: 21627102]
234. Lu N, Gao A, Dai P, Song S, Fan C, Wang Y, Li T. Small. 2014; 10:2022–2028. [PubMed: 24574202]
235. Wang Y, Pu KY, Liu B. Langmuir. 2010; 26:10025–10030. [PubMed: 20491465]
236. Wang Y, Liu B. Anal Chem. 2007; 79:7214–7220. [PubMed: 17711299]
237. Brouard D, Viger ML, Bracamonte AG, Boudreau D. ACS Nano. 2011; 5:1888–1896. [PubMed: 21344882]
238. Lu J, Paulsen IT, Jin D. Anal Chem. 2013; 85:8240–8245. [PubMed: 23919763]
239. Wu C, Chiu DT. Angew Chem, Int Ed. 2013; 52:3086–3109.
240. Lee K, Rouillard JM, Pham T, Gulari E, Kim J. Angew Chem, Int Ed. 2007; 46:4667–4670.
241. Zhu C, Liu L, Yang Q, Lv F, Wang S. Chem Rev. 2012; 112:4687–4735. [PubMed: 22670807]
242. Chang K, Liu Z, Chen H, Sheng L, Zhang SXA, Chiu DT, Yin S, Wu C, Qin W. Small. 2014; 10:4270–4275. [PubMed: 25048985]
243. Li K, Liu B. Polym Chem. 2010; 1:252–259.
244. Feng X, Yang G, Liu L, Lv F, Yang Q, Wang S, Zhu D. Adv Mater. 2012; 24:637–641. [PubMed: 21932281]
245. Feng F, He F, An L, Wang S, Li Y, Zhu D. Adv Mater. 2008; 20:2959–2964.
246. Aslan K, Wu M, Lakowicz JR, Geddes CD. J Am Chem Soc. 2007; 129:1524–1525. [PubMed: 17283994]
247. Bardhan R, Grady NK, Cole JR, Joshi A, Halas NJ. ACS Nano. 2009; 3:744–752. [PubMed: 19231823]
248. Viger M, Live L, Therrien O, Boudreau D. Plasmonics. 2008; 3:33–40.
249. Lessard-Viger M, Rioux M, Rainville L, Boudreau D. Nano Lett. 2009; 9:3066–3071. [PubMed: 19603786]
250. Reil F, Hohenester U, Krenn JR, Leitner A. Nano Lett. 2008; 8:4128–4133. [PubMed: 19367798]
251. Gerasimova YV, Kolpashchikov DM. Chem Soc Rev. 2014; 43:6405–6438. [PubMed: 24901032]
252. Liu S, Lin Y, Wang L, Liu T, Cheng C, Wei W, Tang B. Anal Chem. 2014; 86:4008–4015. [PubMed: 24655032]
253. Zuo X, Xia F, Xiao Y, Plaxco KW. J Am Chem Soc. 2010; 132:1816–1818. [PubMed: 20092337]
254. McErlean B. Nature. 1963; 197:507–508. [PubMed: 13949083]
255. Hsu HL, Huang HH, Liang CC, Lin HC, Liu WT, Lin FP, Kau JH, Sun KH. Anal Chem. 2013; 85:5562–5568. [PubMed: 23627570]
256. Ming K, Kim J, Biondi MJ, Syed A, Chen K, Lam A, Ostrowski M, Rebbapragada A, Feld JJ, Chan WCW. ACS Nano. 2015; 9:3060–3074. [PubMed: 25661584]
257. Piepenburg O, Williams CH, Stemple DL, Armes NA. PLoS Biol. 2006; 4:e204. [PubMed: 16756388]
258. Flagella M, Bui S, Zheng Z, Nguyen CT, Zhang A, Pastor L, Ma Y, Yang W, Crawford KL, McMaster GK, Witney F, Luo Y. Anal Biochem. 2006; 352:50–60. [PubMed: 16545767]

259. Bally M, Syed S, Binkert A, Kauffmann E, Ehrat M, Vörös J. Anal Biochem. 2011; 416:145–151. [PubMed: 21669176]
260. Chen C, Wu J. Sensors. 2012; 12:11684–11696. [PubMed: 23112677]
261. Soto CM, Blum AS, Vora GJ, Lebedev N, Meador CE, Won AP, Chatterji A, Johnson JE, Ratna BR. J Am Chem Soc. 2006; 128:5184–5189. [PubMed: 16608355]
262. Park J, Park Y, Kim S. ACS Nano. 2013; 7:9416–9427. [PubMed: 24063720]
263. Ren W, Liu H, Yang W, Fan Y, Yang L, Wang Y, Liu C, Li Z. Biosens Bioelectron. 2013; 49:380–386. [PubMed: 23807231]
264. Cheng W, Yan F, Ding L, Ju H, Yin Y. Anal Chem. 2010; 82:3337–3342. [PubMed: 20345087]
265. Chapin SC, Doyle PS. Anal Chem. 2011; 83:7179–7185. [PubMed: 21812442]
266. Wang CH, Lien KY, Wu JJ, Lee GB. Lab Chip. 2011; 11:1521–1531. [PubMed: 21399774]
267. Xuan F, Hsing IM. J Am Chem Soc. 2014; 136:9810–9813. [PubMed: 24969438]
268. Bobrow MN, Harris TD, Shaughnessy KJ, Litt GJ. J Immunol Methods. 1989; 125:279–285. [PubMed: 2558138]
269. Lohse J, Petersen K, Woller NC, Pedersen HC, Skladtchikova G, Jørgensen RM. Bioconjugate Chem. 2014; 25:1036–1042.
270. Qi HJ, Chen SH, Zhang ML, Shi H, Wang SQ. Anal Bioanal Chem. 2010; 398:2745–2750. [PubMed: 20852851]
271. Silahtaroglu AN, Nolting D, Dyrskjøt L, Berezikov E, Møller M, Tommerup N, Kauppinen S. Nat Protoc. 2007; 2:2520–2528. [PubMed: 17947994]
272. Yuan L, Xu L, Liu S. Anal Chem. 2012; 84:10737–10744. [PubMed: 23181414]
273. Wu Y, Shi H, Yuan L, Liu S. Chem Commun. 2010; 46:7763–7765.
274. Wang Y, Liu B. Biosens Bioelectron. 2009; 24:3293–3298. [PubMed: 19442508]
275. Deng W, Goldys EM. Langmuir. 2012; 28:10152–10163. [PubMed: 22568517]
276. Chen K, Chou LYT, Song F, Chan WCW. Nano Today. 2013; 8:228–234.
277. Song F, Tang PS, Durst H, Cramb DT, Chan WCW. Angew Chem, Int Ed. 2012; 51:8773–8777.
278. Wu XW, Gong M, Dong CH, Cui JM, Yang Y, Sun FW, Han ZF, Guo GC. Opt Express. 2010; 18:6340–6346. [PubMed: 20389657]
279. Jares-Erijman EA, Jovin TM. Nat Biotechnol. 2003; 21:1387–1395. [PubMed: 14595367]
280. Wagh A, Jyoti F, Mallik S, Qian S, Leclerc E, Law B. Small. 2013; 9:2129–2139. [PubMed: 23359548]
281. Lee J, Lee S, Ragunathan K, Joo C, Ha T, Hohng S. Angew Chem, Int Ed. 2010; 122:10118–10121.
282. Uphoff S, Holden SJ, Le Reste L, Periz J, van de Linde S, Heilemann M, Kapanidis AN. Nat Methods. 2010; 7:831–836. [PubMed: 20818380]
283. Tyrakowski CM, Snee PT. Anal Chem. 2014; 86:2380–2386. [PubMed: 24506832]
284. Wang CX, Sato Y, Kudo M, Nishizawa S, Teramae N. Chem – Eur J. 2012; 18:9481–9484. [PubMed: 22733702]
285. Fan J, Hu M, Zhan P, Peng X. Chem Soc Rev. 2013; 42:29–43. [PubMed: 23059554]
286. Chen G, Song F, Xiong X, Peng X. Ind Eng Chem Res. 2013; 52:11228–11245.
287. Zhang H, Feng G, Guo Y, Zhou D. Nanoscale. 2013; 5:10307–10315. [PubMed: 24056667]
288. Sukhanova A, Susha AS, Bek A, Mayilo S, Rogach AL, Feldmann J, Oleinikov V, Reveil B, Donvito B, Cohen JH. Nano Lett. 2007; 7:2322–2327. [PubMed: 17645364]
289. Li J, Qi H, Wang H, Yang Z, Zhu P, Diao G. Microchim Acta. 2014:1–7.
290. Wang L, Cole K, Gaigalas A, Zhang YZ. Bioconjugate Chem. 2005; 16:194–199.
291. Srinivas ARG, Peng H, Barker D, Travas-Sejdic J. Biosens Bioelectron. 2012; 35:498–502. [PubMed: 22487009]
292. Ocheretina O, Merveille YM, Mabou MM, Escuyer VE, Dunbar SA, Johnson WD, Pape JW, Fitzgerald DW. J Clin Microbiol. 2013; 51:2232–2237. [PubMed: 23658258]
293. Mistlberger G, Klimant I. Bioanal Rev. 2010; 2:61–101.
294. Giri S, Li D, Chan WCW. Chem Commun. 2011; 47:4195–4197.

295. Amendola V, Scaramuzza S, Agnoli S, Polizzi S, Meneghetti M. Nanoscale. 2014; 6:1423–1433. [PubMed: 24309909]
296. Du J, Jing C. J Phys Chem C. 2011; 115:17829–17835.
297. Ellington AA, Kullo IJ, Bailey KR, Klee GG. Clin Chem. 2010; 56:186–193. [PubMed: 19959625]
298. Safarik I, Safarikova M. BioMagn Res Technol. 2004; 2:7. [PubMed: 15566570]
299. Sasso LA, Johnston IH, Zheng M, Gupte RK, Ündar A, Zahn JD. Microfluid Nanofluid. 2012; 13:603–612. [PubMed: 26366143]
300. Golden J, Verbarg J, Howell P Jr, Shriver-Lake L, Ligler F. Biosens Bioelectron. 2013; 40:10–16. [PubMed: 22960010]
301. Ng AH, Uddayasankar U, Wheeler AR. Anal Bioanal Chem. 2010; 397:991–1007. [PubMed: 20422163]
302. Culbertson CT, Mickleburgh TG, Stewart-James SA, Sellens KA, Pressnall M. Anal Chem. 2014; 86:95–118. [PubMed: 24274655]
303. Burger R, Reith P, Kijanka G, Akujobi V, Abgrall P, Ducrée J. Lab Chip. 2012; 12:1289–1295. [PubMed: 22334354]
304. Riegger L, Grumann M, Nann T, Riegler J, Ehlert O, Bessler W, Mittenbuehler K, Urban G, Pastewka L, Brenner T. Sens Actuators, A. 2006; 126:455–462.
305. Tarn MD, Lopez-Martinez MJ, Pamme N. Anal Bioanal Chem. 2014; 406:139–161. [PubMed: 24150283]
306. Nguyen NT. Microfluid Nanofluid. 2012; 13:527–528.
307. Phurimsak C, Yildirim E, Tarn MD, Trietsch SJ, Hankemeier T, Pamme N, Vulto P. Lab Chip. 2014; 14:2334–2343. [PubMed: 24832933]
308. Yang SY, Lien KY, Huang KJ, Lei HY, Lee GB. Biosens Bioelectron. 2008; 24:855–862. [PubMed: 18760591]
309. Ng AH, Choi K, Luoma RP, Robinson JM, Wheeler AR. Anal Chem. 2012; 84:8805–8812. [PubMed: 23013543]
310. Choi K, Ng AH, Fobel R, Chang-Yen DA, Yarnell LE, Pearson EL, Oleksak CM, Fischer AT, Luoma RP, Robinson JM. Anal Chem. 2013; 85:9638–9646. [PubMed: 23978190]
311. Gao Y, Lam AWY, Chan WCW. ACS Appl Mater Interfaces. 2013; 5:2853–2860. [PubMed: 23438061]
312. Klostranec JM, Xiang Q, Farcas GA, Lee JA, Rhee A, Lafferty EI, Perrault SD, Kain KC, Chan WCW. Nano Lett. 2007; 7:2812–2818. [PubMed: 17705551]
313. Giljohann DA, Mirkin CA. Nature. 2009; 462:461–464. [PubMed: 19940916]
314. Lawrie GA, Battersby BJ, Trau M. Adv Funct Mater. 2003; 13:887–896.
315. Grøndahl L, Battersby BJ, Bryant D, Trau M. Langmuir. 2000; 16:9709–9715.
316. Battersby BJ, Bryant D, Meutermans W, Matthews D, Smythe ML, Trau M. J Am Chem Soc. 2000; 122:2138–2139.
317. Chen L, Xu S, Li J. Chem Soc Rev. 2011; 40:2922–2942. [PubMed: 21359355]
318. Sacca B, Niemeyer CM. Chem Soc Rev. 2011; 40:5910–5921. [PubMed: 21975573]
319. Verheyen E, Schillemans JP, van Wijk M, Demeniex M-A, Hennink WE, van Nostrum CF. Biomaterials. 2011; 32:3008–3020. [PubMed: 21288565]
320. Tran TNN, Cui J, Hartman MR, Peng S, Funabashi H, Duan F, Yang D, March JC, Lis JT, Cui H, Luo D. J Am Chem Soc. 2013; 135:14008–14011. [PubMed: 23978265]
321. Niemeyer CM. Angew Chem, Int Ed. 2010; 49:1200–1216.
322. Blokzijl A, Friedman M, Pontén F, Landegren U. J Intern Med. 2010; 268:232–245. [PubMed: 20695973]
323. Stoevesandt O, Taussig MJ. Proteomics. 2007; 7:2738–2750. [PubMed: 17639606]
324. Taussig MJ, Stoevesandt O, Borrebaeck CA, Bradbury AR, Cahill D, Cambillau C, De Daruvar A, Dübel S, Eichler J, Frank R. Nat Methods. 2007; 4:13–17. [PubMed: 17195019]
325. Nery AA, Wrenger C, Ulrich H. J Sep Sci. 2009; 32:1523–1530. [PubMed: 19472283]
326. Egholm M, Buchardt O, Nielsen PE, Berg RH. J Am Chem Soc. 1992; 114:1895–1897.

327. Kaur H, Arora A, Wengel J, Maiti S. Biochemistry. 2006; 45:7347–7355. [PubMed: 16752924]
328. Busch AK, Litman T, Nielsen PS. Nat Methods. 2007; 4:I–ii.
329. Ratilainen T, Holmén A, Tuite E, Nielsen PE, Nordén B. Biochemistry. 2000; 39:7781–7791. [PubMed: 10869183]
330. Chandler DP, Jarrell AE. Anal Biochem. 2003; 312:182–190. [PubMed: 12531204]
331. Nagasaki Y. Polym J. 2011; 43:949–958.
332. Åkerman ME, Chan WCW, Laakkonen P, Bhatia SN, Ruoslahti E. Proc Natl Acad Sci U S A. 2002; 99:12617–12621. [PubMed: 12235356]
333. Barbey R, Lavanant L, Paripovic D, Schüwer N, Sugnaux C, Tugulu S, Klok HA. Chem Rev. 2009; 109:5437–5527. [PubMed: 19845393]
334. Uchida K, Hoshino Y, Tamura A, Yoshimoto K, Kojima S, Yamashita K, Yamanaka I, Otsuka H, Kataoka K, Nagasaki Y. Biointerphases. 2007; 2:126–130. [PubMed: 20408648]
335. Chen A, Kozak D, Battersby BJ, Forrest RM, Scholler N, Urban N, Trau M. Langmuir. 2009; 25:13510–13515. [PubMed: 19928944]
336. Nagasaki Y, Kobayashi H, Katsuyama Y, Jomura T, Sakura T. J Colloid Interface Sci. 2007; 309:524–530. [PubMed: 17368469]
337. Yoshimoto K, Matsumoto S, Asakawa R, Uchida K, Ishii T, Nagasaki Y. Chem Lett. 2007; 36:1444–1445.
338. Mao C, Liu A, Cao B. Angew Chem, Int Ed. 2009; 48:6790–6810.
339. Jeon CS, Hwang I, Chung TD. Adv Funct Mater. 2013; 23:1484–1489.
340. Kwak E-A, Jaworski J. J Mater Chem B. 2013; 1:3486–3493.
341. Park J-S, Cho MK, Lee EJ, Ahn KY, Lee KE, Jung JH, Cho Y, Han S-S, Kim YK, Lee J. Nat Nanotechnol. 2009; 4:259–264. [PubMed: 19350038]
342. Tajima N, Takai M, Ishihara K. Anal Chem. 2011; 83:1969–1976. [PubMed: 21338074]
343. Saha B, Evers TH, Prins MWJ. Anal Chem. 2014; 86:8158–8166. [PubMed: 25048623]
344. Lin PC, Weinrich D, Waldmann H. Macromol Chem Phys. 2010; 211:136–144.
345. Jonkheijm P, Weinrich D, Schröder H, Niemeyer CM, Waldmann H. Angew Chem, Int Ed. 2008; 47:9618–9647.
346. Arrabito G, Reisewitz S, Dehmelt L, Bastiaens PI, Pignataro B, Schroeder H, Niemeyer CM. Small. 2013; 9:4243–4249. [PubMed: 23881817]
347. Seo JS, Lee S, Poulter CD. J Am Chem Soc. 2013; 135:8973–8980. [PubMed: 23746333]
348. Gauchet C, Labadie GR, Poulter CD. J Am Chem Soc. 2006; 128:9274–9275. [PubMed: 16848430]
349. Choi S, Goryll M, Sin L, Wong P, Chae J. Microfluid Nanofluid. 2011; 10:231–247.
350. West J, Becker M, Tombrink S, Manz A. Anal Chem. 2008; 80:4403–4419. [PubMed: 18498178]
351. Nge PN, Rogers CI, Woolley AT. Chem Rev. 2013; 113:2550–2583. [PubMed: 23410114]
352. White AK, VanInsberghe M, Petriv OI, Hamidi M, Sikorski D, Marra MA, Piret J, Aparicio S, Hansen CL. Proc Natl Acad Sci U S A. 2011; 108:13999–14004. [PubMed: 21808033]
353. Spurgeon SL, Jones RC, Ramakrishnan R. PLoS One. 2008:3.
354. Tan WH, Takeuchi S. Proc Natl Acad Sci U S A. 2007; 104:1146–1151. [PubMed: 17227861]
355. Derveaux S, Stubbe BG, Braeckmans K, Roelant C, Sato K, Demeester J, De Smedt SC. Anal Bioanal Chem. 2008; 391:2453–2467. [PubMed: 18458889]
356. Ayas S, Cupallari A, Ekiz OO, Kaya Y, Dana A. ACS Photonics. 2013; 1:17–26.
357. Ozcan A. Lab Chip. 2014; 14:3187–3194. [PubMed: 24647550]
358. Wei Q, Qi H, Luo W, Tseng D, Ki SJ, Wan Z, Göröcs Z, Bentolila LA, Wu TT, Sun R, Ozcan A. ACS Nano. 2013; 7:9147–9155. [PubMed: 24016065]
359. Yuan J, Zhao X, Wang X, Gu Z. Sci Rep. 2014; 4:6755. [PubMed: 25341876]
360. Laksanasopin T, Guo TW, Nayak S, Sridhara AA, Xie S, Olowookere OO, Cadinu P, Meng F, Chee NH, Kim J, Chin CD, Munyazesa E, Mugwaneza P, Rai AJ, Mugisha V, Castro AR, Steinmiller D, Linder V, Justman JE, Nsanzimana S, Sia SK. Science Translational Medicine. 2015; 7:273re1.

361. Ateya DA, Erickson JS, Howell PB Jr, Hilliard LR, Golden JP, Ligler FS. Anal Bioanal Chem. 2008; 391:1485–1498. [PubMed: 18228010]
362. Rosenauer M, Buchegger W, Finoulst I, Verhaert P, Vellekoop M. Microfluid Nanofluid. 2011; 10:761–771.
363. Cho SH, Chen CH, Tsai FS, Godin JM, Lo Y-H. Lab Chip. 2010; 10:1567–1573. [PubMed: 20379604]
364. Schmidt H, Hawkins AR. Nat Photonics. 2011; 5:598–604.
365. Fan X, White IM. Nat Photonics. 2011; 5:591–597. [PubMed: 22059090]
366. Cubillas AM, Unterkofler S, Euser TG, Etzold BJM, Jones AC, Sadler PJ, Wasserscheid P, Russell PSJ. Chem Soc Rev. 2013; 42:8629–8648. [PubMed: 23753016]

Biographies

Yuankui Leng

Yuankui Leng earned his bachelor's degree in 2010 on materials science from Zhejiang University. He then started pursuing his PhD at School of Materials Science and Engineering & State Key Lab of Metal Matrix Composites of Shanghai Jiao Tong University under the supervision of Dr Kang Sun & Dr Wanwan Li. He is focused on the development of optical/magnetic nanoparticle encoded microspheres for multiplexed bio-assays towards his PhD thesis.

Kang Sun

Kang Sun obtained his PhD in materials science from Shanghai Jiao Tong University of China in 1995, then he joined School of Materials Science and Engineering & State Key Lab of Metal Matrix Composites of Shanghai Jiao Tong University, where he was promoted to a Professor in 2003. His research concerns microscale and nanoscale organic/inorganic composite materials and their applications on biomedical diagnosis & therapy. He has published more than 100 articles in scientific peer-reviewed international journals and peer-reviewed papers in these fields.

Xiaoyuan Chen

Xiaoyuan Chen received his PhD in chemistry from the University of Idaho in 1999. He joined the University of Southern California as an Assistant Professor of Radiology in 2002. He then moved to Stanford University in 2004 and was promoted to an Associate Professor in 2008. In the summer of 2009, he joined the Intramural Research Program of the NIBIB as a tenured Senior Investigator and the Chief of the Laboratory of Molecular Imaging and Nanomedicine (LOMIN). Dr Chen has published over 450 papers and numerous books and book chapters. He sits on the editorial board of over 10 peer-reviewed journals and is the founding editor of the journal “Theranostics”. He is interested in developing molecular imaging modalities for better understanding of early diagnosis of disease, monitoring therapy response, and guiding drug discovery/ development. His lab also puts a special emphasis on high-sensitivity nanosensors for biomarker detection and theranostic nanomedicine.

Wanwan Li

Wanwan Li obtained his PhD in materials science from Shanghai University of China in 2004, then he joined the School of Materials Science and Engineering & State Key Lab of Metal Matrix Composites of Shanghai Jiao Tong University in 2005, where he was promoted to a Professor in 2013. During 2012 to 2013, he joined the Laboratory of Molecular Imaging and Nanomedicine (LOMIN) at the National Institute engineering (NIBIB) as a visiting scholar. His research concerns fabrication of inorganic nanocrystals, organic–inorganic hierarchical assemblies, and their applications on biomedical diagnosis & therapy. He has published more than 50 articles in scientific peer-reviewed international journals.

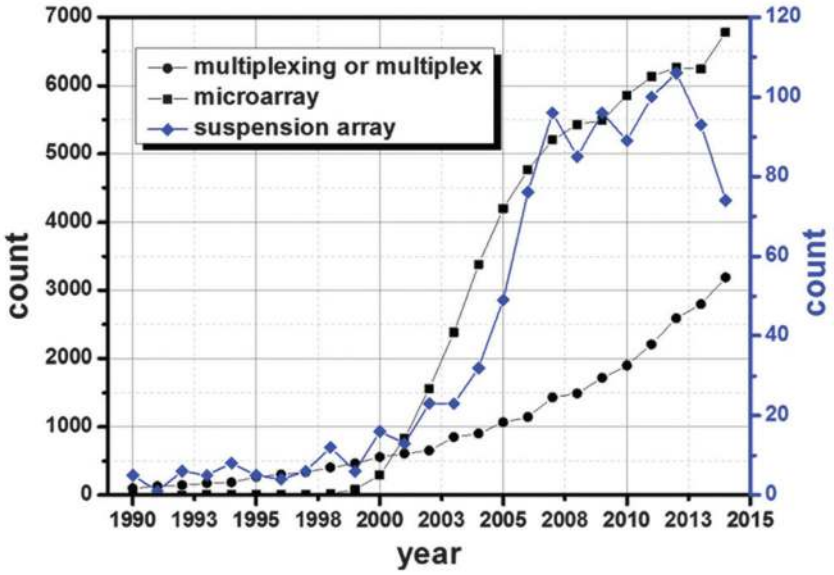

Fig. 1.

The growing interest in multiplexing. A PubMed search illustrating the cumulative numbers of manuscripts by year, containing the keywords ‘multiplexing or multiplex’, ‘microarray’, and ‘suspension array’.

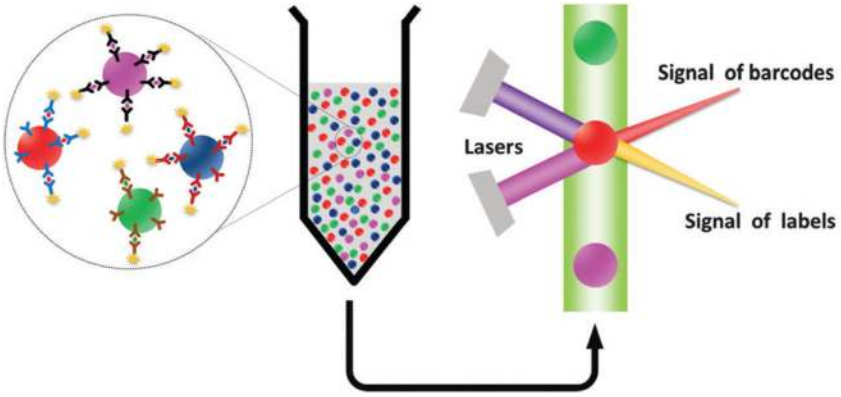

Fig. 2.

Schematic illustration of a typical suspension array platform. The target of interest is identified by the barcode signal and quantified by the label signal.

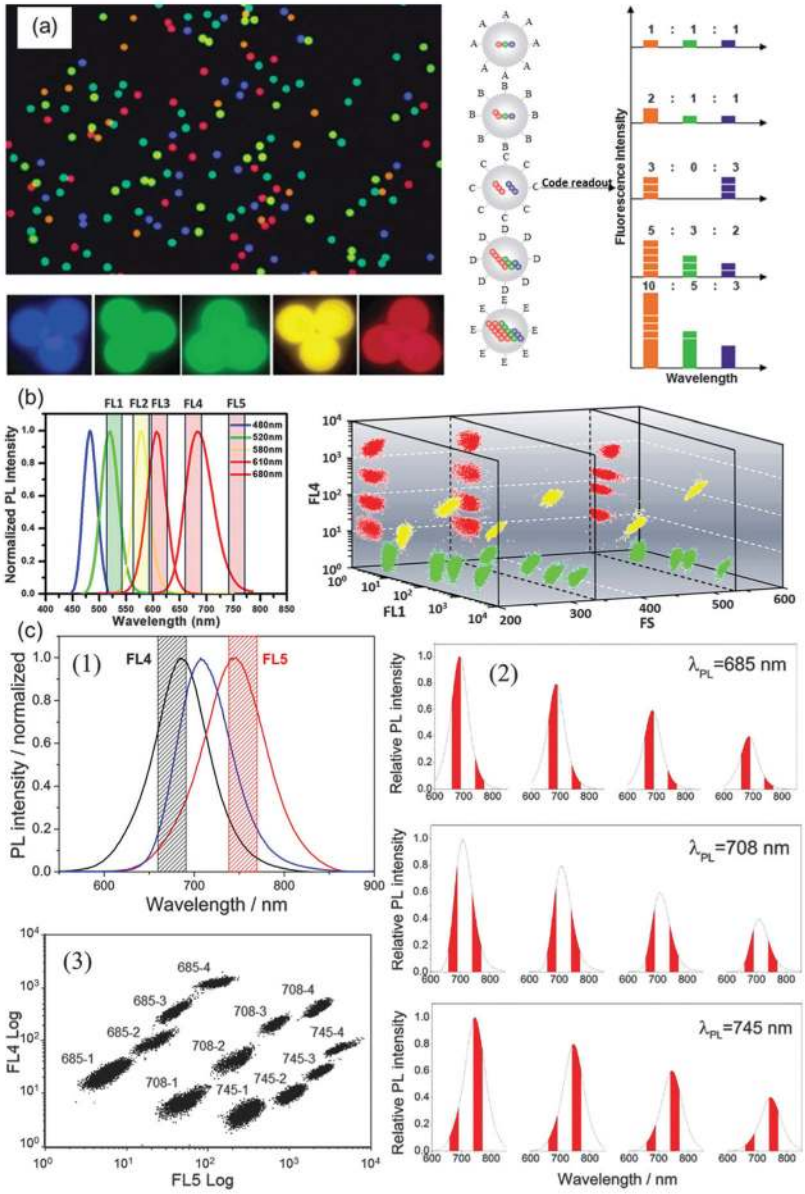

Fig. 3.

(a) The most commonly used encoding principle utilizes colors and intensity levels; (b) A 3D encoding method that combines color, intensity level, and microsphere size; The fluorescent signals from QDs are detected by the flow cytometer's FL1, FL4 fluorescence detection channels, while the size of the microsphere is correlated with the signal intensity of the FS (forward scattering) channel; (c) single wavelength encoding, which is based on the channel ratio (FL4/FL5) and the intensity level. (c-1) The relationship between the PL peak wavelength of 685 nm, 708 nm, and 745 nm QD-encoded microspheres and FL4, FL5 fluorescent detection channels of a flow cytometer. (c-2) Schematic of the relationship of the different barcodes corresponding to FL4 and FL5 fluorescence detection channels of the flow cytometer with wavelength and intensity. (c-3) Fluorescence barcode matrices of 685,

708, and 745 nm QD-encoded microbeads on a flow cytometric FL5-FL4 plot diagram.[12,30,66,68]

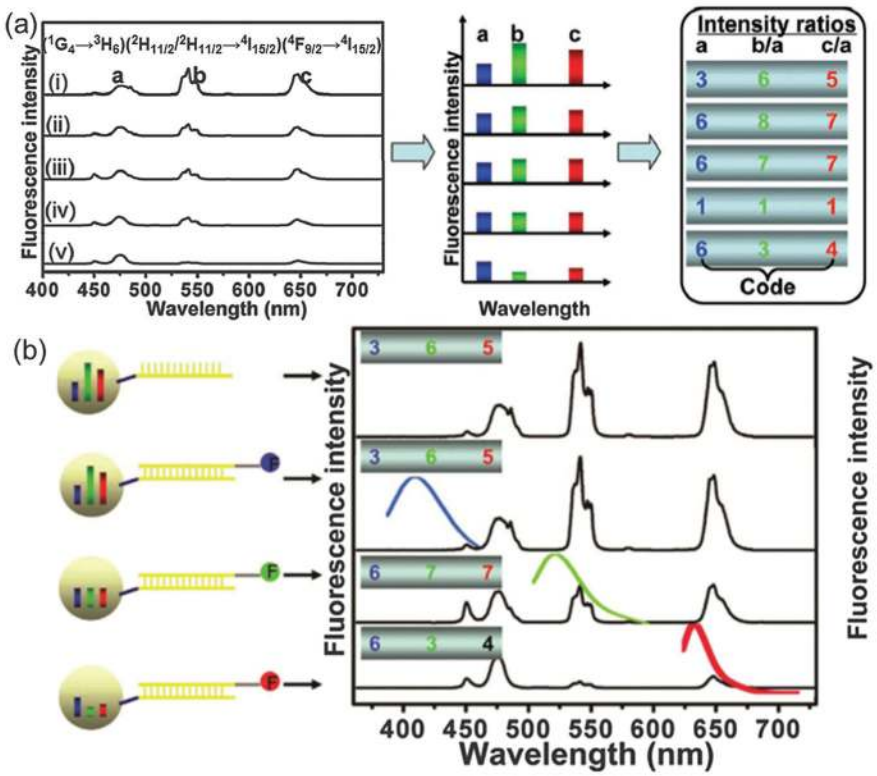

Fig. 4.

(a) Fluorescence signals obtained from the $NaYF_4$:Yb/Ho/Tm (with different Tm doping amounts) upconversion nanocrystal encoded beads. Both the absolute intensities and relative intensity ratios of different emissions are used for coding purposes. (b) Suspension arrays for nucleic acid detection, with different organic dyes used as labels for different targets.[16]

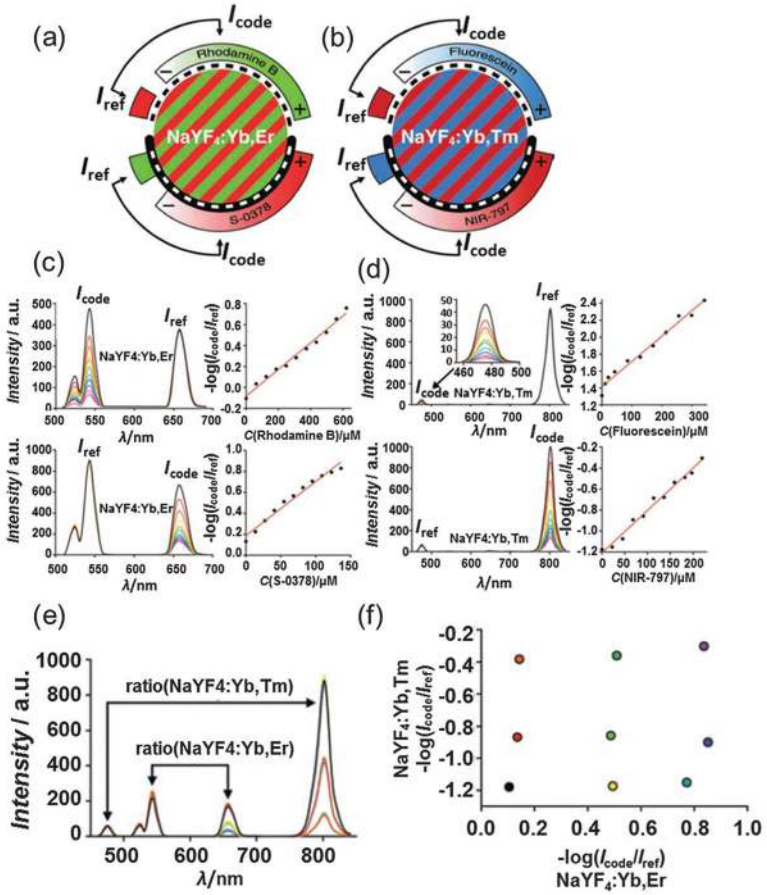

Fig. 5.

Tuning the dual emission bands of two types of upconverting nanoparticles by coating selected organic dyes. (a) Different concentrations of either rhodamine B or the dye S-0378 are used to screen off selectively either the green or the red emission band of $NaYF_4$:Yb,Er UCNPs to various degrees. (b) Fluorescein or the dye NIR-797 is used to screen off the blue or the near-infrared emission band of $NaYF_4$:Yb,Tm UCNPs. (c) $NaYF_4$:Yb,Er UCNPs are coated with various concentrations of either rhodamine B (top) or the dye S-0378 (bottom). Ten different concentrations of rhodamine B are used to selectively reabsorb the green (λ_{max} = 543 nm) emission while the red (λ_{max} = 657 nm) emission remains constant. A linear function is obtained by plotting $-\log(I_{code}/I_{ref})$ against the concentration of rhodamine B. Alternatively, the intensity of the NIR emission can be selectively tuned by S-0378. (d) NaYF4:Yb,Tm upconversion nanoparticles display dual emission lines that can be individually tuned by either fluorescein for the blue emission (λ_{max} = 475 nm) or NIR-797 for the NIR emission (λ_{max} = 802 nm). (e) Mixing equal amounts of NaYF4:Yb,Er and NaYF4:Yb,Tm, which have been tuned by S-0378 and NIR-797, each exhibiting three different values of $-\log(I_{code}/I_{ref})$ and yielding nine (3^2) ratiometric codes. (f) A 2D matrix of the coding combinations. The ratiometric coding elements are independent of absolute signal intensities and are well separated, leading to ready identification.[79]

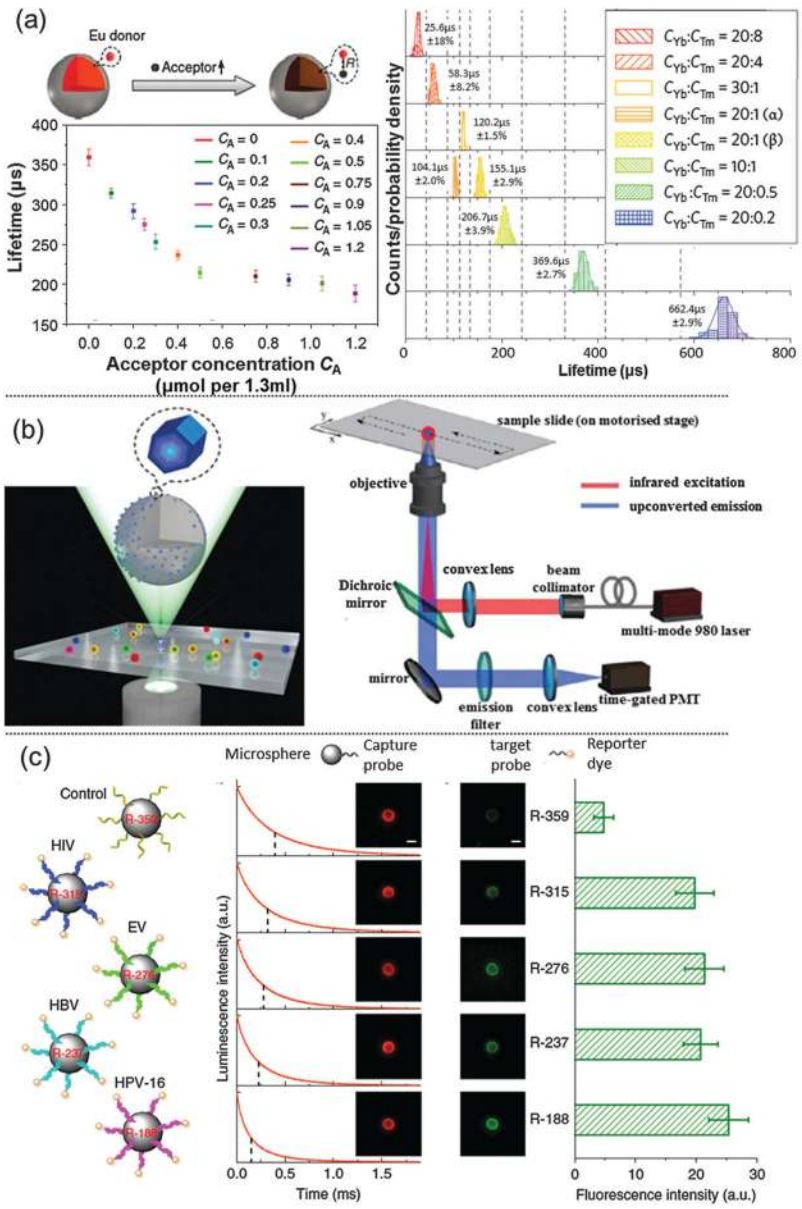

Fig. 6.

(a) Eu-LRET barcodes (left) (donor: Eu complex of thenoyltrifluoroacetonate; Acceptor: hexafluorophosphate salt of cationic coumarin) and τ-dots-encoded populations of microsphere barcodes (right). (b) Concept of τ-dots-encoded microspheres-based lifetime multiplexing suspension array (left), the microsphere barcodes embedded with Tm doped UCNPs can be decoded by the time-resolved scanning cytometry system (right). (c) Lifetime-encoded Eu-LRET microsphere-based multiplexed DNA detection and time-resolved OSAM decoding. The five selected Eu-LRET microsphere barcodes were conjugated to five different DNA sequences, with Qdot 565 used as a universal reporter dye in the bead-based assay. The microspheres were identified based on their lifetime codes while the amount of target DNA in the test samples was determined by the intensities of the fluorescence reporters.[17,100]

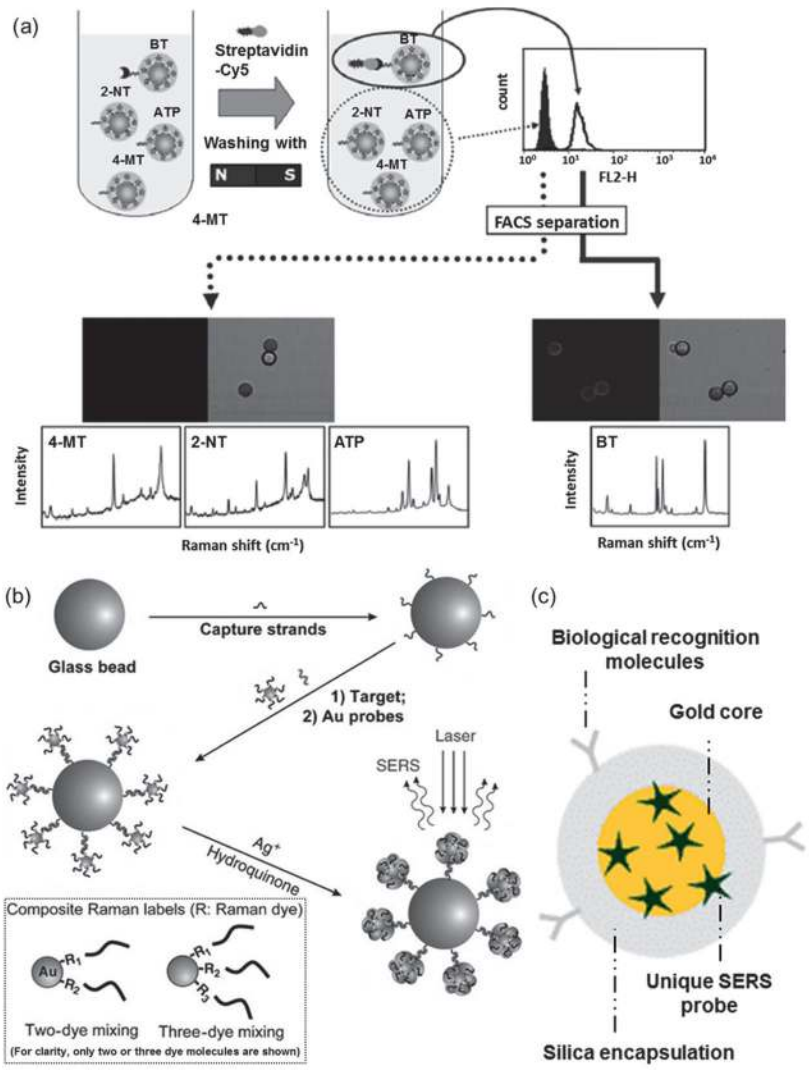

Fig. 7.

(a) SERS barcode microsphere-based suspension assay; (b) suspension assay that uses SERS dots as barcode labels. (c) Nanoplex™ biotag.[125,127,128]

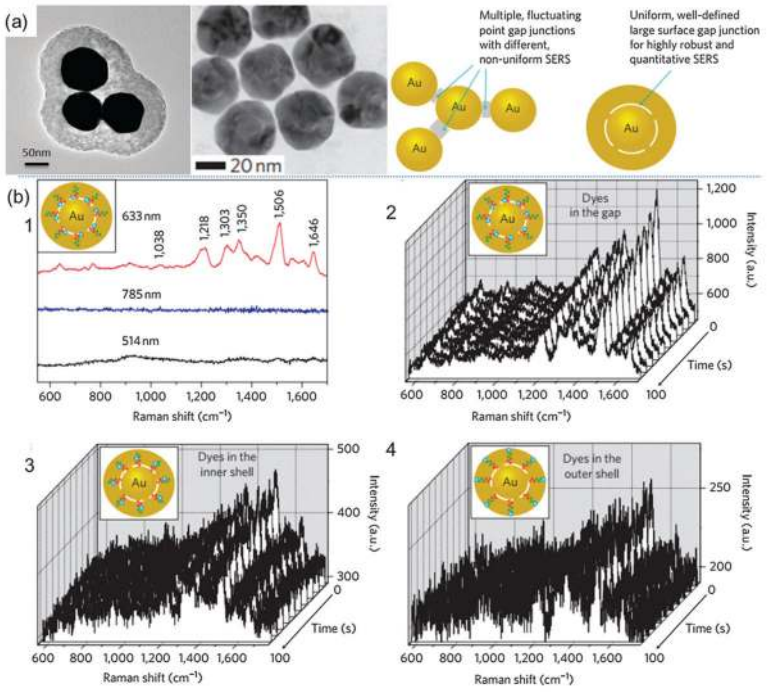

Fig. 8.

(a) TEM images and schematic diagrams of a SERS probe with a multimeric, inter-nanogap structure (left) and a monomeric SERS probe with an interior nanogap structure (right). The monomeric interior nanogap structure has a more uniform surface gap junction, resulting in uniform SERS. (b) Excitation wavelength and dye position dependence of SERS of gold nanobridged nanogap particles (Au-NNPs) in solution. All spectra (2–4) were acquired under the same detection conditions at the same particle concentration.[132,134]

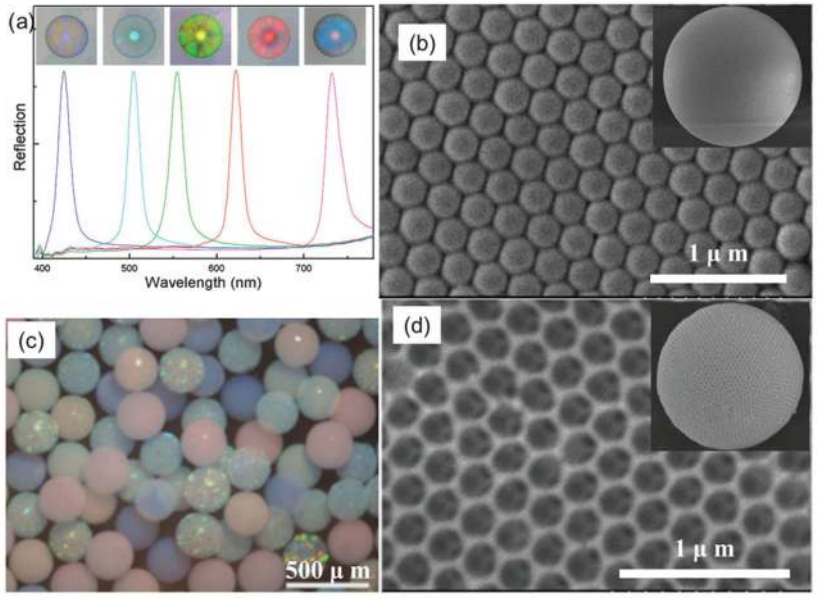

Fig. 9.

(a) Reflection spectra of the opal photonic crystal beads (PCBs) composed of silica nanoparticles with different sizes (left to right, 200, 225, 240, 260, and 295 nm) and (b) the SEM image of opal PCB surface, the inset is a 200 μm opal PCB; (c) the 3D image of the seven kinds of inverse-opaline PCBs in water and (d) the SEM image of the inverse-opaline photonic bead surface. Inset is a 10 μm inverse-opaline PCB.[60,143]

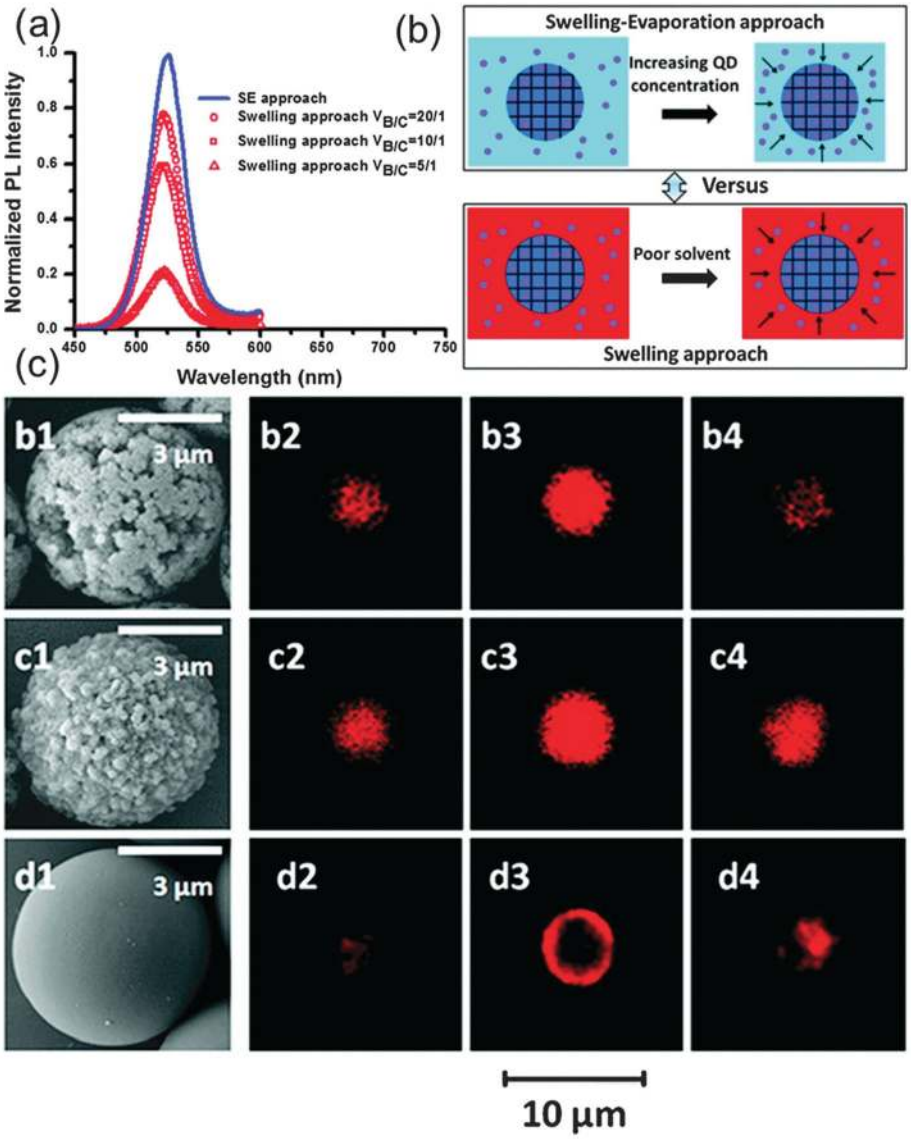

Fig. 10.

(a) and (b) Swelling–Evaporation (SE) method *versus* the swelling method originally proposed by Nie *et al.* (a) Fluorescence spectra of 525 nm QD-microspheres prepared by the two methods. $V_{B/C}$ is the volume ratio of butanol to chloroform. (b) The use of different primary diffusion driving forces in both the SE and the swelling approaches. (c) SEM images and laser confocal fluorescence images of microspheres with suitable pores (b1)–(b4), microspheres with exceedingly large pores (c1)–(c4), and nonporous microspheres (d1)–(d4).[149]

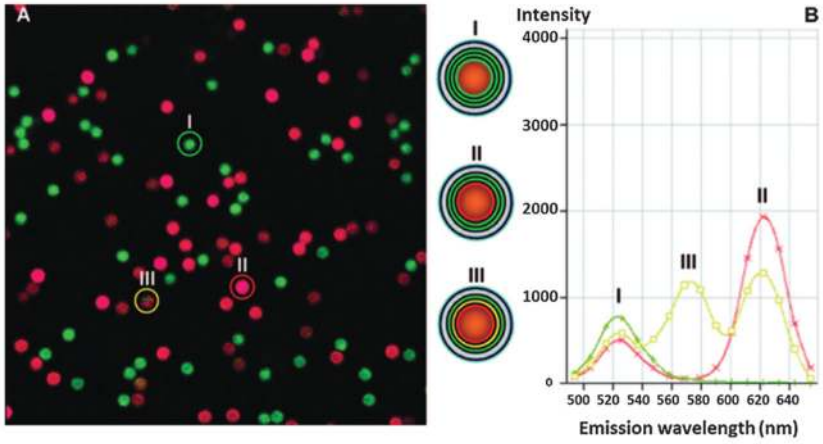

Fig. 11.

(A) Confocal laser scanning microscopy (CLSM) image of three sets of microspheres encoded with (I) three layers of green QDs (three green layers), (II) one red layer and two green layers, and (III) one red layer, one yellow layer, and one green layer. (B) The emission spectrum of one (circled) microsphere from each set. Colors of the circles correspond to the line colors of the emission spectra indicated in panel B.[157]

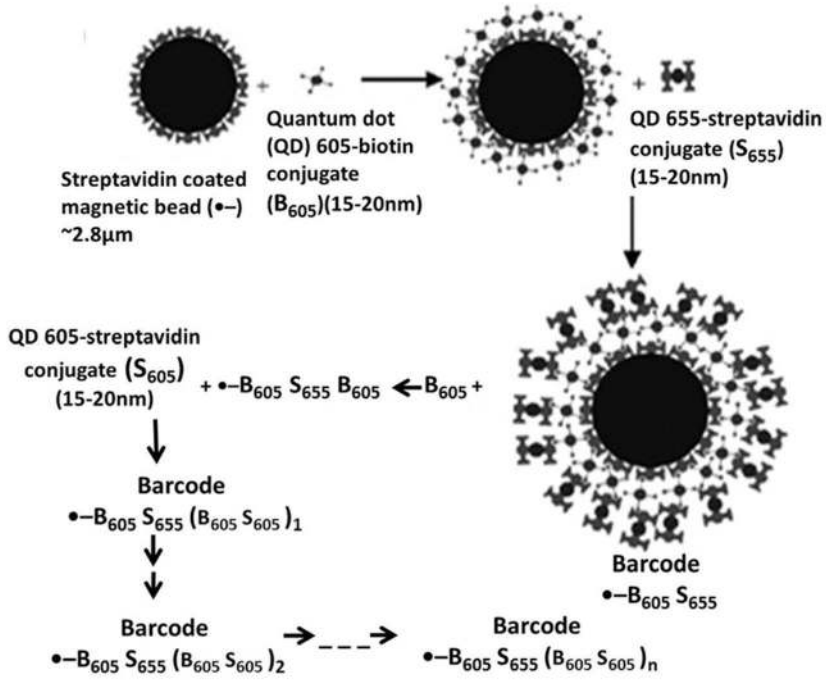

Fig. 12.

Schematic illustration for fabricating inorganic nanoparticle–composite microspheres using the LBL method and *via* the interaction of biological molecules[159]

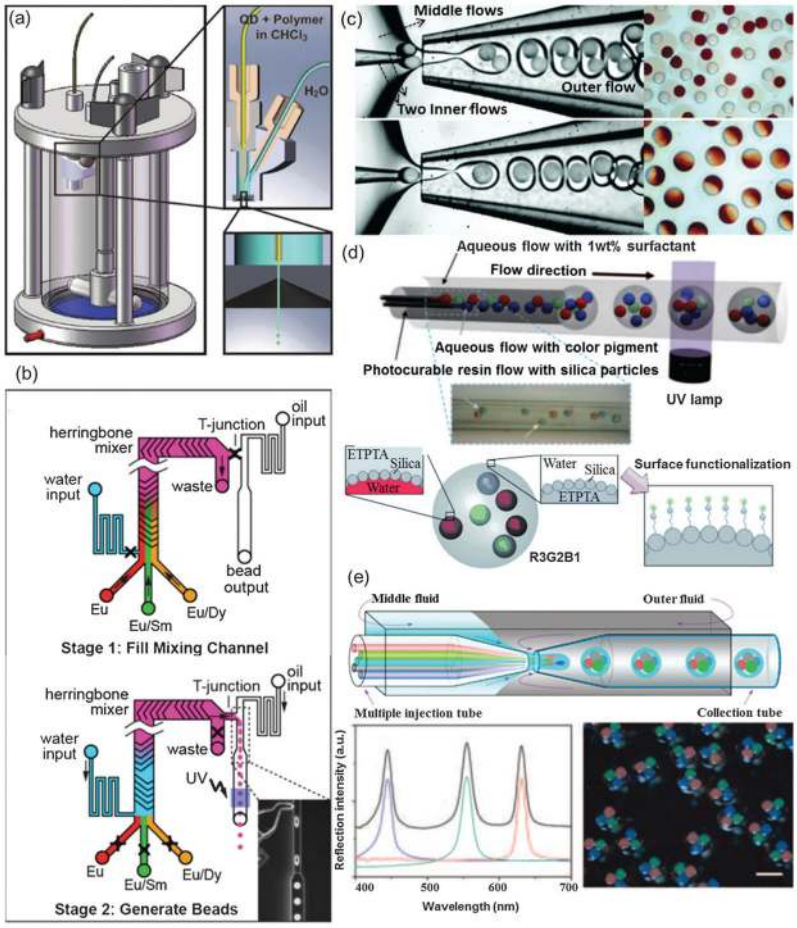

Fig. 13.

Schematic illustration of the fabrication of inorganic nanoparticle–composite microspheres by using various microfluidic devices. Microfluidic generation of monodispersed, single emulsions: (a) a concentration-controlled, flow-focusing (CCFF) device for the preparation of QD barcodes. (b) Lanthanide nanophosphor-encoded microsphere synthesis using a microfluidic device. Stage 1: hydrophilic lanthanide nanoparticle (Eu alone (red), Eu/Sm (green), Eu/Dy (orange)) suspended pre-polymer mixture is mixed on the chip using a herringbone mixer. Stage 2: water (blue) pushes the lanthanide mixture (pink) towards a T-junction, where the water phase breaks it into droplets (inset high-magnification image) by a continuously flowing oil stream. Droplets are polymerized into beads *via* illumination of a downstream UV light and collected for later use. (c) Anisotropic magnetic barcode microspheres prepared *via* controlled double emulsification by using a microfluidic device with two inner jets. (d) Multicore-encoded microsphere with silica particle arrays at the inner and outer surfaces produced *via* double emulsification. (e) Schematic of the capillary microfluidic device used to generate the multiple core double emulsions (top), 3D image and reflection spectra of four-core barcodes with red, green, and blue opal photonic crystal cores and one magnetic core (bottom).[65,82,145,181,185]

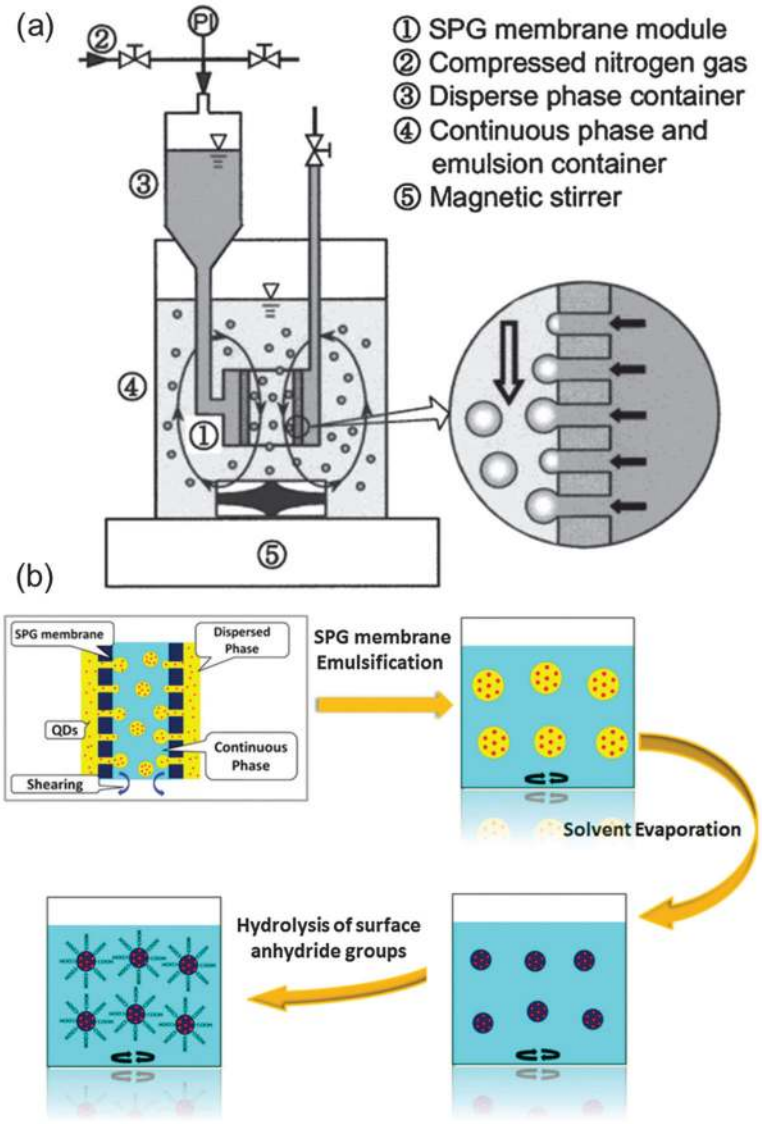

Fig. 14.

(a) Schematic diagram of a SPG membrane emulsification device and the process; (b) schematic illustrating the preparation of carboxylated QD barcodes by a SPG membrane emulsification-solvent evaporation approach.[30,189]

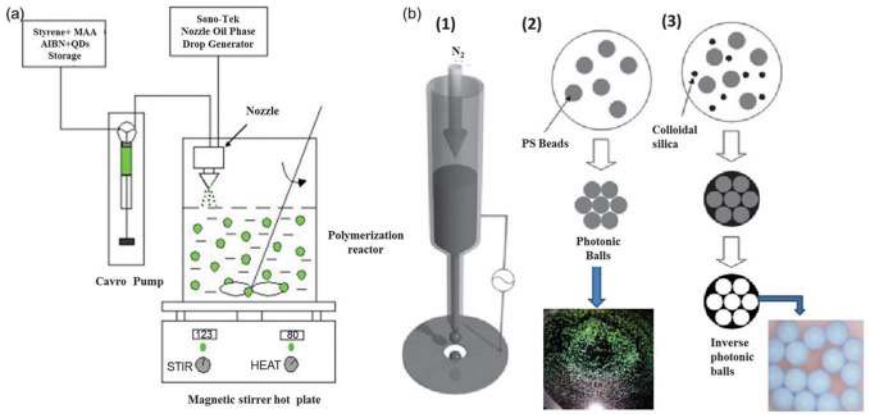

Fig. 15.

(a) Schematic of the experimental set up for the spraying suspension polymerization technique. (b) Preparation of monodisperse opaline photonic crystal balls (2) and inverse opaline photonic crystal balls (3) *via* an electro-spraying method (1).[165,191]

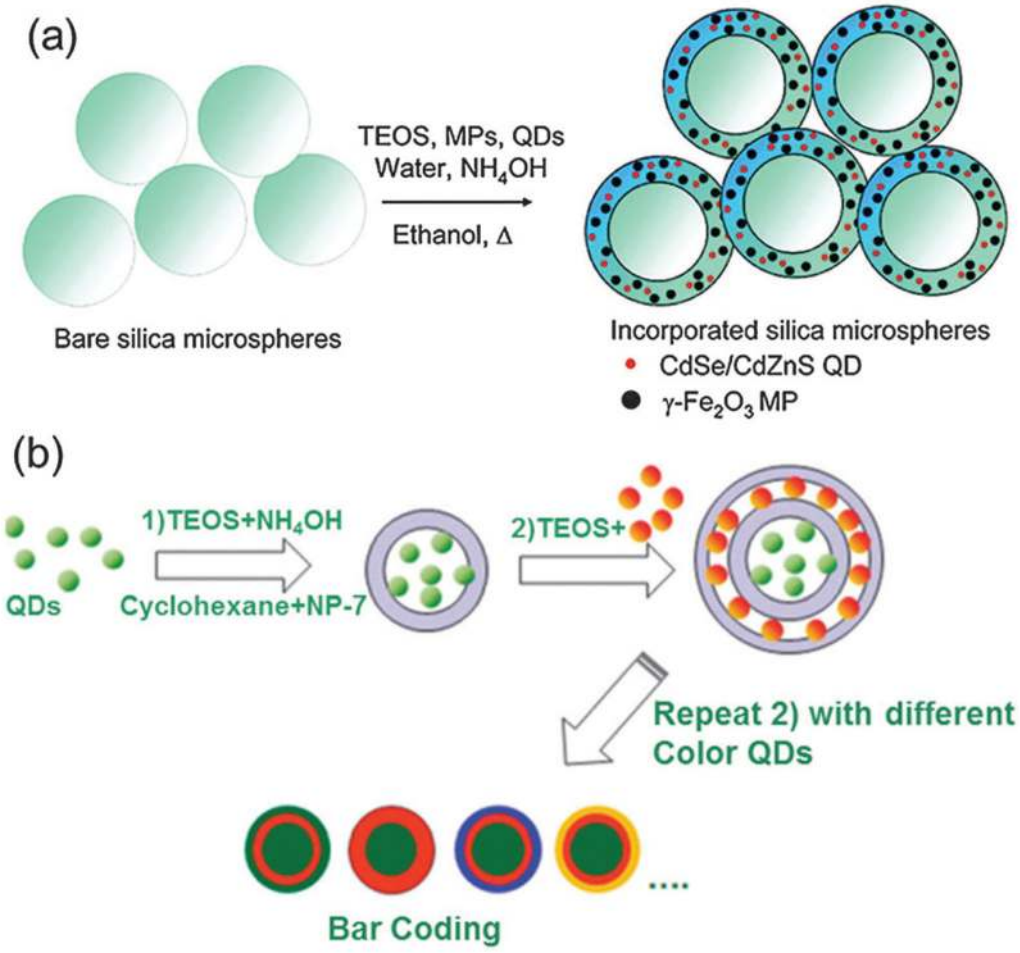

Fig. 16.

(a) Silica-shell-encapsulated nanoparticles made by a sol–gel process (b) Illustration of the procedure used to prepare multiplexed, color-encoded silica nanospheres encapsulating QDs multilayers.[194,196]

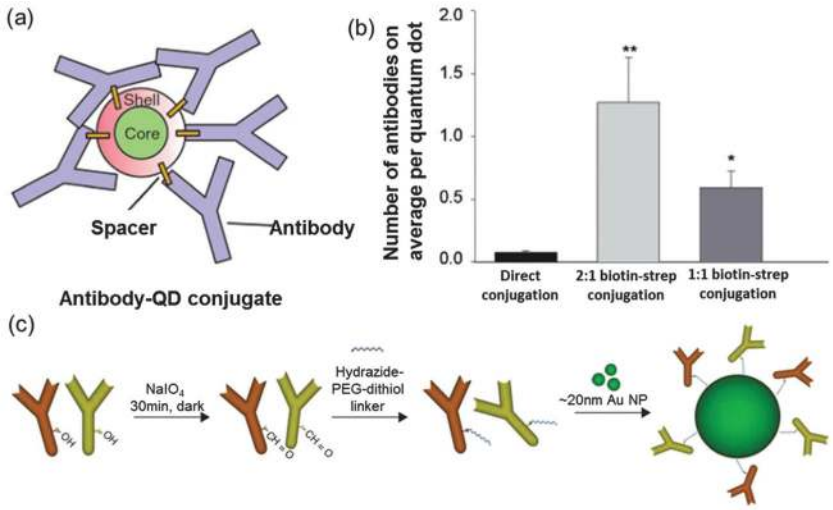

Fig. 17.

(a) Schematics of a QD-antibody conjugate (direct conjugation). Most antibodies show worst-case orientations, meaning that the recognition site (Fab region) of the antibody is oriented close to the support surface, resulting in a lack of target binding. (b) A comparison for two conjugation schemes using calculated values for the average number of antibodies available for target binding on the QD surfaces. (c) Directional-oriented conjugation of antibodies to AuNPs.[57,227,228]

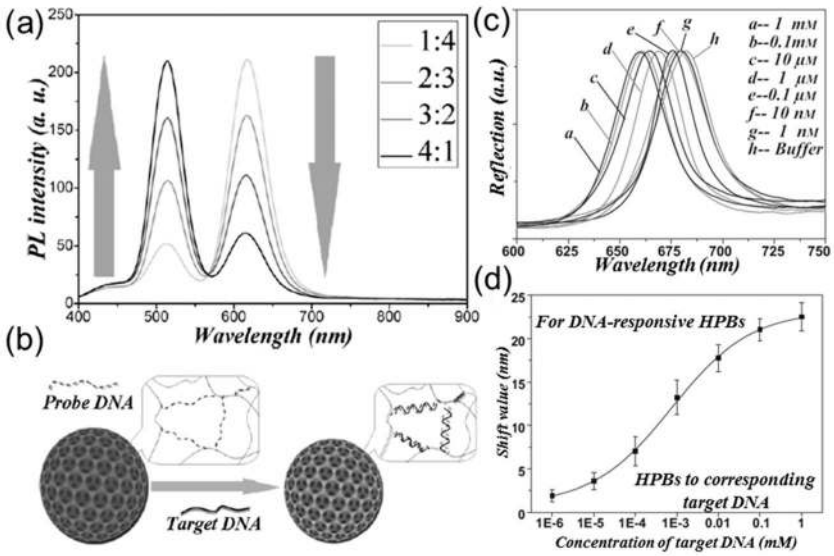

Fig. 18.

(a) Encoding inverse opal colloidal photonic crystal beads by incorporating multicolor QDs into the beads at different intensities. (b) Schematic diagram of the DNA-responsive hydrogel photonic bead-based, label-free DNA detection (c) optical response (reflection-peak shift) of the DNA-responsive hydrogel photonic beads incubated with their corresponding target DNA at different concentrations. (d) Reflection-peak shift of the DNA-responsive hydrogel photonic beads (HPBs) incubated in their corresponding target DNA with different concentrations.[15]

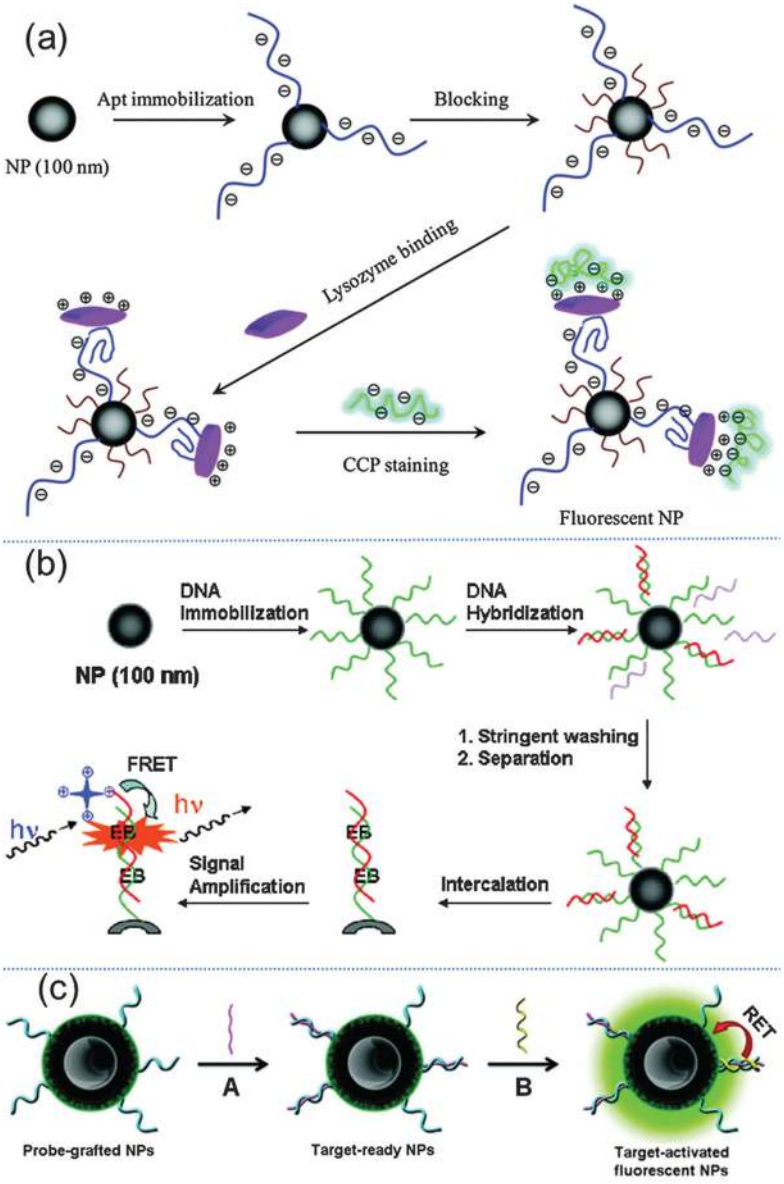

Fig. 19.

Label-free, bead-based assay using conjugate polymers (CP) as signal transducers. (a) Label-free lysozymal detection with aptamer-immobilized silica NP and CPs.[235] (b) FRET-based, label-free SNP DNA detection scheme.[236] (c) DNA detection on fluorescent multilayer core–shell NPs *via* plasmonics-enhanced FRET.[237]

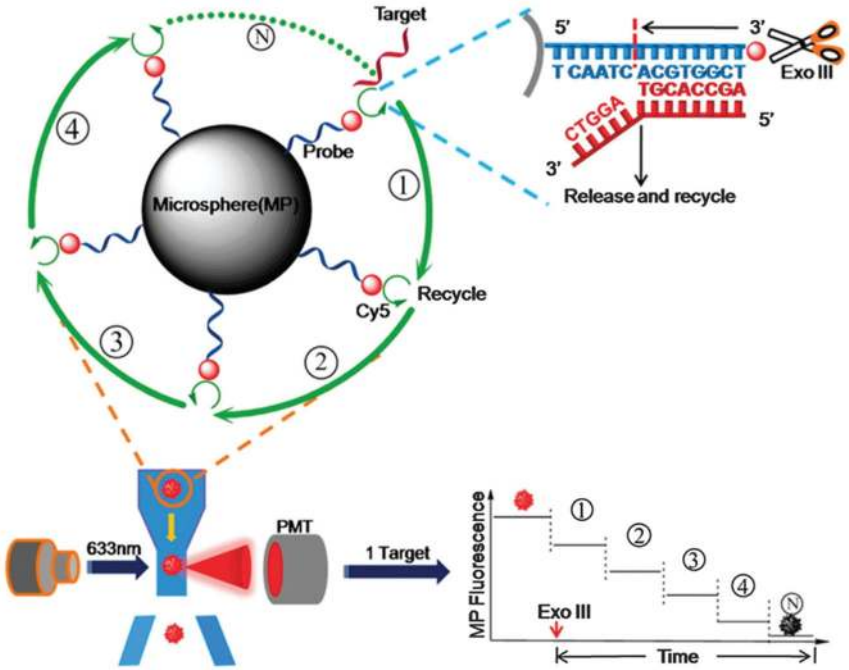

Fig. 20.

Schematic representation of exonuclease III-aided target recycling based amplification flow cytometry, DNA bead assay. Each round of target recycling can remove one Cy5 molecule from the microsphere surface. The resulting drop in fluorescence intensity of individual microspheres that have been functionalized with a Cy5-tagged probe is proportional to the concentration of target DNA. Fluorescence intensity of Cy5 was detected by flow cytometry. As shown in the bottom right graph, the microsphere fluorescence gradually decreased due to the activation of target recycling by exonuclease III.[238]

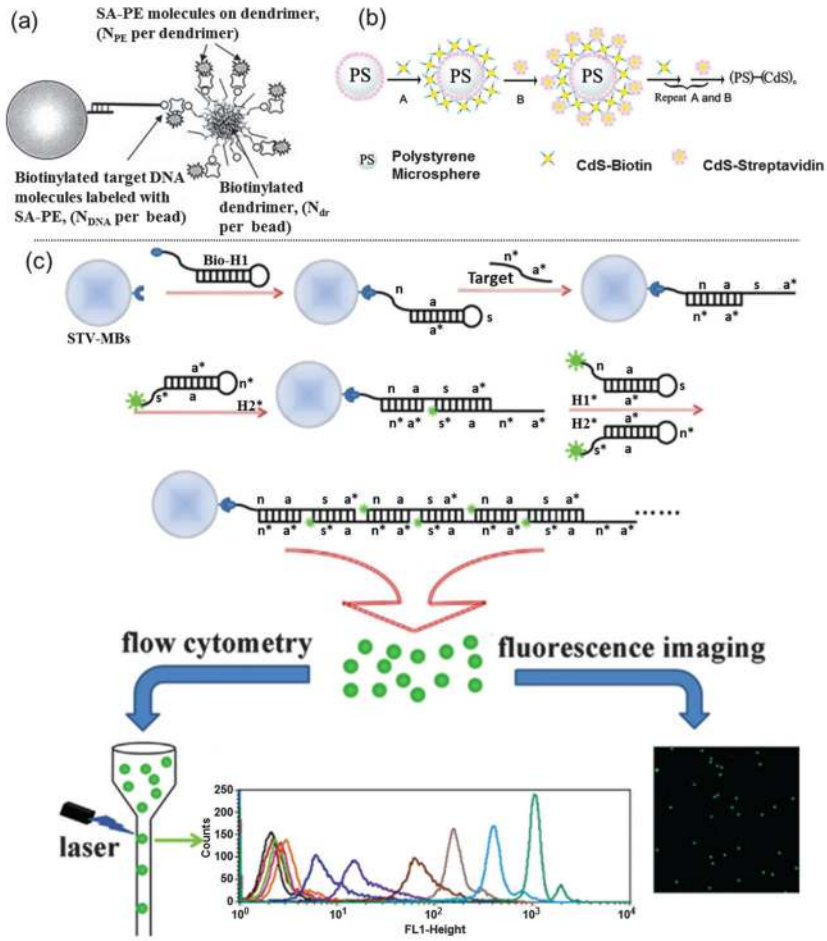

Fig. 21.

(a) Biotinylated dendrimer, (b) biotin–streptavidin system, and (c) hybridization chain reaction-based label amplification methods.[205,206,263]

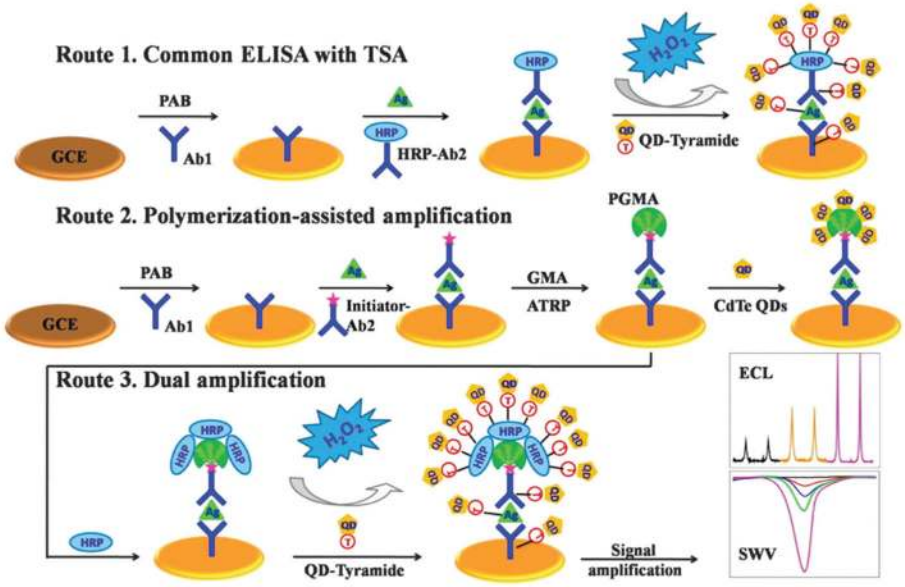

Fig. 22.

Schematic representation of typical tyramide signal amplification (TSA) for common ELISA using QD–tyramide conjugates as labels (route 1), the polymerization-assisted amplification *via* surface-initiated ATRP and subsequent direct binding of CdTe QDs (route 2), and the sandwich immunoassay using QD–tyramide conjugates as labels *via* SI-ATRP and TSA (route 3).[272]

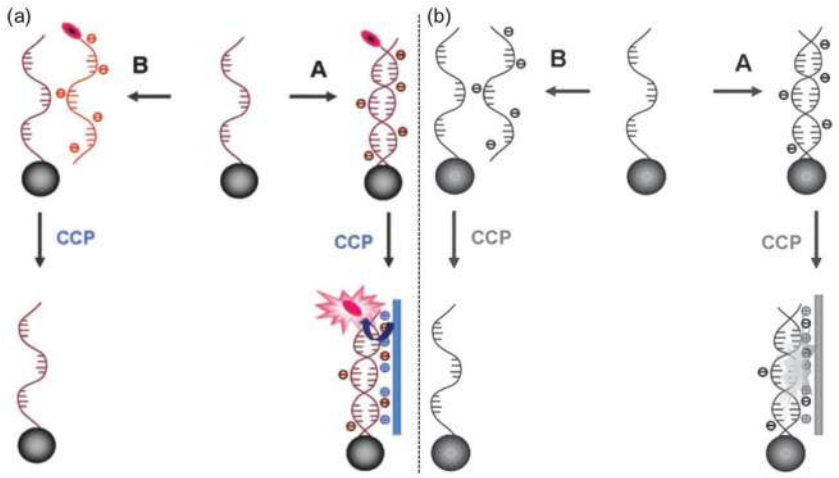

Fig. 23.

Bead-based assay using a cation conjugate polymer (CCP), PFVP as the amplifier (a) or reporter (b). Peptide nucleic acid (PNA) probes immobilized onto PS beads that were hybridized with target DNA. PFVP incorporated into the PNA/DNA duplexes. The Cy5 label (a) and the polymer fluorescence signal (b) were then immediately detected upon excitation at 408 nm.[207]

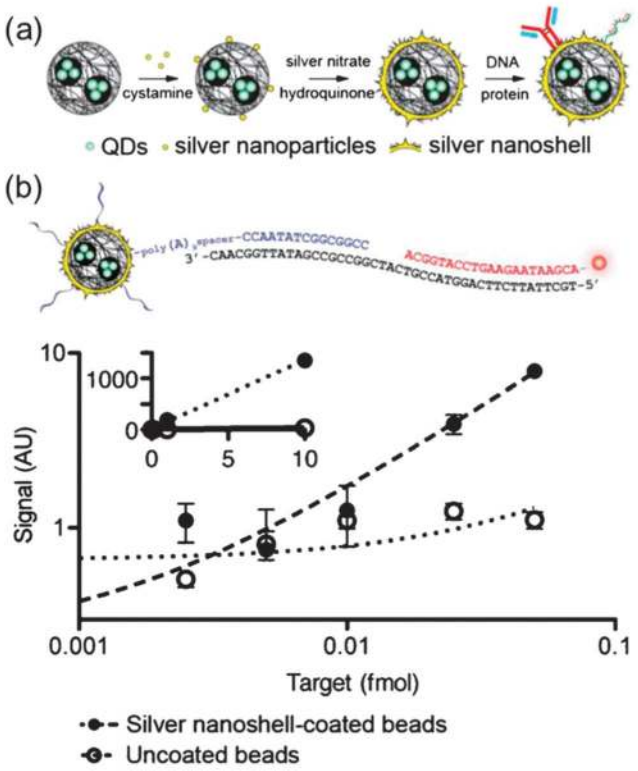

Fig. 24.

(a) Schematic diagram of the fabrication and functionalization process of silver nanoshell-coated QD microbeads. (b) Comparison of assay sensitivities using uncoated and silver nanoshell-coated microbeads.[276]

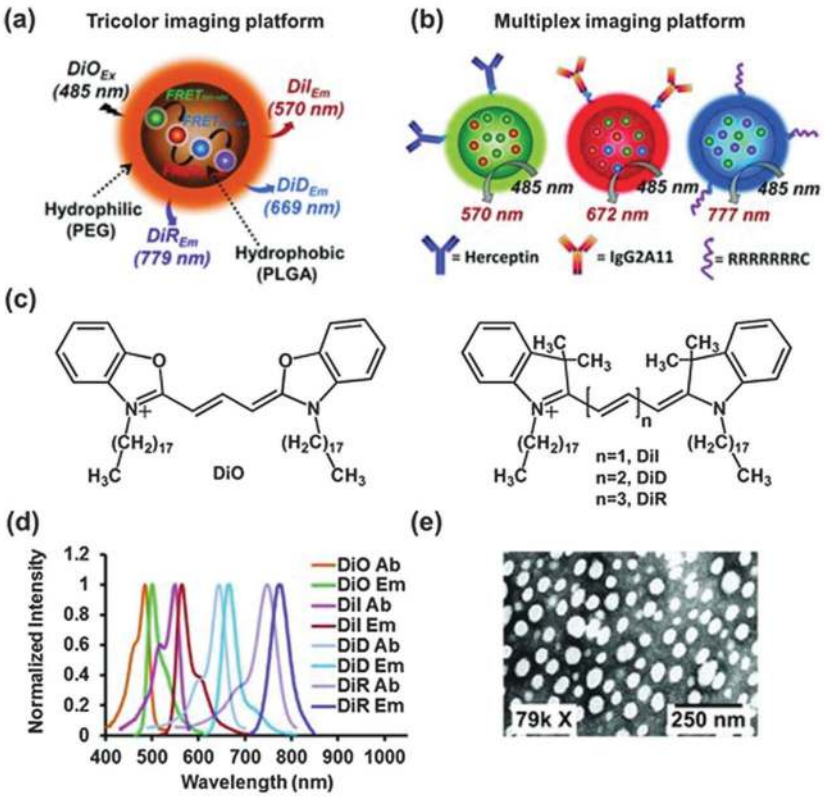

Fig. 25.

Schematic representations of particles designed for (a) multicolor and (b) multiplex imaging. (c) The chemical structures of four lipophilic, carbocyanine-based fluorophores: DiO, DiI, DiD, and DiR. (d) The normalized absorption and fluorescence emission spectra of the fluorophores in methanol. (e) A TEM image of nanoparticles which were negatively stained with 2% (w/v) uranylacetate in deionized water.[280]

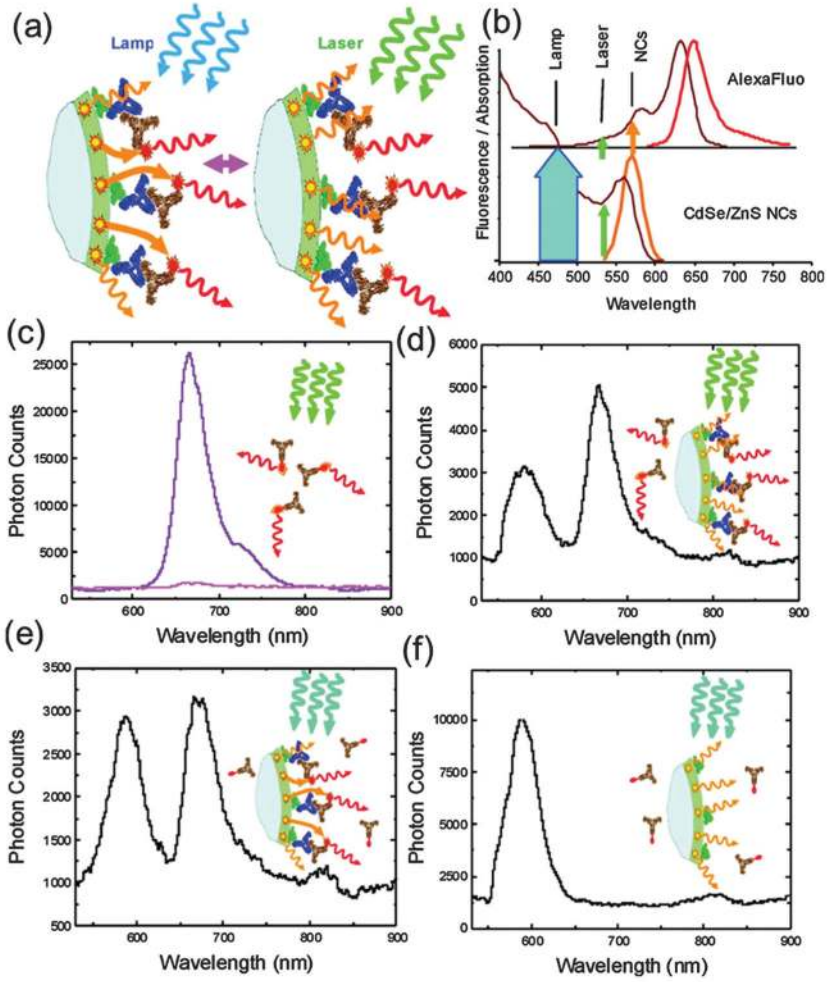

Fig. 26.

Single bead immunoassay. (a) Scheme of a single bead assay, excited by a 532 nm laser or by a 450–500 nm broad band lamp. Microbeads encoded with orange-emitting QDs, coated by monoclonal antibodies, and stained with AlexaFluor633-labeled secondary antibodies. (b) Absorption and emission spectra of QDs and AlexaFluor633. The lamp source was chosen to selectively excite QDs but not the dye, while the laser source excites both QDs and dye. (c) Emission spectra of AlexaFluor633-labeled secondary antibody solution under the laser (purple line) and lamp (pink line) excitations. (d) and (e) Emission spectra from a QD microbead with AlexaFluor633 captured on the surface and excited by either the laser (d) or lamp (e). (f) Negative control: no red emission of the AlexaFluor633 label is detected in the absence of a primary antibody and under the QD-selective lamp excitation focused on a single microbead.[288]

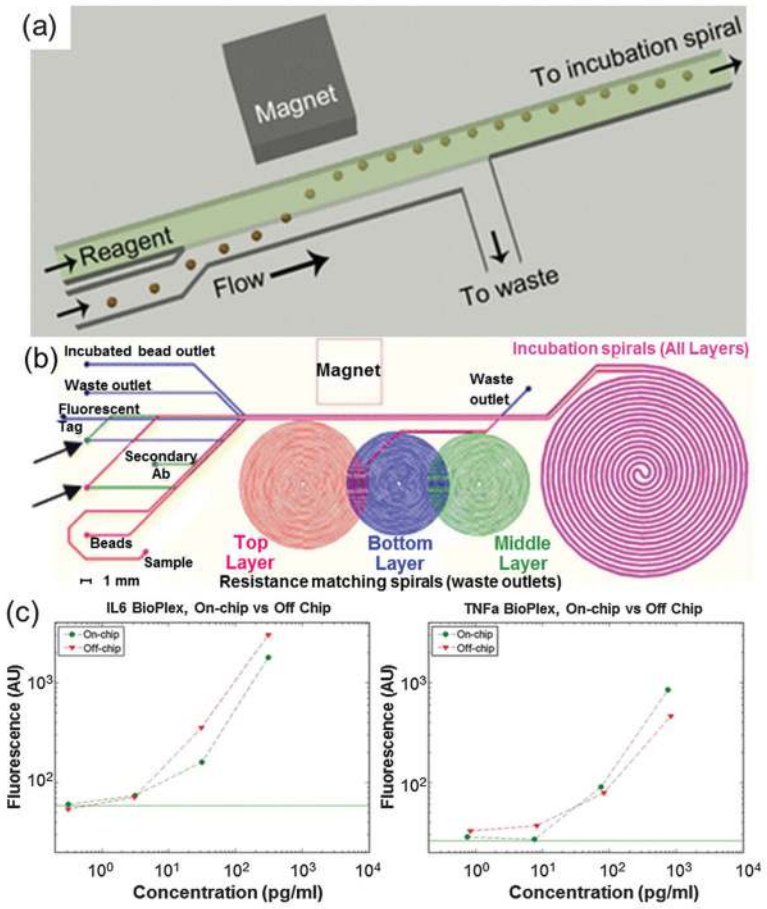

Fig. 27.

(a) Schematic of magnetic-based bead transfer. The external magnet pulls magnetic microbeads from a carrier stream into the reagent stream. The carrier stream is then diverted to waste while microbeads contained within the reagent stream flow to an incubation spiral. The device uses three of these separation regions on three aligned and bonded device layers: first to transfer the microbeads into the plasma sample, second to transfer them into the biotinylated secondary antibody, and third, to transfer them into a streptavidin-PE fluorescent tag. (b) CAD drawing of the entire microfluidic channel layout. The large incubation spiral is identical for all layers. (c) Representative multiplexed calibration curves for a IL-6 (left) and TNF-a (right), compared using an on-chip and off-chip Bio-Plex bead assay.[299]

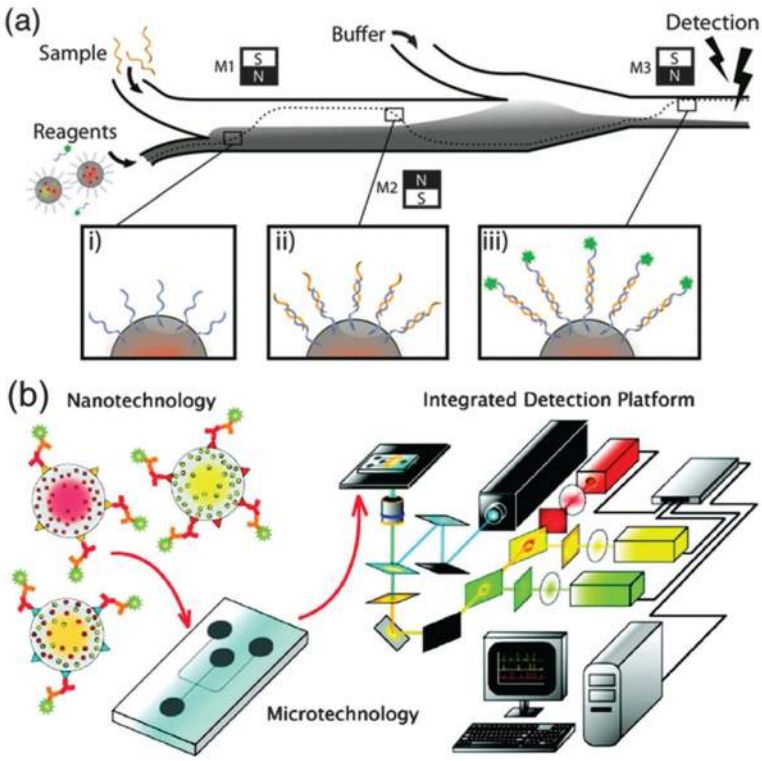

Fig. 28.

(a) Microfluidic biochip capable of automating the entire barcode assay process. Magnetic barcodes were: (i) magnetically attracted toward M1 to capture the target ssDNA in the upper laminar stream, (ii) pulled back to the lower laminar stream and toward M2 to interact with the reporter probe, and (iii) pulled toward M3 to be washed and aligned for detection. (b) Automatic detection platform for suspension arrays composed of a polydimethylsiloxane (PDMS) microfluidic chip, a photon counting detection system, and a signal processing system for deconvolution of QD optical barcode signals.[311,312]

Table 1

Comparison of different encoding methods

Encoding methods	Theoretic encoding capacity	Reported barcode number	Stability	Advantages	Disadvantages or problems to be solved	Ref.
Organic dyes	+ +	Up to 500 (Luminex FLEXMAP 3D™ system)	+	Easy for encoding and decoding; better batch uniformity	Need multiple excitation; limited encoding capacity; poor stability	25
QDs	+ + + +	105 (Warren C. W. Chan *et al.*)	+ + +	Single excitation, narrow emission spectra, providing high encoding capacity	Cross-talk among different QDs (FRET)	65
UCNPs	+ + +	About 10 (Zhang *et al.*)	+ + + +	Single NIR laser for excitation, low background interference	Limited by suitable labels	16
Life-time	+ +	8 (Yiqing Lu *et al.*)	+ + + +	Low background interference	Combination of lifetime, color and intensity for encoding is a challenge; lower decoding speed	17
SERS (encoded carriers)	+ + + +	34 (Jong-Ho Kim *et al.*)	+ + + +	High encoding capacity	Limited by cross-talk between barcodes and fluorescent label; unlikely to produce large numbers of barcodes that have robust and precise readouts	122
SERS (encoded labels)	+ + + +	13 (Mirkn *et al.*)	+ + + +	High encoding capacity; ultrasensitive	Unlikely to produce large numbers of ultrasensitive barcodes that have robust and precise readouts	128
Structure color	+ +	About 10 barcodes with different single structure colors (Gu *et al.*)	+ + + + +	High stability	Limited encoding capacity, lager barcode library has been obtained by combining with QDs; large size limits its multiplexing capacity	60

Chem Soc Rev. Author manuscript; available in PMC 2017 January 10.

Table 2

Comparison of different methods for producing QD barcodes

	Swelling	Layer-by-layer	Polymerization	Concentration-controlled flow-focusing (CCFF)	Membrane emulsification
Synthetic steps	3 or more	More than 3	2	1	1
Purification	Tedious	Tedious	Tedious	No need	No need
Ease of barcoding	Difficult	Easy	Easy	Easy	Easy
Bead monodispersity	Excellent (<3%)	Excellent (<3%)	Poor (>10 000%)	Good (<10%)	Good (<10%)
Size range	100 nm–10 μm	100 nm–100 μm	Undefined	4–20 μm	0.1–20 μm
Yield	High	High	High	Not enough	1000-fold greater than CCFF
Stability	Poor (need protection layer)	Good (due to protection layer)	Good	Good	Good
Bioconjugation	Feasible	Feasible	Feasible	Feasible	Feasible
Problems for application	Poor stability; hard to create large barcode library	Low encoding capacity	Lack of monodispersity and control of size	Does not allow microspheres smaller than 4 μm	Undefined
Ref.	12	157	201	65	30

Chem Soc Rev. Author manuscript; available in PMC 2017 January 10.

Table 3

Comparison of properties of different labels[57,127,214,229]

		Organic dyes				
	Fluorescent protein	**Visible organic dyes**	**NIR organic dyes**	**Quantum dots (QDs)**	**SERS dots**	**Upconversion nanoparticles**
Examples	R-phycoerythrin	FITC Alxea488	Alexa647, CY5	CdS, CdSeS	Nanoplex™ biotag	NaYF4:Yb,Er NaYF4Yb,Tm
Absorption spectra	Narrow absorption spectra	Narrow absorption spectra		Quasi-continuum superposition of absorption bands		Nano absorption spectra in NIR region
Emission spectra	Asymmetric, tailing to long-wavelength side	Asymmetric, often tailing to long-wavelength side		Symmetric, gaussian profile	Fingerprint SERS	Multicolor emission, from UV to NIR
Molar absorption coefficient	1.96×10^6 M^{-1} cm^{-1}	2.5×10^4 –2.5×10^5 M^{-1} cm^{-1}		1×10^5–1×10^6 M^{-1} cm^{-1}		
Quantum yield	0.82	0.5–1.0	0.05–0.25	0.1–0.8 (visible), 0.2–0.7 (NIR)		0.00005–0.03
Stokes shift or anti-Stokes shift	80 nm	Small Stokes shifts		Typically <50 nm for intrinsic QDs		Large anti-Stokes shift
Fluorescence lifetimes	2.9 ns	1–10 ns		10–100 ns		From microseconds to milliseconds
Binding to biomolecules	*Via* functional groups following established protocols	*Via* functional groups following established protocols; several dyes bind to a single biomolecule	*Via* ligand chemistry, few protocols available; several biomolecules bind to a single nanoparticle			
Size (molecular weight)	240 000 Da (M_w)	0.5 nm; molecule		6–60 nm (hydrodynamic diameter); colloid	300–500 nm	10–200 nm
Stability	+ +	+ +	+	+ + +	+ + + +	+ + + +
Sensitivity (signal to noise ratio)	+ + +	+	+ +	+ + +	+ + + +	Have not been used as labels in suspension array
Disadvantages	Background interference, cross talk with barcodes	Background interference, cross talk with barcodes, stability for NIR organic dyes		Background interference, limited by complex structure and surface chemistry	Multiplexing capacity is limited by decoding instrument	Limited by complex structure and surface chemistry

Table 4

Label-free suspension array platforms and bead-based label-free patterns

Method/platform	Quantification signal/signal transducer	Sensitivity	Multiplexing capacity (only considering spectrometrical barcodes)	Ref.
Photonic crystal based method	Reflection-peak shift of photonic crystal microbeads	1 nM for DNA	High, encoded by embedding QDs into the photonic crystal microbeads	15 and 202
Molecular beacon (MB) based method	Fluorescent signal of the molecular beacon	100 nM for thrombin	High, can be QD barcodes, SERS barcodes and so on	203
Conjugated polymers (CPs) coated barcodes based method	Color change of CPs	Undefined, color change of the CPs can be induced not only by targets but also by other stressors from environment	Low, color change of CPs occupies a broad spectral range	204
Conjugated polymer staining method	Fluorescent signal of CPs	~0.36 μg mL^{-1} for lysozymes	Undefined, water soluble anionic CPs with narrow band or near-infrared band emission would be preferable to obtain high multiplexing capacity	235
FRET based SNP detection	FRET from CPs to fluorescent reporter	35 fold higher than fluorescent reporter used alone	Low, fluorescent or SERS barcodes are not proper barcodes to expand this platform for multiplexing	236
Enzyme-assisted target recycling scheme	The signal from reporter binding on the surface of beads	High, 56.8 fold over direct hybridization, bead-based assays	High, clear transferability to suspension arrays with high multiplexing capacity	238

Table 5

Summary of signal/target amplification technologies in suspension assay

Type	Method	Sensitivity/reported enhanced factor	Ref.
Target amplification	Polymerase chain reaction (PCR)	A few target copies to detectable levels	255
	Recombinase polymerase amplification (RPA)	A few target copies to detectable levels	256
	Enzyme-assisted target recycling	56.8	238
Label amplification	Hybridization chain reaction (HCR)	Three orders of magnitude	263
	Layer-by-layer assembly *via* biotin–avidin interaction	17	206
	Dendrimers/branched DNA/polymer chains…(big structures to provide increased binding sites for labels)	8.5/10/100	205, 258 and 260
	Catalyzed reporter deposition (tyramide signal amplification)	100	209
	Polymerization-assisted signal amplification	10	272
Signal enhancement	Conjugated polymer-based FRET	110-fold for DNA detection, 6 fold for protein detection	207 and 274
	Nanoplasmonic-assisted fluorescence enhancement	1–2 orders of magnitude	208 and 276

Table 6

Comparison of different isothermal nucleic acid amplification technologies

Method	Amplification type	Sensitivity	Temperature	Speed/incubation time	Hardware requirement	Ref.
Recombinase polymerase amplification (RPA)	Target amplification	fM	37 °C	10–15 min	Little or no	256
Linear hybridization chain reaction (HCR)	Label amplification	pM	Room temperature	2 h	Little or no	263
Nonlinear HCR		Undefined	Room temperature	30 min	Little or no	267
Rolling circle amplification (RCA)		aM (ref. 264),<fM (ref. 265)	37 °C (ref. 264), 30 °C (ref. 265)	1 h (ref. 264), 4 h (ref. 265)	Little or no	264 and 265
Loop mediated isothermal amplification (LAMP)		10 fg μL^{-1}	63 °C	1 h	Temperature control module required	266